**Universidade de Brasília**
**Faculdade de Tecnologia**
**Departamento de Engenharia Mecânica**

# Semi-blind Receivers for two-hop MIMO relay systems with Multiple Khatri-Rao and Kronecker Codings

Pablo Henrique Ursulino de Pinho

TESE DE DOUTORADO

PROGRAMA DE PÓS-GRADUAÇÃO EM SISTEMAS MECATRÔNICOS

Brasília

2024

**Universidade de Brasília**
**Faculdade de Tecnologia**
**Departamento de Engenharia Mecânica**

# Semi-blind Receivers for two-hop MIMO relay systems with Multiple Khatri-Rao and Kronecker Codings

Pablo Henrique Ursulino de Pinho

Tese de Doutorado submetida ao Departamento de Engenharia Mecânica da Faculdade de Tecnologia da Universidade Brasília como parte dos requisitos necessários para a obtenção do grau de Doutor.

Orientador: Prof. Dr.-Ing. João Paulo J. da Costa
Coorientador: Prof. Dr. Gérard Favier

Brasília
2024

Ursulino de Pinho, Pablo Henrique .
U769s Semi-blind Receivers for two-hop MIMO relay systems with Multiple Khatri-Rao and Kronecker Codings / Pablo Henrique Ursulino de Pinho; orientador João Paulo J. da Costa ; coorientador Gérard Favier . -- Brasília, 2024.
130 p.

Tese de Doutorado (Programa de Pós-Graduação em Sistemas Mecatrônicos) -- Universidade de Brasília, 2024.

1. Decomposição Tensorial. 2. Codificações Khatri-Rao e Kronecker. 3. Receptores Semi-cegos. 4. Sistema MIMO. I. , João Paulo J. da Costa, orient. II. , Gérard Favier, coorient. III. Título

**Universidade de Brasília**
**Faculdade de Tecnologia**
**Departamento de Engenharia Mecânica**

# Semi-blind Receivers for two-hop MIMO relay systems with Multiple Khatri-Rao and Kronecker Codings

Pablo Henrique Ursulino de Pinho

Tese de Doutorado submetida ao Departamento de Engenharia Mecânica da Faculdade de Tecnologia da Universidade Brasília como parte dos requisitos necessários para a obtenção do grau de Doutor.

Trabalho aprovado. Brasília, 30 de Abril de 2024:

---

**Prof. Dr.-Ing. João Paulo Javidi da Costa, UnB/FT/ENM**
Orientador

---

**Prof. Dr. Gérard Favier, Unice/França**
Co-orientador

---

**Ricardo Zelenovsky, UnB/ENE**
Examinador interno

---

**Prof. Dr. José Alfredo Ruiz Vargas, UnB/PPMEC**
Examinador interno

Brasília
2024

**Prof. Dr. Walter Freitas Jr.,**
**UFC/PPGETI**
Examinador externo

**Prof. Dr. Tarcisio F. Maciel,**
**UFC/PPGETI**
Examinador externo

Brasília
2024

*”What we do in life echoes*
*in eternity.” (Maximus)*

# Acknowledgements

I would like to thank all the people who contributed to the development of this Thesis, especially:

To my Friends, Parents, Advisors Prof. Dr. Gérard Favier and Prof. Dr. João Paulo Javidi da Costa. I am especially grateful to Prof. Dr. Gérard Favier, who supported me throughout the thesis. He was my support throughout this research, everything I know about tensor decompositions I owe to his teachings. Thank you so much for the patience you had with me and for all you taught me.

My dear wife Maria de Fátima Kallynna Bezerra Couras all my thanks and gratitude. For all her efforts to embark on this dream of becoming PhDs and for all the support in crucial moments of our personal and academic life.

To my parents Edilson Ursulino de Morais, *in memorian*, and Leny Campelo de Pinho for granting me the gift of life together with our supreme being God. To my brothers Edilson Ursulino de Morais Filho and Fernanda Brígida Ursulino de Pinho for their support at different times.

My dear University of Brasília - UnB and my dear Université Côte D'Azur in particular to the I3S laboratory for the technical support given to the development of this thesis.

To my friends from Brasilia especially Jacinto Bezerra Gomes, Sílvia Martins, Gustavo Martins, João Batista Martins, Gileno Alves Santos, Italene Aparecida Neves da Silva dos Santos, Pedro Lucas Neves dos Santos and João Paulo Neves dos Santos for a beautiful and true friendship.

To my friends in Brazil, Evandson Dantas, Luciano Monteiro, Moisés Hamsses, Emanoel José, Sônia Seabra, Euvaldo Carvalho, Valmir Silvino, Aldenir Sudario, Paulo, Gilberto Sobreira, Emanoel José and Michael Ronnes for the true feeling of friendship.

To the friends that I made during my doctoral stay in the city of Nice in France Danielle Nunes, Danilo Sousa Rocha, Yuri Rodrigues, Davide Coluzzi, Henrique Goulart, Luana Goulart, Jean-Marie Kai, Ninad Manerikar, Pedro Marinho, Fernando Ireta, Miguel Romero, Melissa Sanabria and Michel Gonzaga. I am pleased for the support in a such important period of the development of my Thesis at the I3S laboratory in France.

To a great friend and one of the greatest supporters of my doctorate and my wife at the University of Brasília-UnB, Dr. Ing. Ricardo Kehrle Miranda, an outstanding researcher and an exemplary person in my area of expertise.

To my Parents-in-law, Francisco Bezerra Couras, *in memorian*, a true Father I had

and Pastoura Gomes Bezerra for the welcome in her home and family. To my brothers-in-law Carlos Alberto Bezerra Couras, Vicente Bezerra Couras and my sisters-in-law Célia Lima and Edina Alves. To my nephews and nieces, Ianca Lavigne, Carlos Daniel, Karla Vitorya, Davi Pinho, Igo Alexandre and Sophia Morais. To my grandparents, Maria do Desterro de Pinho, *in memorian* and Luiz Campelo da Silva.

I am also grateful to the LASP laboratory, University of Brasília-UnB and GTEL, Federal University of Ceará-UFC for their technical support and to my posgraduating program, PPMEC / UnB. To the Coordenação de Aperfeiçoamento de Pessoal de Nível Superior-CAPES for the scholarship granted (Coordination of Superior Level Staff Improvement).

To my graduate and master professors, Carlos Alberto, Edina Luz, Nádja Vieira, Luiz Pereira, Silvana da Cunha and Suzete Correia.

To Prof. Dr. João César Mota and Prof. Dr. André de Almeida for their encouragement during my doctoral research and one of the promoters of our trip to Nice in France for his doctorate with Université Côte D'Azur. To Prof. Dr. Walter Freitas, for his encouragement during my doctoral research and his friendship.

*“If you find that you’re spending almost all your time on theory,*
*start turning some attention to practical things,*
*it will improve your theories.*
*If you find that you’re spending almost all your time on practice,*
*start turning some attention to theoretical things,*
*it will improve your practice.”*
*(Donald Knuth)*

# Abstract

In recent years, semi-blind receivers based on tensor models for MIMO communication systems have been widely used as they allow for a better estimation of parameters of interest without prior channel knowledge. This thesis presents developments carried out in the scope of new semi-blind receivers applied to point-to-point and cooperative MIMO communication systems to perform symbols and channel estimation. More specifically, the theoretical contributions of this thesis are linked to the extension of the codings that introduce spatial diversity to symbol matrices. These codings allow for the proposition of semi-blind receivers to estimate the symbol and channel matrices without prior channel knowledge. In the first part of this thesis, a particular case of the multiple Khatri-Rao space-time (MKRST) coding is considered for a point-to-point MIMO system. For the MKRST coding, a symbol matrix is assumed known, which can be considered as a pre-coding matrix. For this coding scheme, a received signal tensor model is proposed, and new semi-blind receivers are presented to jointly estimate the symbols and the channel. In the second part of this thesis, a new coding extension based on the multiple Kronecker product of the symbol matrices is applied to a two-hop MIMO relay system. This system considers a single relay and the coding scheme is combined with a tensor space-time-frequency (TSTF) coding on both, transmit and relay nodes denoted by TSTF-MSMKron coding. For the proposed system, the tensor model is exploited to obtain receivers that jointly estimate channels and symbols in a semi-blind way. In each part of the thesis, conditions related to the uniqueness of tensor decompositions and the identifiability of the proposed algorithms are discussed. Simulation results are provided to evaluate the performance of the proposed coding schemes and the semi-blind receivers.

**Keywords**: Tensor Decomposition. Khatri-Rao and Kronecker codings. Semi-blind receivers. MIMO system.

# Resumo

Nos últimos anos, receptores semi-cegos baseados em modelos tensoriais para sistemas de comunicação MIMO têm sido amplamente utilizados, pois permitem uma melhor estimativa dos parâmetros de interesse sem o conhecimento prévio do canal. Esta tese apresenta desenvolvimentos realizados no âmbito de novos receptores semi-cegos aplicados a sistemas de comunicação MIMO ponto-a-ponto e cooperativo para realizar estimativas das matrizes de símbolos e canais. Mais especificamente, as contribuições teóricas desta tese estão ligadas à extensão das codificações que introduzem a diversidade espacial às matrizes de símbolos. Essas codificações permitem propor receptores semi-cegos para estimar as matrizes de símbolos e o canal sem o seu conhecimento prévio. Na primeira parte desta tese, um caso particular da codificação MKRST (do inglês, *multiple Khatri-Rao space-time*) é considerado para o sistema MIMO ponto-a-ponto. Para a codificação MKRST, uma matriz de símbolos é assumida conhecida, que pode ser considerada como uma matriz de pre-codificação. Para este esquema de codificação, um modelo de tensor do sinal recebido é proposto e novos receptores semi-cegos são apresentados para estimar conjuntamente as matrizes de símbolos e o canal. Na segunda parte desta tese, uma nova extensão de codificação baseada em múltiplos produtos de Kronecker das matrizes de símbolos é aplicada a um sistema de retransmissão MIMO de dois saltos. Esse sistema considera um único relé e o esquema de codificação é combinado com uma codificação TSTF em ambos os nós de transmissão e retransmissão, nomeada como codificação TSTF-MSMKron. Para o sistema proposto, o modelo tensorial é explorado para obter receptores que estimam conjuntamente os canais e as matrizes de símbolos de forma semi-cega. Em cada parte da tese, condições relacionadas à unicidade das decomposições tensoriais e à identificabilidade dos algoritmos propostos são discutidas. Resultados das simulações de Monte Carlo são fornecidos para avaliar o desempenho das codificações e dos receptores semi-cegos propostos.

**Palavras-chave**: Decomposição Tensorial. Codificações Khatri-Rao e Kronecker. Receptores Semi-cegos. Sistema MIMO.

# List of Figures

# List of Tables

# List of abbreviations and acronyms

| | | |
|---|---|---|
| 5G | fifth-generation | 20 |
| 6G | sixth-generation | 20 |
| AF | amplify-and-forward | 80 |
| AI | artificial intelligence | 20 |
| ALS | alternating least squares | 47 |
| AWGN | additive white Gaussian noise | 95 |
| Bi-ALS | bi-alternating least squares | 89 |
| CDMA | code-division multiple-access | 22 |
| CONFAC | constrained factor | 39 |
| CPD | canonical polyadic decomposition | 43 |
| CSI | channel state information | 21 |
| DF | decode-and-forward | 80 |
| DS-CDMA | direct sequence CDMA | 55 |
| GKRF | generalized Khatri-Rao factorization | 33 |
| GKronF | generalized Kronecker factorization | 30 |
| GNSS | global navigation satellite | 25 |
| HOSVD | higher-order singular value decomposition | 28 |
| i.i.d | independent and identically distributed | 82 |
| IOSs | intelligent omnisurfaces | 20 |
| IoT | internet of things | 20 |
| IRS | intelligent reflecting surfaces | 20 |
| KRF | Khatri-Rao factorization | 25 |
| KronF | Kronecker factorization | 25 |
| KronST | Kronecker space-time | 55 |
| KRST | Khatri-Rao space-time | 55 |
| LM | Levenberg-Marquard | 47 |
| MIMO | multiple input multiple output | 20 |

| | | |
|---|---|---|
| MKronST | multiple Kronecker space-time | 55 |
| MKRST | multiple Khatri-Rao space-time | 53 |
| MSMKron | multiple symbol matrices Kronecker | 79 |
| MUI | multi-user interference | 53 |
| NMSE | normalized mean square error | 23 |
| OFDM | orthogonal frequency division multiplexing | 22 |
| PARAFAC | parallel factor analysis | 31 |
| PSK | phase-shift keying | 95 |
| QAM | quadrature amplitude modulation | 69 |
| SER | symbol error rate | 20 |
| SNR | signal-noise ratio | 80 |
| ST | space-time | 55 |
| STF | space-time-frequency | 55 |
| STM | space-time multiplexing | 55 |
| SVD | singular value decomposition | 25 |
| TDD | time division duplex | 55 |
| THOSVD | truncated higher-order singular value decomposition | 32 |
| TST | tensor space-time | 55 |
| TSTF | tensor space-time-frequency | 21 |
| ZF | zero-forcing | 66 |

# List of symbols

# Contents

# 1 Introduction

## 1.1 Thesis scope and motivation

Wireless communication systems have experienced great growth in the number of users since the early 1990s [1]. The emergence of connected devices and the introduction of new applications, such as autonomous vehicles, smart homes and cities, Internet of Things (IoT) and virtual reality have paved the way for the integration of the multiple input multiple output (MIMO) technologies that meet the requirements of 5G (fifth-generation) wireless systems [2]. MIMO systems have been designed to support the growing demand for high-quality multimedia services, with the best trade-offs between error performance in terms of symbol error rate (SER), transmission rate in symbols per channel use, power efficiency, and receiver complexity for symbol recovery. These systems use multiple antennas at both transmitter and receiver ends, which allow for the increase of spatial diversity and lead to communication systems with MIMO channels. The deployment of multiple antennas on wireless systems allows for improved reliability in terms of the error rate and transmission rate concerning single transmit antenna systems while keeping the same power and transmission bandwidth [3, 4, 5, 6].

5G technology offers advantages in terms of data rate, reliability, latency, energy efficiency and mobility [7, 8]. On the other hand, 5G technology brings some challenges in the bag, such as, needing high frequency bands that are expensive. As the necessary waves are high frequency, the length of the waves is shorter, not being able to travel for long distances, thus requiring more base stations to a smaller area to give reliability to the user in addition to the development of new low-cost devices that support the 5G technology [8]. Massive MIMO systems have emerged to solve most challenges faced by 5G technology. These systems are composed of hundreds to thousands of receive and transmit antennas and provide an increase in spectral efficiency, reduction of dead zones and calls being discarded, also providing a uniform quality of services for different environments such as in urban and rural areas [8, 9]. Now, the idea of future 6G (sixth-generation) wireless systems and networks is specifically emerging to improve the functions and performance of future massive MIMO systems, combining other innovative technologies, architectures, and strategies such as intelligent omnisurfaces (IOSs)/intelligent reflecting surfaces (IRSs), artificial intelligence (AI), THz communications, cell-free architecture, etc [10, 11]. In the last years, cooperative MIMO systems have attracted a lot of attention to 5G mobile networks to increase the transmission coverage area, data rates and performance of wireless communications [12]. The gains of the cooperative MIMO systems are related to spatial diversity by the use of multiple antennas to transmit and receive signals and spatial multiplexing related to the use

of multiple antennas to transmit independent data streams.

During the last two decades, tensor models have been widely used for designing wireless communication systems [13, 14, 15, 16, 17]. See for instance their use in the context of point-to-point MIMO systems [18, 19], and cooperative MIMO systems [20, 21, 22, 23, 24, 25]. Tensor models have the ability to capture the multidimensional nature of the wireless channel, as well as their unique properties [26, 27]. These approaches also allow us to bring into consideration different diversities (space, time, frequency, code, polarization, ...) during system design, and to develop semi-blind receivers to jointly estimate the channels and symbol matrices, under more relaxed conditions than the matrix-based methods.

In the context of cooperative systems, some results have been published on tensor-based receivers. Some works are dedicated to the use of training sequences for estimating the channels in a supervised way, as in [28, 29] where a scenario of a three-hop multi-relay system is considered and multiple relay links are exploited at the receiver to estimate all partial channels involved in the communication. These works rely on supervised channel estimation methods, which can be bandwidth-consuming, especially for moderate to large number of antennas. This explains the development of semi-blind receivers for jointly estimating the transmitted information symbols and channels, i.e., without the use of training sequences, as in the case of the systems briefly introduced.

To improve the estimation of the transmitted information, it is also necessary to exploit the space, time, and frequency codings. Diversity techniques aim to enhance the quality of received signals in communication systems, where we create redundancies in the signal, exploiting the random nature of radio propagation [12, 30, 31]. In addition to introducing diversity into the system, codings allow the proposition of semi-blind receivers that estimate channel and symbol matrices without prior knowledge of the channel. In cooperative MIMO systems, the accuracy of channel state information (CSI) at each hop influences the effectiveness of exploiting available diversities [23]. Several works combine cooperative MIMO systems with space/time/frequency codings to increase system diversity and obtain the best performance in channel and symbol estimation [17, 32, 33, 34]. Depending on the coding chosen for the relay system, different tensor models are obtained for the signals received at the relay and destination nodes. The exploitation of these models makes it possible to derive two families of receivers: the one of supervised receivers and the one of semi-blind receivers.

In this thesis, new semi-blind receivers are addressed to jointly estimate channels and symbol matrices in point-to-point and cooperative MIMO communication systems. In particular, one of the main contributions of this thesis relies on the new coding scheme obtained by combining the tensor space-time-frequency (TSTF) coding and the multiple Kronecker product of symbol matrices (MSMKron) at the source and relay nodes. This new coding scheme, called TSTF-MSMKron coding, can be viewed as a generalization of the

codings proposed in [33] and [35]. TSTF-MSMKron coding is applied to a two-hop orthogonal frequency division multiplexing and code-division multiple-access (OFDM-CDMA) MIMO relay communication system. In addition, a particular case of the multiple Khatri-Rao space-time (MKRST) coding presented in [33] for multi-hop MIMO relay systems is considered. This coding is applied to a point-to-point MIMO system, where the pre-coding matrix corresponds to a symbol matrix that is assumed known. By applying the proposed codings, new received signal models based on tensor decomposition are presented and by exploiting these system models, semi-blind receivers are proposed to jointly estimate the channels and transmitted symbols for point-to-point and two-hop MIMO relay systems. Extensive Monte Carlo simulations are performed to illustrate the behavior and the effectiveness of the proposed schemes.

## 1.2 Thesis organization

This thesis is divided into five chapters, including this introductory chapter. In the following, we briefly describe the content of the four remaining chapters.

**Chapter 2:** *Tensor Prerequisites*: This chapter provides a theoretical basis for the methods developed in this thesis. First, a review of the definitions and operations of multilinear algebra is presented, where the notations and operations involving matrices and tensors are summarized. Second, some tensor approaches and algorithms are presented to model systems and estimate the factor matrices in tensor decompositions.

**Chapter 3:** *Semi-blind receivers for point-to-point MIMO system with MKRST coding*: This chapter presents a bibliography review of existing MIMO communication systems and coding techniques. Furthermore, the first contributions of this thesis are introduced. A particular case of the MKRST coding is considered, where the pre-coding matrix corresponds to a symbol matrix that is assumed known. Considering the MKRST coding, a point-to-point MIMO system is proposed based on tensor decompositions. By exploiting the tensor model of the received signal, tensor-based semi-blind iterative and non-iterative receivers are proposed to simultaneously estimate symbol and channel matrices. Simulation results are provided to evaluate the performance of the proposed coding and receivers in terms of symbol and channel estimation.

**Chapter 4:** *Semi-blind receivers for two-hop MIMO relay communication system with TSTF-MSMKron Coding*: This chapter introduces a new coding scheme based on the Kronecker product of multiple symbol matrices combined with a TSTF coding at the source and relay nodes, denoted as TSTF-MSMKron coding. A new two-hop OFDM-CDMA MIMO relay system is proposed based on this new coding scheme. In this system, the DF protocol is

considered to transmit the symbols between the relay and the destination nodes. Then, the proposed two-hop relay system is exploited to derive semi-blind receivers that jointly estimate the source-relay and relay-destination channels and the transmitted symbol matrices. The identifiability conditions of each receiver are analyzed. Monte Carlo simulation results are provided to illustrate the effectiveness of the proposed coding scheme and semi-blind receivers.

**Chapter 5:** *Conclusions and Perspective*: In the first part, a raising of the main conclusions on the contributions of this work is presented. Some advantages and limitations of the proposed methods and systems are highlighted. In the second part, some perspectives for future research are outlined.

## 1.3 Main original contributions

Briefly, the main contributions of this thesis can be summarized as follows:

***Chapter 3***

- The presentation of the particular case of the MKRST coding scheme used to encode signals to be transmitted in a point-to-point MIMO system;
- Proposition of the point-to-point MIMO communication system, which uses the MKRST coding. It is established that the received signals tensor satisfies a PARAFAC model;
- By exploiting the received signals tensor, proposition of new semi-blind receivers to jointly estimate channel and symbol matrices;
- Discussion on identifiability conditions of the proposed algorithms;
- Study of MKRST coding performance and the impact of design parameters under the assumption of perfect channel knowledge, by means of extensive Monte Carlo simulations;
- Study of proposed semi-blind receivers in terms of SER for symbols estimation and normalized mean square error (NMSE) for channel estimation.

***Chapter 4***

- Proposition of the new TSTF-MSMKron coding scheme as a combination of the TSTF coding and the proposed MSMKron coding used to code the signals to be transmitted in a two-hop MIMO system;

- Proposition of the new two-hop MIMO relay communication system, which uses the TSTF-MSMKron coding to code the symbols. It is established that the tensor of received signals at each hop satisfies a generalized Tucker model;
- By exploiting the signals received model at each hop, new semi-blind receivers are proposed based on iterative and non-iterative (closed-form) algorithms. These receivers are composed of two stages to jointly estimate the transmitted symbols and individual channels;
- Discussion on identifiability conditions of the proposed semi-blind receivers;
- Study of the performance of the combined TSTF-MSMKron coding and the impact of the design parameters under the assumption of perfect channel knowledge, by means of extensive Monte Carlo simulations;
- Study of the proposed semi-blind receivers in terms of SER for symbols estimation and NMSE for channel estimation.

## 1.4 Scientific production

This thesis gave rise to two conference publications and two journals/magazine publications. The list of publications is as follows:

**Conference papers:**

- **P. H. de Pinho**, M. F. K. B. Couras, G. Favier, J. P. J. da Costa, de A. L. F. Almeida, J. P. A. Maranhão, Semi-supervised receivers for MIMO systems with multiple Khatri-Rao coding. In: **13th International Conference on Signal Processing and Communication Systems (ICSPCS)**. **IEEE**, p. 1-7, 2019.
- M. F. K. B. Couras, **P. H. de Pinho**, G. Favier, J. P. J. da Costa, V. Zarzoso, and de A. L. F. Almeida, Multidimensional CX decomposition of tensors. In: **2019 Workshop on Communication Networks and Power Systems (WCNPS). IEEE**, p. 1-4, 2019.

**Journal/Magazine papers:**

- **P. H. de Pinho**, M. F. K. B. Couras, G. Favier, de A. L. F. Almeida, J. P. J. da Costa, Semi-blind receivers for two-hop MIMO relay systems with a combined TSTF-MSMKron coding. **Sensors**, 2023, 23(13), 5963.
- M. F. K. B. Couras, **P. H. de Pinho**, G. Favier, V. Zarzoso, de A. L. F. Almeida, and J. P. J. da Costa, Semi-blind receivers based on a coupled nested Tucker-PARAFAC model for dual-polarized MIMO systems using combined TST and MSMKron codings. **Digital Signal Processing**, 2023, 137, p. 104043.

# 2 Tensor Prerequisites

*Tensors theory is the basis of multilinear algebra. In literature, there are several approaches to defining tensors. One of the definitions deals with tensors as multimodal arrays with orders greater than two. System models based on tensor approaches are applied in many areas such as chemometrics, psychometrics, numerical analysis, telecommunication systems, signal and image processing, global navigation satellite systems (GNSSs), cyber attack detection, sub Nyquist sampling, RADAR system and intracranial biosignals area* [17, 26, 37, 38, 39, 40, 41, 42, 43, 36]. *In particular, tensor models have been widely used in communication systems over the last decades* [14, 17, 39, 44, 45].

*In this chapter, we review some important multilinear algebra definitions and operations necessary for the development of this thesis. The chapter is divided into five sections. In Section 2.1, we define the notations. In Section 2.2, the Kronecker and Khatri-Rao products are presented. In Section 2.3, a review of singular value decomposition (SVD), Kronecker factorization (KronF), Khatri-Rao factorization (KRF) and their generalizations are derived. Section 2.4 presents some concepts of multilinear algebra and basic operations involving matrices and tensors. Section 2.5 recalls the main tensor decompositions explored in the literature and some algorithms used for matrices estimation in tensor decompositions. All content presented here will be widely used throughout this thesis.*

## 2.1 Notation

$\mathbb{R}$ and $\mathbb{C}$ denote the real and complex number fields, respectively. Scalars, column vectors, matrices and tensors are denoted by lowercase, boldface lowercase, boldface uppercase and calligraphic letters, e.g., $y$, $\mathbf{y}$, $\mathbf{Y}$, $\mathcal{Y}$, respectively. The transpose, complex conjugate, complex conjugate transpose and Moore-Penrose pseudo-inverse of $\mathbf{Y}$ are represented by $\mathbf{Y}^{\mathrm{T}}$, $\mathbf{Y}^{*}$, $\mathbf{Y}^{\mathrm{H}}$ and $\mathbf{Y}^{\dagger}$, respectively, while $\mathbf{Y}_{i_.}$ (resp. $\mathbf{Y}_{.j}$) represents the $i^{th}$ row (resp. $j^{th}$ column) of $\mathbf{Y} \in \mathbf{C}^{I \times J}$. The Kronecker, Khatri-Rao, Hadamard, inner and outer products are denoted by $\otimes$, $\diamond$, $\odot$, $\langle \cdot \rangle$ and $\circ$, respectively. And the Frobenius norm is represented as the symbol $\| \cdot \|_F$.

$\mathbf{1}_N$ stands the all-ones column vector of dimension $N$. $\mathbf{I}_R$ and $\mathcal{I}_{N,R}$ represent the identity matrix of size $R \times R$ and the identity tensor of $N$-order and size $R \times R \times .... \times R$, respectively. $\mathbf{e}_r^{(R)}$ stands for the $r^{th}$ canonical vector of Euclidean space $\mathbb{R}^R$, while $r_{\mathbf{Y}}$ represents the rank of $\mathbf{Y}$. $\hat{\mathbf{Y}}$ denotes an estimate of $\mathbf{Y}$, while $\hat{\hat{\mathbf{Y}}}$ represents the matrix $\hat{\mathbf{Y}}$ after the correction of ambiguities.

$\mathbf{Y}_{I_1 \times I_2 I_3}$ is an unfolding of $\mathcal{Y} \in \mathbb{C}^{I_1 \times I_2 \times I_3}$ with dimension $I_1 \times I_2 I_3$. The vec$(\cdot)$ and

unvec(·) operators are defined by $\mathbf{y}_{I_2I_3I_1} = \text{vec}\left(\mathbf{Y}_{I_1\times I_2I_3}\right) \in \mathbb{C}^{I_2I_3I_1} \leftrightarrow \mathbf{Y}_{I_1\times I_2I_3} = \text{unvec}\left(\mathbf{y}_{I_2I_3I_1}\right)$. The operator bdiag$(\cdot)$ forms a block-diagonal matrix from its matrix arguments, where bdiag$(\mathbf{X}_{..k}) \triangleq$ bdiag$(\mathbf{X}_{..1}, ..., \mathbf{X}_{..K}) \in \mathbb{C}^{KI\times KJ}$, and $\mathbf{X}_{..k} \in \mathbb{C}^{I\times J}$ is the $k^{th}$ block on the diagonal of $\mathcal{X} \in \mathbb{C}^{I\times J\times K}$.

The $i^{th}$ element of $\mathbf{a} \in \mathbb{C}^I$ is denoted by $a_i$, the $(i,j)^{th}$ element of $\mathbf{A} \in \mathbb{C}^{I\times J}$ is denoted by $a_{i,j}$ and the $(i_1,...,i_N)^{th}$ element of the $N$-order tensor $\mathcal{A} \in \mathbb{C}^{I_1\times...\times I_N}$ is given by $a_{i_1,...,i_N}$.

## 2.2 Matrix operations

The Kronecker and Khatri-Rao products are important operations in multilinear algebra. Often, these products are used to represent in a simplified way the matrix unfoldings of tensor decompositions. Below, Kronecker and Khatri-Rao products are described in detail.

**Definition 1.** (Kronecker product) *Given $\boldsymbol{A} \in \mathbb{C}^{I\times J}$ and $\boldsymbol{B} \in \mathbb{C}^{K\times M}$, a Kronecker product to the right of $\boldsymbol{A}$ by $\boldsymbol{B}$ is defined as:*

$$\mathbf{A}\otimes\mathbf{B} = \begin{bmatrix} a_{1,1}\mathbf{B} & a_{1,2}\mathbf{B} & ... & a_{1,J}\mathbf{B} \\ a_{2,1}\mathbf{B} & a_{2,2}\mathbf{B} & ... & a_{2,J}\mathbf{B} \\ \vdots & \vdots & \vdots & \vdots \\ a_{I,1}\mathbf{B} & a_{I,2}\mathbf{B} & ... & a_{I,J}\mathbf{B} \end{bmatrix} \in \mathbb{C}^{IK\times JM}. \tag{2.1}$$

Note that the dimensions of $\mathbf{A}$ and $\mathbf{B}$ do not necessarily have to be the same to calculate the Kronecker product. The Kronecker product of two matrices can be seen as a matrix of blocks with $I$ blocks in the rows, $J$ blocks in the columns and each block is a matrix of size $K \times M$.

**Definition 2.** (Khatri-Rao product) *Given $\boldsymbol{A} \in \mathbb{C}^{I\times J}$ and $\boldsymbol{C} \in \mathbb{C}^{K\times J}$, the Khatri-Rao product is equivalent to a column-wise Kronecker product defined as:*

$$\mathbf{A}\diamond\mathbf{C} = \begin{bmatrix} \mathbf{A}_{.1}\otimes\mathbf{C}_{.1} & \mathbf{A}_{.2}\otimes\mathbf{C}_{.2} & ... & \mathbf{A}_{.J}\otimes\mathbf{C}_{.J} \end{bmatrix} \in \mathbb{C}^{IK\times J}. \tag{2.2}$$

The Khatri-Rao product of $\mathbf{A}$ and $\mathbf{C}$ only exists if the matrices have the same number of columns. Let us define some useful matrix properties that involve the present operations. For this, we consider the matrices $\mathbf{A} \in \mathbb{C}^{I\times M}$, $\mathbf{B} \in \mathbb{C}^{J\times N}$, $\mathbf{C} \in \mathbb{C}^{J\times M}$, $\mathbf{D} \in \mathbb{C}^{I\times N}$, $\mathbf{E} \in \mathbb{C}^{M\times N}$, $\mathbf{F} \in \mathbb{C}^{M\times K}$ and $\mathbf{G} \in \mathbb{C}^{N\times L}$.

**Property 1.**

$$(\mathbf{A}\otimes\mathbf{B})^H = \mathbf{A}^H\otimes\mathbf{B}^H, \tag{2.3}$$

**Property 2.**

$$(\mathbf{A}\otimes\mathbf{B})(\mathbf{F}\otimes\mathbf{G}) = \mathbf{AF}\otimes\mathbf{BG}, \tag{2.4}$$

**Property 3.**

$$(\mathbf{A}\diamond\mathbf{C})^H(\mathbf{D}\diamond\mathbf{B}) = \mathbf{A}^H\mathbf{D}\odot\mathbf{C}^H\mathbf{B}, \tag{2.5}$$

**Property 4.**

$$\text{vec}\left(\mathbf{AEB}^T\right) = (\mathbf{B} \otimes \mathbf{A})\,\text{vec}\,(\mathbf{E})\,, \tag{2.6}$$

**Property 5.**

$$\text{vec}\left(\mathbf{a}^{(N)} \circ ... \circ \mathbf{a}^{(1)}\right) = \mathbf{a}^{(1)} \otimes ... \otimes \mathbf{a}^{(N)}. \tag{2.7}$$

**Property 6.** *The rank of the product* $\boldsymbol{AB}$ *is less than or equal to the minimum between the ranks of* $\boldsymbol{A}$ *and* $\boldsymbol{B}$ *[27]:*

$$r_{\mathbf{AB}} \leq \min\left(r_{\mathbf{A}}, r_{\mathbf{B}}\right). \tag{2.8}$$

**Property 7.** *Given* $\boldsymbol{M} = \boldsymbol{A} \otimes \boldsymbol{C}$*, then* $r_{\boldsymbol{M}} = r_{\boldsymbol{A}} r_{\boldsymbol{C}}$*. This implies that* $\boldsymbol{M}$ *is full column rank if and only if* $\boldsymbol{A}$ *and* $\boldsymbol{C}$ *are full column rank.*

**Definition 3.** (Outer product of two vectors) *Given two vectors* $\boldsymbol{a} = \begin{bmatrix} a_1, & a_2, & ..., & a_M \end{bmatrix} \in \mathbb{C}^M$ *and* $\boldsymbol{b} = \begin{bmatrix} b_1, & b_2, & ..., & b_N \end{bmatrix} \in \mathbb{C}^N$*, their outer product* $\boldsymbol{C} = \boldsymbol{a} \circ \boldsymbol{b} \in \mathbb{C}^{M \times N}$ *is defined as:*

$$\mathbf{C} = \mathbf{a} \circ \mathbf{b} = \mathbf{a}\mathbf{b}^T. \tag{2.9}$$

This product can also be represented as:

$$c_{m,n} = a_m b_n. \tag{2.10}$$

**Definition 4.** (Outer product of two matrices) *Given* $\boldsymbol{A} \in \mathbb{C}^{I \times J}$ *and* $\boldsymbol{B} \in \mathbb{C}^{K \times M}$*, their outer product is defined as:*

$$\mathcal{D} = \mathbf{A} \circ \mathbf{B} \in \mathbb{C}^{I \times J \times K \times M}. \tag{2.11}$$

This product can also be represented as:

$$d_{i,j,k,m} = a_{i,j} b_{k,m}. \tag{2.12}$$

Eq.(2.11) is a generalization of the concept of the outer product of two vectors.

**Definition 5.** (Kruskal rank) *The Kruskal rank, also called k-rank, of a matrix* $\boldsymbol{A} \in \mathbb{C}^{I \times J}$ *is the maximum number* $k_{\boldsymbol{A}}$ *such that any set of* $k_{\boldsymbol{A}}$ *columns of* $\boldsymbol{A}$ *is linearly independent. Note that the k-rank is always less than or equal to the rank of the matrix:* $k_{\boldsymbol{A}} \leq r_{\boldsymbol{A}} \leq min\,(I, J)$*.*

**Definition 6.** (vec(·) operator) *Given* $\boldsymbol{B} \in \mathbb{C}^{K \times M}$ *as:*

$$\mathbf{B} = \begin{bmatrix} | & \vdots & | \\ \mathbf{B}_{.1} & \cdots & \mathbf{B}_{.M} \\ | & \vdots & | \end{bmatrix} \in \mathbb{C}^{K \times M}. \tag{2.13}$$

The vectorization of $\mathbf{B}$ consists of stacking its columns as:

$$\text{vec}\,(\mathbf{B}) = \begin{bmatrix} \mathbf{B}_{.1} \\ \vdots \\ \mathbf{B}_{.M} \end{bmatrix} \in \mathbb{C}^{MK}. \tag{2.14}$$

The unvec(·) operator is the inverse operator of the vec(·) operator.

## 2.3 Matrix factorizations

In this section, singular value decomposition (SVD), Kronecker factorization (KronF), and Khatri-Rao factorization (KRF) are presented. The first is an important concept to define the higher-order singular value decomposition (HOSVD) in the next sections. The second and third are used to estimate the matrices of a Kronecker or a Khatri-Rao product, respectively. These factorizations are closed-form algorithms to solve a set of rank-one approximation problems. In some applications addressed in this thesis, we will be interested in approximating a Khatri-Rao or a Kronecker product of $N$ matrices. These problems repeatedly appear over the next chapters in the context of our applications.

### 2.3.1 Singular value decomposition (SVD)

The SVD was discovered independently by Eugenio Beltrani and Camille Jordan, in 1873 and 1874, respectively. This decomposition can be viewed as a generalization of the eigendecomposition to a rectangular matrix $\mathbf{A} \in \mathbb{C}^{I \times J}$ in the sense of a diagonalization by means of two unitary matrices [46]. SVD corresponds to a matrix factorization technique that consists of representing a matrix $\mathbf{A}$ as:

$$\mathbf{A} = \mathbf{U}\boldsymbol{\Sigma}\mathbf{V}^H = \sum_{r=1}^{\min(I,J)} \sigma_r \mathbf{u}_r \mathbf{v}_r^H, \tag{2.15}$$

where $\mathbf{U} \in \mathbb{C}^{I \times I}$ is the matrix of the left singular vectors, $\mathbf{V} \in \mathbb{C}^{J \times J}$ represents the matrix of the right singular vectors and $\boldsymbol{\Sigma} \in \mathbb{C}^{I \times J}$ is a pseudo-diagonal matrix that contains the non-zero singular values $\sigma_1 \geq \sigma_2 \geq ... \geq \sigma_R > 0$ ordered by the magnitude on its main diagonal and zero elsewhere, with $R \leq \min(I,J)$.

The derivation of the SVD is directly related to the property which, to $\mathbf{A}$, the products $\mathbf{A}\mathbf{A}^H$ and $\mathbf{A}^H\mathbf{A}$ (or $\mathbf{A}\mathbf{A}^T$ and $\mathbf{A}^T\mathbf{A}$, in the case of a real matrix) are Hermitian matrices (or real symmetric matrices) and therefore, they are diagonalizable by means of their eigendecompositions, namely [46]:

$$\mathbf{A}\mathbf{A}^H = \mathbf{U}\mathbf{D}_1\mathbf{U}^H, \tag{2.16}$$

$$\mathbf{A}^H\mathbf{A} = \mathbf{V}\mathbf{D}_2\mathbf{V}^H, \tag{2.17}$$

where $\mathbf{U}$ is the matrix of eigenvectors of $\mathbf{A}\mathbf{A}^H$ and $\mathbf{V}$ is the matrix of eigenvectors of $\mathbf{A}^H\mathbf{A}$, whose columns form two orthonormal bases, which implies: $\mathbf{U}\mathbf{U}^H = \mathbf{U}^H\mathbf{U} = \mathbf{I}_I$ and $\mathbf{V}\mathbf{V}^H = \mathbf{V}^H\mathbf{V} = \mathbf{I}_J$. The non-zero eigenvalues of $\mathbf{A}\mathbf{A}^H$ and $\mathbf{A}^H\mathbf{A}$ are equal, non-negative and ordered by the magnitude, i.e, $\lambda_1 \geq \lambda_2 \geq ... \geq ... \geq \lambda_R > 0$.

Eq.(2.15) can be expressed as an economy SVD notation. The idea is to obtain the same data matrix, reducing the number of columns of $\mathbf{U}$ and $\mathbf{V}$. The economy SVD of $\mathbf{A}$ is defined as:

$$\mathbf{A} = \mathbf{U}_r\boldsymbol{\Sigma}_r\mathbf{V}_r^H = \sum_{r=1}^{R} \sigma_r \mathbf{u}_r \mathbf{v}_r^H, \tag{2.18}$$

where $\mathbf{U}_r \in \mathbb{C}^{I\times R}$ and $\mathbf{V}_r \in \mathbb{C}^{J\times R}$ contain the first $R$ columns of $\mathbf{U}$ and $\mathbf{V}$, respectively, and $\mathbf{\Sigma}_r \in \mathbb{C}^{R\times R}$ contains only the first $R$ non-zero singular values on its main diagonal. If $\mathbf{A}$ is a rank-one matrix, the low-rank approximation of $\mathbf{A}$ is obtained by truncating its SVD to a rank-one approximation as follows:

$$\mathbf{A} = \sigma_1 \mathbf{u}_1 \mathbf{v}_1^H, \tag{2.19}$$

where $\mathbf{u}_1 \in \mathbb{C}^I$ is the left dominant singular vector of $\mathbf{U}$, $\mathbf{v}_1 \in \mathbb{C}^J$ is the right dominant singular vector of $\mathbf{V}$, and $\sigma_1$ is the dominant singular value.

### 2.3.2 Kronecker factorization (KronF)

In this section, the KronF algorithm is summarized according to [14, 44, 45]. KronF algorithm introduced by [47] presents a rank-one estimation of the Kronecker product of two matrices. Consider the following product $\mathbf{C} = \mathbf{A} \otimes \mathbf{B} \in \mathbb{C}^{IJ\times KQ}$ and the minimization problem as:

$$\min_{\mathbf{A},\mathbf{B}} \parallel \mathbf{C} - \mathbf{A} \otimes \mathbf{B} \parallel_F^2, \tag{2.20}$$

where $\mathbf{A} \in \mathbb{C}^{I\times K}$ and $\mathbf{B} \in \mathbb{C}^{J\times Q}$. The matrices can be estimated by calculating the rank-one approximation of $\mathbf{C}$ defined as:

$$\min_{\mathbf{a},\mathbf{b}} \parallel \tilde{\mathbf{C}} - \mathrm{vec}(\mathbf{B})\,\mathrm{vec}(\mathbf{A})^T \parallel_F^2, \tag{2.21}$$

where $\tilde{\mathbf{C}} \in \mathbb{C}^{QJ\times KI}$, $\mathbf{a} = \mathrm{vec}(\mathbf{A}) \in \mathbb{C}^{KI}$ and $\mathbf{b} = \mathrm{vec}(\mathbf{B}) \in \mathbb{C}^{QJ}$. Defining $\tilde{\mathbf{C}} = \mathbf{U}\mathbf{\Sigma}\mathbf{V}^H$, $\mathbf{a}$ and $\mathbf{b}$ can be estimated as [14]:

$$\hat{\mathbf{a}} = \sqrt{\sigma_1}\mathbf{V}_{.1}^* \quad \hat{\mathbf{b}} = \sqrt{\sigma_1}\mathbf{U}_{.1} \ , \tag{2.22}$$

where $\mathbf{U}_{.1} \in \mathbb{C}^{QJ}$ and $\mathbf{V}_{.1} \in \mathbb{C}^{KI}$ are the first columns of the left and right singular vector matrices, respectively, and $\sigma_1$ is the dominant singular value. To find the estimated matrices $(\hat{\mathbf{A}}, \hat{\mathbf{B}})$, $\hat{\mathbf{a}}$ and $\hat{\mathbf{b}}$ must be unvectorized as:

$$\hat{\mathbf{A}} = \mathrm{unvec}(\hat{\mathbf{a}}) \in \mathbb{C}^{I\times K}, \tag{2.23}$$

$$\hat{\mathbf{B}} = \mathrm{unvec}\left(\hat{\mathbf{b}}\right) \in \mathbb{C}^{J\times Q}. \tag{2.24}$$

The KronF solution is not unique. $\hat{\mathbf{A}}$ and $\hat{\mathbf{B}}$ are subject to a scaling ambiguity given by:

$$\begin{cases} \hat{\mathbf{A}} = \mathbf{A}\lambda^{(1)}, \\ \hat{\mathbf{B}} = \mathbf{B}\lambda^{(2)} \end{cases} \quad \lambda^{(1)}\lambda^{(2)} = 1 \ , \tag{2.25}$$

where the scaling $\lambda^{(n)}$ for $n \in \{1, 2\}$ is determined from knowledge of one element of $\mathbf{A}$ or $\mathbf{B}$ [14, 33]. Let us consider the element $a_{1,1}$ of $\mathbf{A}$ known. For $\lambda^{(1)}$, we have:

$$\lambda^{(1)} = \frac{\hat{a}_{1,1}}{a_{1,1}}, \tag{2.26}$$

where $\hat{a}_{1,1}$ is the element (1,1) of $\hat{\mathbf{A}}$. For $\hat{\mathbf{B}}$, we have:

$$\lambda^{(2)} = \left(\lambda^{(1)}\right)^{-1}. \tag{2.27}$$

Then, the final estimates are given by:

$$\hat{\hat{\mathbf{A}}} = \hat{\mathbf{A}}\left(\lambda^{(1)}\right)^{-1}, \quad \hat{\hat{\mathbf{B}}} = \hat{\mathbf{B}}\lambda^{(1)} \ . \tag{2.28}$$

The KronF algorithm is described in Table 1

Table 1 – KronF algorithm.

| **KronF algorithm for estimating the factor matrices of a Kronecker product** |
|---|
| **Input:** matrix $\mathbf{C}$, $I$, $J$, $K$ and $Q$ |
| **Output:** Estimated matrices $\hat{\hat{\mathbf{A}}}$ and $\hat{\hat{\mathbf{B}}}$ |
| 1) Reshape $\mathbf{C} \in \mathbb{C}^{IJ\times KQ}$ as: $$\tilde{\mathbf{C}} = \text{reshape}\left(\mathbf{C},[QJ, KI]\right). \tag{2.29}$$ |
| 2) Calculate the SVD of $\tilde{\mathbf{C}}$: $$\tilde{\mathbf{C}} = \mathbf{U}\mathbf{\Sigma}\mathbf{V}^H. \tag{2.30}$$ |
| 3) Estimate $\hat{\mathbf{a}}$ and $\hat{\mathbf{b}}$ using Eq.(2.22) and unvectorize $\hat{\mathbf{a}}$ and $\hat{\mathbf{b}}$ using Eqs. (2.23)-(2.24), respectively. |
| 4) Eliminate the scaling ambiguities using Eqs.(2.25)-(2.28). |

#### 2.3.2.1 Generalized Kronecker factorization (GKronF)

In this subsection, the generalized KronF algorithm is summarized according to [45]. Before presenting this procedure, let us present the following formula for row and column permutation of the Kronecker product $\mathbf{B} \otimes \mathbf{C}$:

$$\mathbf{C} \otimes \mathbf{B} = \mathbf{\Pi}_{I,J}\left(\mathbf{B} \otimes \mathbf{C}\right)\mathbf{\Pi}_{S,R} \in \mathbb{C}^{IJ\times RS}, \tag{2.31}$$

with $\mathbf{C} \in \mathbb{C}^{I\times R}$, $\mathbf{B} \in \mathbb{C}^{J\times S}$ and $\mathbf{\Pi}_{I,J} \in \mathbb{C}^{IJ\times JI}$, $\mathbf{\Pi}_{S,R} \in \mathbb{C}^{SR\times RS}$ being permutation matrices defined as:

$$\mathbf{\Pi}_{I,J} = \sum_i \sum_j \left(\mathbf{e}_i^{(I)}\mathbf{e}_j^{(J)T}\right) \otimes \left(\mathbf{e}_j^{(J)}\mathbf{e}_i^{(I)T}\right) \in \mathbb{C}^{IJ\times JI}, \tag{2.32}$$

$$\mathbf{\Pi}_{S,R} = \sum_s \sum_r \left(\mathbf{e}_s^{(S)}\mathbf{e}_r^{(R)T}\right) \otimes \left(\mathbf{e}_r^{(R)}\mathbf{e}_s^{(S)T}\right) \in \mathbb{C}^{SR\times RS}, \tag{2.33}$$

where $\mathbf{e}_i^{(I)}$ is the $i^{th}$ canonical basis vector of the Euclidean space $\mathbb{R}^I$, similarly for $\mathbf{e}_j^{(J)}$, $\mathbf{e}_s^{(S)}$ and $\mathbf{e}_r^{(R)}$. Now, let us consider the following product $\mathbf{A} = \otimes_{n=1}^N \mathbf{A}^{(n)} \in \mathbb{C}^{I\times R}$ and the minimization problem as:

$$\min_{\mathbf{A}^{(n)}, n\in\{1,N\}} \| \mathbf{A} - \otimes_{n=1}^N \mathbf{A}^{(n)} \|_F^2, \tag{2.34}$$

where $\mathbf{A}^{(n)} \in \mathbb{C}^{I_n \times R_n}$ are the matrices to be estimated, with $I = \prod_{n=1}^{N} I_n$ and $R = \prod_{n=1}^{N} R_n$. This problem can be solved by determining $\mathbf{A}^{(n)}$, for $n \in \{1, N\}$ with a two-by-two search. This basic algorithm was proposed by [47] to estimate two factor matrices of a Kronecker product associated with third-order parallel factor analysis (PARAFAC) model presented in the next sections. To illustrate the GKronF algorithm, consider the case $N = 3$, with $\mathbf{A} = \mathbf{A}^{(1)} \otimes \mathbf{A}^{(2)} \otimes \mathbf{A}^{(3)}$. The optimization problem becomes:

$$\min_{\mathbf{A}^{(1)},\mathbf{A}^{(2)},\mathbf{A}^{(3)}} \| \mathbf{A} - \mathbf{A}^{(1)} \otimes \mathbf{A}^{(2)} \otimes \mathbf{A}^{(3)} \|_F^2 . \tag{2.35}$$

$\mathbf{A}^{(1)}$ and $\mathbf{A}^{(3)}$ can be estimated by applying the KronF algorithm presented in Table 1 to the following two decompositions of $\mathbf{A}$:

$$\mathbf{A} = \mathbf{A}^{(1)} \otimes \mathbf{A}^{(2,3)} \in \mathbb{C}^{I_1 I_2 I_3 \times R_1 R_2 R_3}, \tag{2.36}$$

$$\mathbf{A} = \mathbf{A}^{(1,2)} \otimes \mathbf{A}^{(3)} \in \mathbb{C}^{I_1 I_2 I_3 \times R_1 R_2 R_3}, \tag{2.37}$$

where $\mathbf{A}^{(2,3)} = \mathbf{A}^{(2)} \otimes \mathbf{A}^{(3)}$ and $\mathbf{A}^{(1,2)} = \mathbf{A}^{(1)} \otimes \mathbf{A}^{(2)}$. To estimate $\mathbf{A}^{(2)}$, we use the following equation obtained by permuting the matrices $\mathbf{A}^{(1)}$ and $\mathbf{A}^{(2)}$:

$$\mathbf{A}_{\pi}^{(2)} = \left(\mathbf{\Pi}_{I_2,I_1} \otimes \mathbf{I}_{I_3}\right) \mathbf{A} \left(\mathbf{\Pi}_{R_2,R_1} \otimes \mathbf{I}_{R_3}\right) = \mathbf{A}^{(2)} \otimes \mathbf{A}^{(1)} \otimes \mathbf{A}^{(3)} \in \mathbb{C}^{I_2 I_1 I_3 \times R_2 R_1 R_3}, \tag{2.38}$$

$$\mathbf{A}_{\pi}^{(2)} = \mathbf{A}^{(2)} \otimes \mathbf{A}^{(1,3)} \in \mathbb{C}^{I_2 I_1 I_3 \times R_2 R_1 R_3}, \tag{2.39}$$

where $\mathbf{A}^{(1,3)} = \mathbf{A}^{(1)} \otimes \mathbf{A}^{(3)}$ and $\mathbf{A}_{\pi}^{(2)}$ indicates the permutation between $\mathbf{A}^{(1)}$ and $\mathbf{A}^{(2)}$. From Eq.(2.39), we apply again the KronF algorithm in Table 1 that allows estimating $\mathbf{A}^{(2)}$.

#### 2.3.2.2 Kronecker product approximation to rank-one tensors

This section presents how a Kronecker product of $N$ matrices can be reorganized as a tensor. Let us consider the following Kronecker product:

$$\mathbf{A} = \mathbf{A}^{(1)} \otimes \ldots \otimes \mathbf{A}^{(N)} \in \mathbb{C}^{I_1 \ldots I_N \times R_1 \ldots R_N}, \tag{2.40}$$

where $\mathbf{A}^{(n)}$ are the matrices to be estimated for $n \in \{1,N\}$. This operation was defined in [48] for Kronecker product of multiple matrices. The problem (2.40) becomes:

$$\min_{\mathbf{A}^{(n)}, n \in \{1,N\}} \| \mathbf{A} - \mathbf{A}^{(1)} \otimes \ldots \otimes \mathbf{A}^{(N)} \|_F^2 . \tag{2.41}$$

$\mathbf{A}$ can be expressed as a rank-one tensor rearranging the Kronecker product into an outer product. The problem (2.41) now becomes:

$$\min_{\mathbf{a}^{(n)}, n \in \{1,N\}} \| \mathcal{A} - \mathbf{a}^{(1)} \circ \ldots \circ \mathbf{a}^{(N)} \|_F^2, \tag{2.42}$$

where $\mathbf{a}^{(n)} = \text{vec}(\mathbf{A}^{(n)}) \in \mathbb{C}^{R_n I_n}$ and $\mathcal{A} \in \mathbb{C}^{R_1 I_1 \times \ldots \times R_N I_N}$ is a rank-one tensor defined as:

$$\mathcal{A} = \text{reshape}\left(\mathbf{A}, [R_1 I_1, ..., R_N I_N]\right). \tag{2.43}$$

Therefore, find the matrices $\mathbf{A}^{(n)}$ through the cost function (2.41) is equivalent to finding vectors $\mathbf{a}^{(n)}$ that minimizes the cost function (2.42), i.e., the solution of a Kronecker approximation problem can be recast as the solution of a rank-one tensor approximation problem [46, 48, 49]. The matrices can be estimated using the truncated HOSVD (THOSVD) [50] where the matrices are unique with some scaling factors, similar to the KronF algorithm presented above:

$$\begin{cases} \hat{\mathbf{A}}^{(n)} = \mathbf{A}^{(n)} \lambda^{(n)} \\ \prod_{n=1}^{N} \lambda^{(n)} = 1 \end{cases}. \tag{2.44}$$

### 2.3.3 Khatri-Rao factorization (KRF)

This section summarizes the KRF algorithm presented in [51, 52]. It features a rank-one estimate via the Khatri-Rao product. Let us assume $\mathbf{C} = \mathbf{D} \diamond \mathbf{E} \in \mathbb{C}^{IJ \times K}$ and the following minimization problem:

$$\min_{\mathbf{D},\mathbf{E}} \| \mathbf{C} - \mathbf{D} \diamond \mathbf{E} \|_F^2, \tag{2.45}$$

where $\mathbf{D} \in \mathbb{C}^{I \times K}$ and $\mathbf{E} \in \mathbb{C}^{J \times K}$ can be estimated by calculating the rank-one approximation of $\mathbf{C}$ defined for each column $k \in \{1, K\}$ as:

$$\mathbf{Z}_k = \text{unvec}\left(\mathbf{C}_{.k}\right) = \mathbf{E}_{.k} \mathbf{D}_{.k}^T \in \mathbb{C}^{IJ}, \tag{2.46}$$

where $\mathbf{D}_{.k}$ and $\mathbf{E}_{.k}$ represents the $k^{th}$ column of $\mathbf{D}$ and $\mathbf{E}$, respectively. Defining the SVD of $\mathbf{Z}_k = \mathbf{U}_k \mathbf{\Sigma}_k \mathbf{V}_k^H$, $\hat{\mathbf{D}}_{.k}$ and $\hat{\mathbf{E}}_{.k}$ are given by [52]:

$$\hat{\mathbf{D}}_{.k} = \sqrt{\sigma_{1,k}} \left(\mathbf{V}_k^*\right)_{.1} \quad \hat{\mathbf{E}}_{.k} = \sqrt{\sigma_{1,k}} \left(\mathbf{U}_k\right)_{.1}, \tag{2.47}$$

where $\left(\mathbf{U}_k\right)_{.1} \in \mathbb{C}^J$ and $\left(\mathbf{V}_k\right)_{.1} \in \mathbb{C}^I$ are the first columns of the $k^{th}$ left and right singular vector matrices, respectively, and $\sigma_{1k}$ is the dominant singular value. The KRF solution is not unique. There is a scaling ambiguity per column $k$ in each Khatri-Rao product [52]. For this, we have the following relation:

$$\begin{cases} \hat{\mathbf{D}} = \mathbf{D} \mathbf{\Lambda}^{(1)}, \\ \hat{\mathbf{E}} = \mathbf{E} \mathbf{\Lambda}^{(2)} \end{cases} \quad \mathbf{\Lambda}^{(1)} \mathbf{\Lambda}^{(2)} = \mathbf{I}_K \ . \tag{2.48}$$

To find the scaling matrices, it is necessary to know a row of $\mathbf{D}$ or $\mathbf{E}$ [52]. Let us consider the first row of $\mathbf{D}$ known. We have for each element of $\mathbf{\Lambda}^{(1)}$ the following equation:

$$\lambda_k^{(1)} = \frac{\hat{d}_{1,k}}{d_{1,k}}, \tag{2.49}$$

where $\hat{d}_{1,k}$ and $d_{1,k}$ are the elements of the first row of $\hat{\mathbf{D}}$ and $\mathbf{D}$, respectively. $\mathbf{\Lambda}^{(1)}$ corresponds to a matrix with the elements $\lambda_k^{(1)}$ on the main diagonal. For $\mathbf{E}$, we have:

$$\mathbf{\Lambda}^{(2)} = \left(\mathbf{\Lambda}^{(1)}\right)^{-1}. \tag{2.50}$$

So, the final estimates of $\mathbf{D}$ and $\mathbf{E}$ are:

$$\hat{\hat{\mathbf{D}}} = \hat{\mathbf{D}}\left(\mathbf{\Lambda}^{(1)}\right)^{-1}, \quad \hat{\hat{\mathbf{E}}} = \hat{\mathbf{E}}\mathbf{\Lambda}^{(1)}\ . \tag{2.51}$$

The KRF algorithm is described in Table 2.

Table 2 – KRF algorithm.

| **KRF algorithm for estimating the factor matrices of a Khatri-Rao product** |
|---|
| **Input:** matrix $\mathbf{C}$, $I$, $J$ and $K$ |
| **Output:** Estimated matrices $\hat{\hat{\mathbf{D}}}$ and $\hat{\hat{\mathbf{E}}}$ |
| 1) Unvectorize $\mathbf{C}$: |
| **for** $k \in \{1, K\}$ |
| $$\mathbf{Z}_k = \text{unvec}\left(\mathbf{C}_{.k}\right). \tag{2.52}$$ |
| 2) Calculate the SVD for each column $k$: |
| $$\mathbf{Z}_k = \mathbf{U}_k\mathbf{\Sigma}_k\mathbf{V}_k^H. \tag{2.53}$$ |
| 3) Estimate $\hat{\mathbf{D}}$ and $\hat{\mathbf{E}}$ using Eq.(2.47). |
| **end** |
| 4) Store in the matrices as: |
| $$\hat{\mathbf{D}} = \left[\ \sqrt{\sigma_{1,1}}\left(\mathbf{V}_1\right)_{.1} \quad \ldots \quad \sqrt{\sigma_{1,K}}\left(\mathbf{V}_K\right)_{.1}\ \right]^* \in \mathbb{C}^{I\times K}, \tag{2.54}$$ |
| $$\hat{\mathbf{E}} = \left[\ \sqrt{\sigma_{1,1}}\left(\mathbf{U}_1\right)_{.1} \quad \ldots \quad \sqrt{\sigma_{1,K}}\left(\mathbf{U}_K\right)_{.1}\ \right] \in \mathbb{C}^{J\times K}. \tag{2.55}$$ |
| 5) Eliminate the scaling ambiguities using Eqs.(2.48)-(2.51). |

#### 2.3.3.1 Generalized Khatri-Rao factorization (GKRF)

In this subsection, the GKRF algorithm is summarized according to [45]. Before presenting this procedure, let us present the following equation for the row permutation of a Khatri-Rao product $\mathbf{C} \diamond \mathbf{A}$ as:

$$\mathbf{A} \diamond \mathbf{C} = \mathbf{\Pi}_{I,J}\left(\mathbf{C} \diamond \mathbf{A}\right) \in \mathbb{C}^{IJ\times K}, \tag{2.56}$$

where $\mathbf{A} \in \mathbb{C}^{I\times K}$, $\mathbf{C} \in \mathbb{C}^{J\times K}$ and $\mathbf{\Pi}_{I,J} \in \mathbb{C}^{IJ\times JI}$ defined as Eq.(2.32). Now, let us consider the following product $\mathbf{B} = \diamond_{n=1}^{N}\mathbf{B}^{(n)} \in \mathbb{C}^{I\times R}$ and the minimization problem as:

$$\min_{\mathbf{B}^{(n)}, n\in\{1,N\}} \| \mathbf{B} - \diamond_{n=1}^{N}\mathbf{B}^{(n)} \|_F^2, \tag{2.57}$$

where $\mathbf{B}^{(n)} = \left[ \begin{array}{ccc} \mathbf{B}_{.1}^{(n)}, & ..., & \mathbf{B}_{.R}^{(n)} \end{array} \right] \in \mathbb{C}^{I_n \times R}$ are the matrices to be estimated with $I = \prod_{n=1}^{N} I_n$. To illustrate the GKRF algorithm, consider $N = 3$ and $\mathbf{B} = \mathbf{B}^{(1)} \diamond \mathbf{B}^{(2)} \diamond \mathbf{B}^{(3)}$. The minimization problem in Eq.(2.57) becomes now:

$$\min_{\mathbf{B}^{(1)},\mathbf{B}^{(2)},\mathbf{B}^{(3)}} \| \mathbf{B} - \mathbf{B}^{(1)} \diamond \mathbf{B}^{(2)} \diamond \mathbf{B}^{(3)} \|_F^2 . \tag{2.58}$$

$\mathbf{B}^{(1)}$ and $\mathbf{B}^{(3)}$ can be estimated by applying the KRF algorithm presented in Table 2 to the following two decompositions of $\mathbf{B}$:

$$\mathbf{B} = \mathbf{B}^{(1)} \diamond \mathbf{B}^{(2,3)} \in \mathbb{C}^{I_1 I_2 I_3 \times R}, \tag{2.59}$$

$$\mathbf{B} = \mathbf{B}^{(1,2)} \diamond \mathbf{B}^{(3)} \in \mathbb{C}^{I_1 I_2 I_3 \times R}, \tag{2.60}$$

where $\mathbf{B}^{(2,3)} = \mathbf{B}^{(2)} \diamond \mathbf{B}^{(3)}$ and $\mathbf{B}^{(1,2)} = \mathbf{B}^{(1)} \diamond \mathbf{B}^{(2)}$. By vectorizing $\mathbf{B}$ in both equations, the following LS criteria must be minimized:

$$\min_{\mathbf{B}^{(1)},\mathbf{B}^{(2,3)}} \| \operatorname{vec}(\mathbf{B}) - \operatorname{vec}\left(\mathbf{B}^{(1)} \diamond \mathbf{B}^{(2,3)}\right) \|_F^2 = \min_{\mathbf{B}_{.r}^{(1)},\mathbf{B}_{.r}^{(2,3)}} \sum_{r=1}^{R} \| \mathbf{B}_{.r} - \mathbf{B}_{.r}^{(1)} \diamond \mathbf{B}_{.r}^{(2,3)} \|_F^2, \tag{2.61}$$

$$\min_{\mathbf{B}^{(1,2)},\mathbf{B}^{(3)}} \| \operatorname{vec}(\mathbf{B}) - \operatorname{vec}\left(\mathbf{B}^{(1,2)} \diamond \mathbf{B}^{(3)}\right) \|_F^2 = \min_{\mathbf{B}_{.r}^{(1,2)},\mathbf{B}_{.r}^{(3)}} \sum_{r=1}^{R} \| \mathbf{B}_{.r} - \mathbf{B}_{.r}^{(1,2)} \diamond \mathbf{B}_{.r}^{(3)} \|_F^2 . \tag{2.62}$$

Since each term in this sum can be minimized separately, the columns $\mathbf{B}_{.r}^{(1)} \in \mathbb{C}^{I_1}$, $\mathbf{B}_{.r}^{(2,3)} \in \mathbb{C}^{I_2 I_3}$, $\mathbf{B}_{.r}^{(1,2)} \in \mathbb{C}^{I_1 I_2}$ and $\mathbf{B}_{.r}^{(3)} \in \mathbb{C}^{I_3}$ are estimated by minimizing the criteria $\min_{\mathbf{B}_{.r}^{(1)},\mathbf{B}_{.r}^{(2,3)}} \sum_{r=1}^{R} \| \mathbf{B}_{.r} - \mathbf{B}_{.r}^{(1)} \diamond \mathbf{B}_{.r}^{(2,3)} \|_F^2$ and $\min_{\mathbf{B}_{.r}^{(1,2)},\mathbf{B}_{.r}^{(3)}} \sum_{r=1}^{R} \| \mathbf{B}_{.r} - \mathbf{B}_{.r}^{(1,2)} \diamond \mathbf{B}_{.r}^{(3)} \|_F^2$, respectively.

Let us define $\mathbf{B}_r \triangleq \operatorname{unvec}(\mathbf{B}_{.r})$ as the matrix obtained by inverting the vectorization operation for $r \in \{1, R\}$. Applying Definition 3, then gives us:

$$\min_{\mathbf{B}_{.r}^{(1)},\mathbf{B}_{.r}^{(2,3)}} \| \mathbf{B}_r - \mathbf{B}_{.r}^{(2,3)} \mathbf{B}_{.r}^{(1)T} \|_F^2 = \min_{\mathbf{B}_{.r}^{(1)},\mathbf{B}_{.r}^{(2,3)}} \| \mathbf{B}_r - \mathbf{B}_{.r}^{(2,3)} \circ \mathbf{B}_{.r}^{(1)} \|_F^2, \tag{2.63}$$

$$\min_{\mathbf{B}_{.r}^{(1,2)},\mathbf{B}_{.r}^{(3)}} \| \mathbf{B}_r - \mathbf{B}_{.r}^{(3)} \mathbf{B}_{.r}^{(1,2)T} \|_F^2 = \min_{\mathbf{B}_{.r}^{(1,2)},\mathbf{B}_{.r}^{(3)}} \| \mathbf{B}_r - \mathbf{B}_{.r}^{(3)} \circ \mathbf{B}_{.r}^{(1,2)} \|_F^2 . \tag{2.64}$$

The vectors $\mathbf{B}_{.r}^{(1)}$, $\mathbf{B}_{.r}^{(2,3)}$, $\mathbf{B}_{.r}^{(1,2)}$ and $\mathbf{B}_{.r}^{(3)}$ can be estimated by computing the rank-one reduced SVD of $\mathbf{B}_r$ as in Eq.(2.47) using the KRF algorithm described in Table 2. To estimate $\mathbf{B}^{(2)}$, we permute the matrices $\mathbf{B}^{(1)}$ and $\mathbf{B}^{(2)}$ as:

$$\mathbf{B}_{\pi}^{(2)} = \left(\mathbf{\Pi}_{I_2,I_1} \otimes \mathbf{I}_{I_3}\right) \mathbf{B} = \mathbf{B}^{(2)} \diamond \mathbf{B}^{(1)} \diamond \mathbf{B}^{(3)} \in \mathbb{C}^{I_2 I_1 I_3 \times R}, \tag{2.65}$$

$$\mathbf{B}_{\pi}^{(2)} = \mathbf{B}^{(2)} \diamond \mathbf{B}^{(1,3)} \in \mathbb{C}^{I_2 I_1 I_3 \times R}, \tag{2.66}$$

where $\mathbf{B}^{(1,3)} = \mathbf{B}^{(1)} \otimes \mathbf{B}^{(3)}$ and $\mathbf{B}^{(2)}_{\pi}$ indicates the permutation between $\mathbf{B}^{(1)}$ and $\mathbf{B}^{(2)}$. For KRF, it is only necessary to permute the rows. For Eq.(2.66), the minimization problem becomes:

$$\min_{\mathbf{B}^{(2)}_{.r},\mathbf{B}^{(1,3)}_{.r}} \| \mathbf{B}^{(2)}_{\pi r} - \mathbf{B}^{(2)}_{.r}\mathbf{B}^{(1,3)T}_{.r} \|^2_F = \min_{\mathbf{B}^{(2)}_{.r},\mathbf{B}^{(1,3)}_{.r}} \| \mathbf{B}^{(2)}_{\pi r} - \mathbf{B}^{(2)}_{.r} \circ \mathbf{B}^{(1,3)}_{.r} \|^2_F . \tag{2.67}$$

where $\mathbf{B}^{(2)}_{\pi r} \triangleq \text{unvec}\left([\mathbf{B}^{(2)}_{\pi}]_{.r}\right)$. From (2.67) we apply again the KRF algorithm in Table 2 that allows to estimate $\mathbf{B}^{(2)}$.

## 2.4 Basics of tensor algebra

This section presents some concepts used in the multilinear algebra. For demonstrations and discussions of these properties, see [42, 46]. A tensor is an array with an order greater than two. It can be called a multidimensional array. For the next definitions presented in this section, unless otherwise indicated, we consider the following tensors:

- an $N$-order tensor $\mathcal{Y} \in \mathbb{C}^{I_1 \times \ldots \times I_N}$;
- a third-order tensor $\mathcal{X} \in \mathbb{C}^{I \times J \times K}$.

**Definition 7.** (Fiber) *For a third-order tensor $\mathcal{X} \in \mathbb{C}^{I \times J \times K}$, there are three types of fibers: (i) column fibers $\left(\boldsymbol{X}_{.jk} \in \mathbb{C}^{I}\right)$, where the indexes $j$ and $k$ are fixed and the index $i$ is varying, forming a vector of size $I$; (ii) row fibers $\left(\boldsymbol{X}_{i.k} \in \mathbb{C}^{J}\right)$, in this case the fixed indexes are $i$ and $k$, and the index $j$ is varying. And finally, (iii) tubes fibers $\left(\boldsymbol{X}_{ij.} \in \mathbb{C}^{K}\right)$, creating a vector of size $K$ by fixing the indexes $i$ and $j$, and varying the index $k$ along the $K$ dimension as illustrated in Figure 1.*

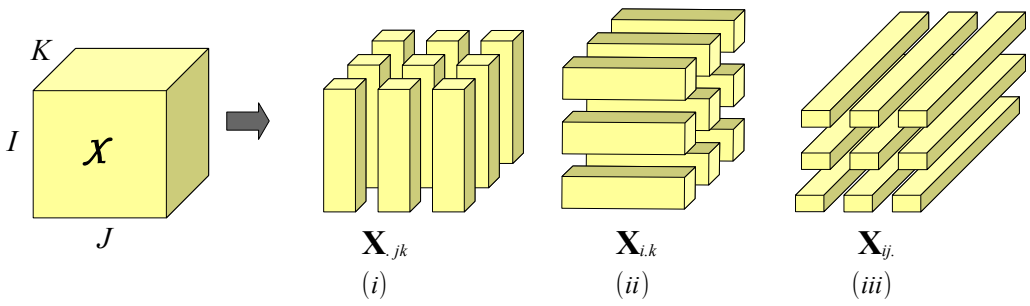


Figure 1 – (i) Column fibers; (ii) row fibers; (iii) tube fibers

**Definition 8.** (Matrix slice) *The matrix slices are matrices obtained by varying the indexes of two modes and fixing all others. For an $N$-order tensor, there are $\binom{N}{2}$ ways to slice it, where*

$\binom{N}{2}$ *denotes the binomial coefficient, i.e., the number of possibilities to choose* 2 *elements from a set of* $N$ *elements. For the third-order tensor* $\mathcal{X}$*, the three types of slices are (i) frontal slice* $\left(\boldsymbol{X}_{..k} \in \mathbb{C}^{I \times J}\right)$*; (ii) lateral slice* $\left(\boldsymbol{X}_{.j.} \in \mathbb{C}^{I \times K}\right)$*; and (iii) horizontal slice* $\left(\boldsymbol{X}_{i..} \in \mathbb{C}^{J \times K}\right)$*. Figure 2 illustrates the three types of slices of a third-order tensor.*

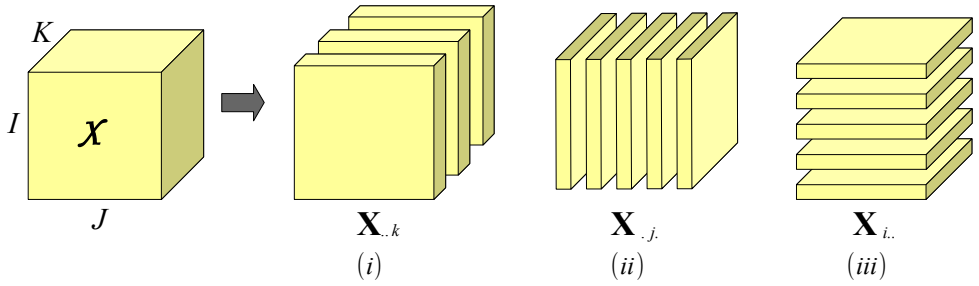


Figure 2 – (i) Frontal slice; (ii) lateral slice; (iii) horizontal slice

**Definition 9.** (Matrix unfoldings) *Matricization or matrix unfolding, is the process of reordering the elements of an* $N$*-way array into a matrix [42]. Given two ordered subset* $\mathbb{S}_1$ *and* $\mathbb{S}_2$ *constituted of* $p$ *and* $N-p$ *indexes, respectively. A general unfolding of* $\mathcal{Y}$*, for* $p \in \{1, N-1\}$*, is given by [53]:*

$$\mathbf{Y}_{\mathbb{S}_1 \times \mathbb{S}_2} = \sum_{i_1}^{I_1} \cdots \sum_{i_N}^{I_N} y_{i_1,\ldots,i_N} \left( \bigotimes_{n \in \mathbb{S}_1} \mathbf{e}_{i_n}^{(I_n)} \right) \left( \bigotimes_{n \in \mathbb{S}_2} \mathbf{e}_{i_n}^{(I_n)} \right)^T \in \mathbb{C}^{J_1 \times J_2}, \tag{2.68}$$

with $J_{n_1} = \prod_{n \in \mathbb{S}_{n_1}} I_n$, for $n_1 \in \{1, 2\}$. From Definition 9, we can see a mode-$n$ unfolding as a rearrangement of the elements of $\mathcal{Y}$ obtained by varying an index $i_n$ and keeping the others indexes fixed, so that the fibers of the $n^{th}$ mode are placed along rows (flat unfolding) or columns (tall unfolding). In Figure 3 we present an example for the third-order tensor $\mathcal{X}$. Note that a matrix unfolding can be obtained by stacking the slices in a certain mode. In our notation, the subscribed characters show the order in which the modes are combined and consequently, the size of the matrix unfolding.

**Definition 10.** (Inner product) *Let us consider a tensor* $\mathcal{T} \in \mathbb{C}^{I_1 \times \ldots \times I_N}$ *of the same order and dimension of* $\mathcal{Y}$*. The inner product between* $\mathcal{Y}$ *and* $\mathcal{T}$ *is defined as:*

$$\langle \mathcal{Y}, \mathcal{T} \rangle = \sum_{i_1=1}^{I_1} \cdots \sum_{i_N=1}^{I_N} y_{i_1,\ldots,i_N} t_{i_1,\ldots,i_N}. \tag{2.69}$$

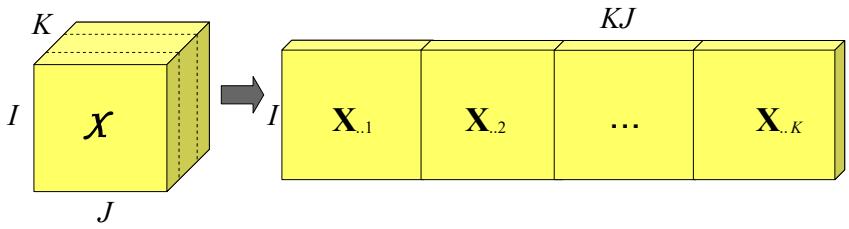


Figure 3 – The matrix unfolding representation $\mathbf{X}_{I\times KJ}$ for the third-order tensor $\mathcal{X}$

**Definition 11.** (Frobenius norm) *Frobenius norm of the tensor $\mathcal{Y}$ is defined as:*

$$\| \mathcal{Y} \|_F = \sqrt{\langle \mathcal{Y}\mathcal{Y} \rangle} = \left( \sum_{i_1=1}^{I_1} \cdots \sum_{i_N=1}^{I_N} |y|^2_{i_1,\ldots,i_N} \right)^{1/2}. \tag{2.70}$$

The Frobenius norm can be interpreted as a measure of "energy" in the tensor.

**Definition 12.** (Outer product of tensors) *The outer product between the N-order tensor $\mathcal{Y}$ and the M-order tensor $\mathcal{Z}$ produces a new tensor, whose entries are defined as:*

$$[\mathcal{Y} \circ \mathcal{Z}]_{i_1,\ldots,i_N j_1,\ldots,j_M} = y_{i_1,\ldots,i_N} z_{j_1,\ldots,j_M}. \tag{2.71}$$

Eq.(2.71) defines a $(N+M)$-order tensor of size $I_1 \times \ldots \times I_N \times J_1 \times \ldots \times J_M$ and can be interpreted as a generalization of the concept of outer product of two vectors.

**Definition 13.** (Rank-one tensor) *The tensor $\mathcal{Y}$ is considered a rank-one tensor if it can be written as the outer product of N vectors $\boldsymbol{a}^{(n)} \in \mathbb{C}^{I_n}$, with $n \in \{1, N\}$, as follows:*

$$\mathcal{Y} = \mathbf{a}^{(1)} \circ \ldots \circ \mathbf{a}^{(N)} \in \mathbb{C}^{I_1 \times \ldots \times I_N}, \tag{2.72}$$

whose entries are $y_{i_1,\ldots,i_N} = a^{(1)}_{i_1} \ldots a^{(N)}_{i_N}$. This definition is a generalization of the concept of rank-one matrix, where a matrix $\mathbf{Y} \in \mathbb{C}^{I_1 \times I_2}$ has rank equal to one if there are two vectors $\mathbf{a}^{(1)} \in \mathbb{C}^{I_1}$ and $\mathbf{a}^{(2)} \in \mathbb{C}^{I_2}$, such that $\mathbf{Y} = \mathbf{a}^{(1)} \circ \mathbf{a}^{(2)} = \mathbf{a}^{(1)} \mathbf{a}^{(2)T}$. Some tensor decompositions express the tensor as linear combinations of rank-one tensors.

**Definition 14.** (Tensor rank) *The rank of a tensor is the smallest number of rank-one tensors needed to write it as a linear combination.*

The above definition implies that any arbitrary tensor of rank $R \geq 1$ can be written as a sum of $R$ rank-one tensors as:

$$\mathcal{Y} = \sum_{r=1}^{R} \mathbf{A}^{(1)}_{.r} \circ \ldots \circ \mathbf{A}^{(N)}_{.r} \in \mathbb{C}^{I_1 \times \ldots \times I_N}, \tag{2.73}$$

where $\mathbf{A}_r^{(n)} \in \mathbb{C}^{I_n}$ is the $r^{th}$ column vector of $\mathbf{A}^{(n)} \in \mathbb{C}^{I_n \times R}$, for $r \in \{1, R\}$ and $n \in \{1, N\}$.

**Definition 15.** (Multilinear rank) *Considering an N-order tensor $\mathcal{Y}$, the columns vectors of the matricized form $\mathbf{Y}^{(n)} \in \mathbb{C}^{I_n \times I_{n+1} \ldots I_N I_1 \ldots I_{n-1}}$ are the mode-n vectors and $R_n = r\left(\mathbf{Y}^{(n)}\right) = r_n(\mathcal{Y}) \leq I_n$ is the mode-n rank of $\mathcal{Y}$. The N-tuplet $(R_1,...,R_N)$ is called multilinear rank of $\mathcal{Y}$ [50].*

**Definition 16.** (Identity tensor) *An N-order identity tensor, denoted by $\mathcal{I}_{N,R} \in \mathbb{R}^{R \times R \times \ldots \times R}$, is a diagonal tensor containing elements equal to 1 at positions where all indices are the same and equal to zero elsewhere.*

**Definition 17.** (mode-$n$ product) *Corresponds to the multiplication of a tensor by a matrix (or a vector) in mode-n. For the matrix case, the mode-n product of an N-order tensor $\mathcal{Y}$ with a matrix $\boldsymbol{U} \in \mathbb{C}^{J \times I_n}$ along the $n^{th}$ mode is denoted by $\mathcal{B} = \mathcal{Y} \times_n \boldsymbol{U}$ and it is of size $I_1 \times \ldots I_{n-1} \times J \times I_{n+1} \times \ldots \times I_N$. The element-wise is:*

$$b_{i_1,\ldots,i_{n-1},j,i_{n+1},\ldots,i_N} = \sum_{i_n=1}^{I_n} y_{i_1,\ldots,i_{n-1},i_n,i_{n+1},\ldots,i_N} u_{j,i_n}. \tag{2.74}$$

*Each mode-n fiber is multiplied by the matrix $\boldsymbol{U}$ [53]. This idea can also be expressed in terms of unfolded tensors as:*

$$\mathcal{B} = \mathcal{Y} \times_n \mathbf{U} \Leftrightarrow \mathbf{B}^{(n)} = \mathbf{U}\mathbf{Y}^{(n)}, \tag{2.75}$$

*with $\boldsymbol{Y}^{(n)} \in \mathbb{C}^{I_n \times I_{n+1} \ldots I_N I_1 \ldots I_{n-1}}$ and $\boldsymbol{B}^{(n)} \in \mathbb{C}^{J \times I_{n+1} \ldots I_N I_1 \ldots I_{n-1}}$. The mode-n product of a tensor with a matrix is related to a change of basis in the case where a tensor defines a multilinear operator. We have the following properties for the mode-n product:*

**Property 8.** *Consider a third-order tensor $\mathcal{X} \in \mathbb{C}^{I \times J \times K}$ and the matrices $\boldsymbol{A} \in \mathbb{C}^{M \times J}$ and $\boldsymbol{B} \in \mathbb{C}^{N \times K}$. For distinct modes in a series of multiplications, the order of the multiplication is irrelevant, i.e.:*

$$\left(\mathcal{X} \times_j \mathbf{A}\right) \times_k \mathbf{B} = \left(\mathcal{X} \times_k \mathbf{B}\right) \times_j \mathbf{A}, \quad j \neq k. \tag{2.76}$$

**Property 9.** *Consider $\boldsymbol{A} \in \mathbb{C}^{M \times J}$ and $\boldsymbol{C} \in \mathbb{C}^{P \times M}$. As the modes are the same, then:*

$$\mathcal{X} \times_j \mathbf{A} \times_j \mathbf{C} = \mathcal{X} \times_j (\mathbf{C}\mathbf{A}). \tag{2.77}$$

The order of multiplication is relevant.

**Definition 18.** (mode-$n$ product between tensors) *Let us consider $\mathbb{S}$ as an ordered subset of $\{i_{j_1}, ..., i_{j_M}\}$ of $\mathbb{J} = \{i_{N_1+1}, ..., i_N\}$, with $j_m \in \{N_1 + 1, N\}$, for $m \in \{1, M\}$. The mode-n product of $\mathcal{B} \in \mathbb{C}^{R_1 \times \ldots \times R_{N_1} \times I_{N_1+1} \times \ldots \times I_N}$ with $\mathcal{A} \in \mathbb{C}^{I_n \times R_n \times I_{\mathbb{S}}}$ is denoted by $\mathcal{B} \times_n \mathcal{A}$, where $n \in \{1, N_1\}$ and $I_{\mathbb{S}}$ is a shortened writing for $I_{j_1} \times \ldots \times I_{j_M}$. This product gives an N-order tensor $\mathcal{Y} \in \mathbb{C}^{R_1 \times \ldots \times R_{n-1} \times I_n \times R_{n+1} \times \ldots \times R_{N_1} \times I_{N_1+1} \times \ldots \times I_N}$, defined as [35]:*

$$y_{r_1,\ldots,r_{n-1},i_n,r_{n+1},\ldots,r_{N_1},\mathbb{J}} = \sum_{r_n=1}^{R_n} b_{r_1,\ldots,r_{n-1},r_n,r_{n+1},\ldots,r_{N_1},\mathbb{J}} a_{i_n,r_n,\mathbb{S}}. \tag{2.78}$$

The sum is over the second index of the tensor $\mathcal{A}$.

## 2.5 Theoretical background on tensor decompositions

This section presents some tensor decompositions that will be useful in the next chapters, namely, Tucker, HOSVD and PARAFAC. During the past decade, other decompositions were developed with applications in communication systems, such as CONFAC [54], PARATUCK [55], Tensor train [56], among others.

### 2.5.1 Tucker decomposition

Tucker decomposition was introduced in [57]. Tucker model decomposes a third-order tensor $\mathcal{X} \in \mathbb{C}^{I_1 \times I_2 \times I_3}$ into a core tensor multiplied by a matrix along each mode. Thus, for $\mathcal{X}$ we have:

$$x_{i_1,i_2,i_3} = \sum_{r_1=1}^{R_1} \sum_{r_2=1}^{R_2} \sum_{r_3=1}^{R_3} g_{r_1,r_2,r_3} a_{i_1,r_1} b_{i_2,r_2} c_{i_3,r_3}, \tag{2.79}$$

where $a_{i_1,r_1}$, $b_{i_2,r_2}$ and $c_{i_3,r_3}$ are the $(i_1,r_1)^{th}$, $(i_2,r_2)^{th}$ and $(i_3,r_3)^{th}$ elements of $\mathbf{A} \in \mathbb{C}^{I_1 \times R_1}$, $\mathbf{B} \in \mathbb{C}^{I_2 \times R_2}$ and $\mathbf{C} \in \mathbb{C}^{I_3 \times R_3}$, respectively, and $g_{r_1,r_2,r_3}$ is the $(r_1,r_2,r_3)^{th}$ element of $\mathcal{G} \in \mathbb{C}^{R_1 \times R_2 \times R_3}$. Tucker decomposition of $\mathcal{X}$ is illustrated in Figure 4.

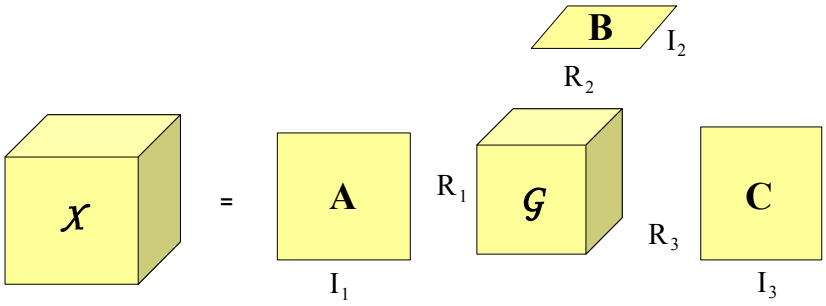


Figure 4 – Tucker decomposition of a third-order tensor $\mathcal{X} \in \mathbb{C}^{I_1 \times I_2 \times I_3}$.

This decomposition can be written in terms of mode-$n$ product as:

$$\mathcal{X} = \mathcal{G} \times_1 \mathbf{A} \times_2 \mathbf{B} \times_3 \mathbf{C} \in \mathbb{C}^{I_1 \times I_2 \times I_3}, \tag{2.80}$$

where $\mathbf{A}$, $\mathbf{B}$ and $\mathbf{C}$ are the factor matrices and can be considered the principal components in each mode. $\mathcal{G}$ is called the core tensor and its entries show the level of interaction between the different components. The mode-$n$ matrix unfoldings of $\mathcal{X}$ are:

$$\mathbf{X}_{I_2 I_3 \times I_1} = (\mathbf{B} \otimes \mathbf{C})\, \mathbf{G}_{R_2 R_3 \times R_1} \mathbf{A}^T, \tag{2.81}$$

$$\mathbf{X}_{I_3 I_1 \times I_2} = (\mathbf{C} \otimes \mathbf{A})\, \mathbf{G}_{R_3 R_1 \times R_2} \mathbf{B}^T, \tag{2.82}$$

$$\mathbf{X}_{I_1 I_2 \times I_3} = (\mathbf{A} \otimes \mathbf{B})\, \mathbf{G}_{R_1 R_2 \times R_3} \mathbf{C}^T, \tag{2.83}$$

where $\mathbf{G}_{R_2 R_3 \times R_1}$, $\mathbf{G}_{R_3 R_1 \times R_2}$ and $\mathbf{G}_{R_1 R_2 \times R_3}$ are the mode-1, mode-2 and mode-3 matrix unfoldings of $\mathcal{G}$, respectively.

*Uniqueness*

In general, the Tucker decomposition is not unique. The singularity can be obtained by imposing some constraints on the core tensor $\mathcal{G}$ or on the factor matrices $\mathbf{A}$, $\mathbf{B}$ and $\mathbf{C}$. To demonstrate the non-uniqueness of the Tucker model we have $\mathcal{X}$ decomposed as:

$$\mathcal{X} = \hat{\mathcal{G}} \times_1 \hat{\mathbf{A}} \times_2 \hat{\mathbf{B}} \times_3 \hat{\mathbf{C}}, \tag{2.84}$$

where $\hat{\mathcal{G}} \in \mathbb{C}^{R_1 \times R_2 \times R_3}$, $\hat{\mathbf{A}} \in \mathbb{C}^{I_1 \times R_1}$, $\hat{\mathbf{B}} \in \mathbb{C}^{I_2 \times R_2}$ and $\hat{\mathbf{C}} \in \mathbb{C}^{I_3 \times R_3}$. This decomposition is not unique because it has freedom of rotation. Defining:

$$\begin{cases} \hat{\mathcal{G}} = \mathcal{G} \times_1 \mathbf{T}^{(1)} \times_2 \mathbf{T}^{(2)} \times_3 \mathbf{T}^{(3)}, \\ \hat{\mathbf{A}} = \mathbf{A} \left(\mathbf{T}^{(1)}\right)^{-1}, \\ \hat{\mathbf{B}} = \mathbf{B} \left(\mathbf{T}^{(2)}\right)^{-1}, \\ \hat{\mathbf{C}} = \mathbf{C} \left(\mathbf{T}^{(3)}\right)^{-1}, \end{cases} \tag{2.85}$$

where $\mathbf{T}^{(n)} \in \mathbb{C}^{R_n \times R_n}$. Substituting Eq.(2.85) in Eq.(2.84) and applying the Property 9 we have:

$$\begin{aligned} \mathcal{X} &= \mathcal{G} \times_1 \mathbf{T}^{(1)} \times_2 \mathbf{T}^{(2)} \times_3 \mathbf{T}^{(3)} \times_1 \mathbf{A} \left(\mathbf{T}^{(1)}\right)^{-1} \times_2 \mathbf{B} (\mathbf{T}^{(2)})^{-1} \times_3 \mathbf{C} \left(\mathbf{T}^{(3)}\right)^{-1} \\ &= \mathcal{G} \times_1 \mathbf{A} \left(\mathbf{T}^{(1)}\right)^{-1} \mathbf{T}^{(1)} \times_2 \mathbf{B} \left(\mathbf{T}^{(2)}\right)^{-1} \mathbf{T}^{(2)} \times_3 \mathbf{C} \left(\mathbf{T}^{(3)}\right)^{-1} \mathbf{T}^{(3)} \\ &= \mathcal{G} \times_1 \mathbf{A} \times_2 \mathbf{B} \times_3 \mathbf{C}, \end{aligned} \tag{2.86}$$

where $\left(\mathbf{T}^{(n)}\right)^{-1} \mathbf{T}^{(n)} = \mathbf{I}_{R_n}$. From Eq.(2.86), note that Tucker decomposition is not unique since its factor matrices are affected by arbitrary linear transformations, while the inverse of these transformations affect the core tensor, leading to the same tensor $\mathcal{X}$.

#### 2.5.1.1 $N$-order Tucker decomposition

Let us consider a $N$-order tensor $\mathcal{Y} \in \mathbb{C}^{I_1 \times \ldots \times I_N}$. The Tucker decomposition is given by:

$$y_{i_1,\ldots,i_N} = \sum_{r_1=1}^{R_1} \ldots \sum_{r_N=1}^{R_N} g_{r_1,\ldots,r_N} \prod_{n=1}^{N} a^{(n)}_{i_n,r_n}, \tag{2.87}$$

where $a^{(n)}_{i_n,r_n}$ and $g_{r_1,\ldots,r_N}$ are the elements of $\mathbf{A}^{(n)} \in \mathbb{C}^{I_n \times R_n}$ and $\mathcal{G} \in \mathbb{C}^{I_1 \times I_2 \times \ldots \times I_N}$ for $n \in \{1, N\}$, respectively. The Tucker decomposition can be written as the mode-$n$ product such that:

$$\mathcal{Y} = \mathcal{G} \times_1 \mathbf{A}^{(1)} \times_2 \ldots \times_N \mathbf{A}^{(N)}. \tag{2.88}$$

The mode-$n$ matrix unfolding of $\mathcal{Y}$ is given by:

$$\mathbf{Y}_{I_{n+1}\ldots I_N I_1\ldots I_{n-1}\times I_n} = \left(\mathbf{A}^{(n+1)} \otimes \ldots \otimes \mathbf{A}^{(N)} \otimes \mathbf{A}^{(1)} \otimes \ldots \otimes \mathbf{A}^{(n-1)}\right) \mathbf{G}_{R_{n+1}\ldots R_N R_1\ldots R_{n-1}\times R_n} \mathbf{A}^{(n)T}, \quad (2.89)$$

where $\mathbf{G}_{R_{n+1}\ldots R_N R_1\ldots R_{n-1}\times R_n} \in \mathbb{C}^{R_{n+1}\ldots R_N R_1\ldots R_{n-1}\times R_n}$ is the corresponding mode-$n$ unfolding of $\mathcal{G}$.

### 2.5.1.2 Special Tucker decompositions

Consider an $N$-order tensor that has $N_1$ factor matrices, and $N-N_1$ matrices equal to identity matrices, where $N_1 < N$. Considering $\mathbf{A}^{(n)} = \mathbf{I}_{I_n}$ for $n \in \{N_1+1, N\}$, which implies $R_n = I_n$, the Tucker-($N_1$,$N$) model [53] corresponds to:

$$\mathcal{Y} = \mathcal{G} \times_1 \mathbf{A}^{(1)} \times_2 \ldots \times_{N_1} \mathbf{A}^{(N_1)} \times_{N_1+1} \mathbf{I}_{I_{N_1+1}} \times_{N_1+2} \ldots \times_N \mathbf{I}_{I_N}, \quad (2.90)$$

or simply:

$$\mathcal{Y} = \mathcal{G} \times_1 \mathbf{A}^{(1)} \times_2 \ldots \times_{N_1} \mathbf{A}^{(N_1)} = \mathcal{G} \times_{n=1}^{N_1} \mathbf{A}^{(n)}. \quad (2.91)$$

with $\mathcal{G} \in \mathbb{C}^{R_1\times\ldots\times R_{N_1}\times I_{N_1+1}\times\ldots\times I_N}$. Now, considering a third-order tensor $\mathcal{X} \in \mathbb{C}^{I_1\times I_2\times I_3}$, there are two important variations of the Tucker-($N_1$,$N$) decomposition. The Tucker-(2,3) decomposition or simply Tucker-2 has one of the factor matrices equal to the identity matrix, i.e.:

$$\mathcal{X} = \mathcal{G} \times_1 \mathbf{A} \times_2 \mathbf{B} \in \mathbb{C}^{I_1\times I_2\times I_3}. \quad (2.92)$$

This is the same as Eq.(2.80) except that $\mathcal{G} \in \mathbb{C}^{R_1\times R_2\times I_3}$, where $I_3 = R_3$ and $\mathbf{C} = \mathbf{I}_{I_3} \in \mathbb{R}^{I_3\times I_3}$. The Tucker-2 decomposition is illustrated in Figure 5.

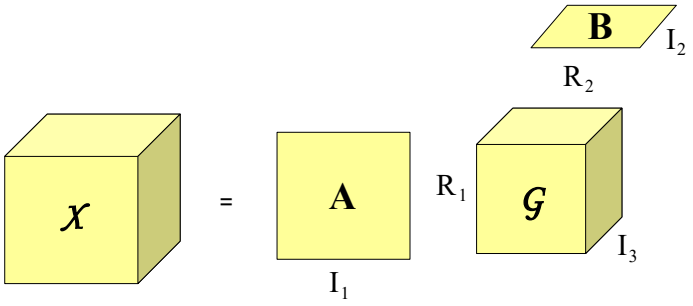


Figure 5 – Tucker-2 decomposition of a third-order tensor $\mathcal{X} \in \mathbb{C}^{I_1\times I_2\times I_3}$.

Likewise, the Tucker-(1,3) decomposition, or simply Tucker-1 has two of the factor matrices equal to the identity matrix. For example, if $\mathbf{B} = \mathbf{I}_{I_2} \in \mathbb{R}^{I_2\times I_2}$ and $\mathbf{C} = \mathbf{I}_{I_3} \in \mathbb{R}^{I_3\times I_3}$, then we have:

$$\mathcal{X} = \mathcal{G} \times_1 \mathbf{A} \in \mathbb{C}^{I_1\times I_2\times I_3}, \quad (2.93)$$

where $\mathcal{G} \in \mathbb{C}^{R_1\times I_2\times I_3}$. The Tucker-1 decomposition is illustrated in Figure 6.

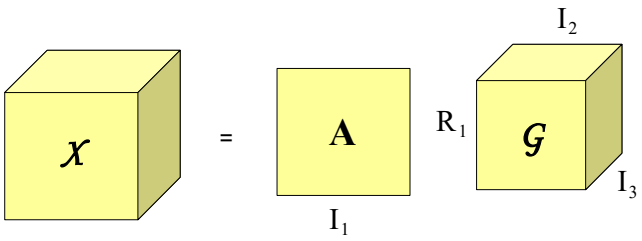


Figure 6 – Tucker-1 decomposition of a third-order tensor $\mathcal{X} \in \mathbb{C}^{I_1 \times I_2 \times I_3}$.

#### 2.5.1.3 Generalized Tucker decomposition

The generalized Tucker decomposition has been introduced for wireless communication systems in [35]. Let us consider an $N$-order tensor $\mathcal{Y} \in \mathbb{C}^{I_1 \times \ldots \times I_N}$ modeled by a generalized Tucker-$(N_1, N)$ decomposition, with $N_1 < N$ as:

$$y_{i_1,\ldots,i_N} = \sum_{r_1=1}^{R_1} \cdots \sum_{r_{N_1}=1}^{R_{N_1}} g_{r_1,\ldots,r_{N_1},i_{N_1+1},\ldots,i_N} \prod_{n=1}^{N_1} a^{(n)}_{i_n,r_n,\mathbb{S}_n}, \tag{2.94}$$

where $\mathbb{S}_n$ is an ordered subset of the set $\mathbb{J} \in \{i_{N_1+1}, \ldots, i_N\}$. In terms of mode-$n$ product the generalized Tucker-$(N_1, N)$ decomposition can be written as:

$$\mathcal{Y} = \mathcal{G} \times_{n=1}^{N_1} \mathcal{A}^{(n)} \in \mathbb{C}^{I_1 \times \ldots \times I_N}, \tag{2.95}$$

where $\mathcal{G} \in \mathbb{C}^{R_1 \times \ldots \times R_{N_1} \times I_{N_1+1} \times \ldots \times I_N}$ is the core tensor and $\mathcal{A}^{(n)} \in \mathbb{C}^{I_n \times R_n \times \mathbb{S}_n}$ are the tensor factors, for $n \in \{1, N_1\}$. For example, let us consider two factors, where the first factor is a third-order tensor $\mathcal{A}^{(1)} \in \mathbb{C}^{I_1 \times R_1 \times I_3}$ and the second factor is a matrix $\mathbf{A}^{(2)} \in \mathbb{C}^{I_2 \times R_2}$. The generalized Tucker-(2,4) decomposition is given by:

$$y_{i_1,i_2,i_3,i_4} = \sum_{r_1=1}^{R_1} \sum_{r_2=1}^{R_2} g_{r_1,r_2,i_3,i_4} a^{(1)}_{i_1,r_1,i_3} a^{(2)}_{i_2,r_2}, \tag{2.96}$$

where $\mathcal{G} \in \mathbb{C}^{R_1 \times R_2 \times I_3 \times I_4}$. In terms of mode-$n$ product, Eq.(2.96) can be written as:

$$\mathcal{Y} = \mathcal{G} \times_1 \mathcal{A}^{(1)} \times_2 \mathbf{A}^{(2)} \in \mathbb{C}^{I_1 \times I_2 \times I_3 \times I_4}. \tag{2.97}$$

### 2.5.2 Higher-order singular value decomposition (HOSVD)

HOSVD, introduced by [50], is a generalization of the matrix SVD for $N$-order tensors. HOSVD is a way to compute the basis for each factor matrix of the Tucker decomposition.

Every $N$-order tensor $\mathcal{Y} \in \mathbb{C}^{I_1 \times \ldots \times I_N}$ can be written as the mode-$n$ product:

$$\mathcal{Y} = \mathcal{S} \times_1 \mathbf{U}^{(1)} \times_2 \ldots \times_N \mathbf{U}^{(N)} \in \mathbb{C}^{I_1 \times \ldots \times I_N}, \tag{2.98}$$

where $\mathcal{S} \in \mathbb{C}^{R_1 \times \ldots \times R_N}$ is the core tensor and $\mathbf{U}^{(n)} \in \mathbb{C}^{I_n \times R_n}$ are the left singular vector matrices, with $n \in \{1, N\}$. The set $(R_1, \ldots, R_N)$ denotes the multilinear rank of $\mathcal{Y}$. The matrix $\mathbf{U}^{(n)}$ is computed as the $R_n$ left singular vectors of the $n^{th}$ matrix unfolding of $\mathcal{Y}$, i.e.:

$$\mathbf{Y}_{I_n \times I_{n+1} \ldots I_N I_1 \ldots I_{n-1}} = \mathbf{U}^{(n)} \mathbf{\Sigma}^{(n)} \mathbf{V}^{(n)H}. \tag{2.99}$$

From $\mathbf{U}^{(n)}$ computed according to Eq.(2.99), the core tensor can be obtained as:

$$\mathcal{S} = \mathcal{Y} \times_1 \mathbf{U}^{(1)H} \times_2 \mathbf{U}^{(2)H} \times_3 \ldots \times_N \mathbf{U}^{(N)H}. \tag{2.100}$$

For a Tucker decomposition, HOSVD algorithm computes a basis for each factor matrix via the SVD for each mode-$n$ unfolding of the tensor. For the explanation, let us consider the third-order tensor $\mathcal{X} \in \mathbb{C}^{I_1 \times I_2 \times I_3}$ modeled by Tucker decomposition as Eq.(2.80). Computing the SVD we have:

$$\mathbf{X}_{I_1 \times I_2 I_3} = \mathbf{U}^{(1)} \mathbf{\Sigma}^{(1)} \mathbf{V}^{(1)H}, \tag{2.101}$$

$$\mathbf{X}_{I_2 \times I_3 I_1} = \mathbf{U}^{(2)} \mathbf{\Sigma}^{(2)} \mathbf{V}^{(2)H}, \tag{2.102}$$

$$\mathbf{X}_{I_3 \times I_1 I_2} = \mathbf{U}^{(3)} \mathbf{\Sigma}^{(3)} \mathbf{V}^{(3)H}. \tag{2.103}$$

Since $\mathbf{U}^{(n)}$ is an unitary matrix of size $I_n \times R_n$, with $n \in \{1, 2, 3\}$, that spans the subspace of **A**, **B** and **C**. The HOSVD procedure is described in the pseudo-code form in Table 3. In this thesis, HOSVD decomposition is applied to formulate efficient denoising strategies in the following chapters.

### 2.5.3 Parallel factor analysis (PARAFAC) decomposition

PARAFAC decomposition was introduced in 1970 [58]. This decomposition can also be called CPD (canonical polyadic decomposition). It expresses a tensor as the sum of a finite number of rank-one tensors. The PARAFAC decomposition of a given third-order tensor $\mathcal{X} \in \mathbb{C}^{I_1 \times I_2 \times I_3}$ can be represented as:

$$x_{i_1, i_2, i_3} = \sum_{r=1}^{R} a_{i_1, r} b_{i_2, r} c_{i_3, r}, \tag{2.111}$$

where $a_{i_1,r}$, $b_{i_2,r}$ and $c_{i_3,r}$ are scalar elements of $\mathbf{A} \in \mathbb{C}^{I_1 \times R}$, $\mathbf{B} \in \mathbb{C}^{I_2 \times R}$ and $\mathbf{C} \in \mathbb{C}^{I_3 \times R}$, respectively. PARAFAC decomposition is expressed by a sum of triads as follows:

$$\mathcal{X} = \sum_{r=1}^{R} \mathbf{A}_{.r} \circ \mathbf{B}_{.r} \circ \mathbf{C}_{.r} \in \mathbb{C}^{I_1 \times I_2 \times I_3}, \tag{2.112}$$

Table 3 – HOSVD algorithm.

**HOSVD algorithm for estimation of $\hat{\mathbf{A}}$, $\hat{\mathbf{B}}$, $\hat{\mathbf{C}}$ and $\hat{\mathcal{G}}$**

**Input:** tensor $\mathcal{X}$ and $R_n$, with $n \in \{1, 2, 3\}$

**Output:** Estimated matrices $\hat{\mathbf{A}}$, $\hat{\mathbf{B}}$, $\hat{\mathbf{C}}$ and $\hat{\mathcal{G}}$

1) Compute the SVD for each mode-$n$ unfolding of $\mathcal{X}$:

$$\mathbf{X}_{I_1 \times I_2 I_3} = \mathbf{U}^{(1)} \mathbf{\Sigma}^{(1)} \mathbf{V}^{(1)H}, \tag{2.104}$$

$$\mathbf{X}_{I_2 \times I_3 I_1} = \mathbf{U}^{(2)} \mathbf{\Sigma}^{(2)} \mathbf{V}^{(2)H}, \tag{2.105}$$

$$\mathbf{X}_{I_3 \times I_1 I_2} = \mathbf{U}^{(3)} \mathbf{\Sigma}^{(3)} \mathbf{V}^{(3)H}. \tag{2.106}$$

2) Compute $\hat{\mathbf{A}}$, $\hat{\mathbf{B}}$ and $\hat{\mathbf{C}}$ using the matrices $\mathbf{U}^{(n)}$:

$$\hat{\mathbf{A}} = \mathbf{U}^{(1)}, \tag{2.107}$$

$$\hat{\mathbf{B}} = \mathbf{U}^{(2)}, \tag{2.108}$$

$$\hat{\mathbf{C}} = \mathbf{U}^{(3)}. \tag{2.109}$$

3) Compute the core tensor $\hat{\mathcal{G}}$:

$$\hat{\mathcal{G}} = \mathcal{X} \times_1 \hat{\mathbf{A}}^H \times_2 \hat{\mathbf{B}}^H \times_3 \hat{\mathbf{C}}^H. \tag{2.110}$$

where $\mathbf{A}_{.r} \in \mathbb{C}^{I_1}$, $\mathbf{B}_{.r} \in \mathbb{C}^{I_2}$ and $\mathbf{C}_{.r} \in \mathbb{C}^{I_3}$ are the columns vectors of $\mathbf{A}$, $\mathbf{B}$ and $\mathbf{C}$, respectively. $R$ is the number of factors, also known as the *rank* of the decomposition. Figure 7 illustrates the PARAFAC decomposition of the third-order tensor in Eq.(2.112). PARAFAC decomposition can also be represented in terms of the mode-$n$ product as:

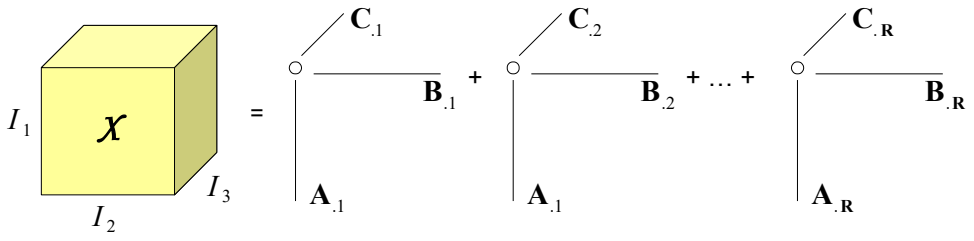


Figure 7 – PARAFAC decomposition of third-order tensor $\mathcal{X} \in \mathbb{C}^{I_1 \times I_2 \times I_3}$ into $R$ components.

$$\mathcal{X} = \mathcal{I}_{3,R} \times_1 \mathbf{A} \times_2 \mathbf{B} \times_3 \mathbf{C} \in \mathbb{C}^{I_1 \times I_2 \times I_3}, \tag{2.113}$$

where $\mathcal{I}_{3,R}$ represents the third-order identity tensor of size $R \times R \times R$. The matrix unfoldings

of the third-order PARAFAC decomposition are given by:

$$\mathbf{X}_{I_3 I_2 \times I_1} = (\mathbf{C} \diamond \mathbf{B})\, \mathbf{A}^T, \tag{2.114}$$

$$\mathbf{X}_{I_1 I_3 \times I_2} = (\mathbf{A} \diamond \mathbf{C})\, \mathbf{B}^T, \tag{2.115}$$

$$\mathbf{X}_{I_2 I_1 \times I_3} = (\mathbf{B} \diamond \mathbf{A})\, \mathbf{C}^T. \tag{2.116}$$

#### 2.5.3.1 $N$-order PARAFAC decomposition

Let us consider an $N$-order tensor $\mathcal{Y} \in \mathbb{C}^{I_1 \times \ldots \times I_N}$ that satisfies the PARAFAC decomposition. This tensor can be expressed as:

$$y_{i_1,\ldots,i_N} = \sum_{r=1}^{R} \prod_{n=1}^{N} a_{i_n,r}^{(n)}, \tag{2.117}$$

where $a_{i_n,r}^{(n)}$ are the elements of $\mathbf{A}^{(n)} \in \mathbb{C}^{I_n \times R}$, for $n \in \{1, N\}$. Note that $R$ represents the rank of $\mathcal{Y}$. The PARAFAC model can be represented by the following outer product:

$$\mathcal{Y} = \sum_{r=1}^{R} \mathbf{A}_{.r}^{(1)} \circ \ldots \circ \mathbf{A}_{.r}^{(N)}, \tag{2.118}$$

where $\mathbf{A}_{.r}^{(n)} \in \mathbb{C}^{I_n}$ is the $r^{th}$ column vector of $\mathbf{A}^{(n)}$. PARAFAC decomposition can also be interpreted as a special case of the Tucker decomposition with an identity core tensor, as introduced in Definition 16. For PARAFAC decomposition, we have the following formulation in terms of the mode-$n$ product:

$$\mathcal{Y} = \mathcal{I}_{N,R} \times_1 \mathbf{A}^{(1)} \times_2 \ldots \times_N \mathbf{A}^{(N)}. \tag{2.119}$$

By using Definition 9, we have the following generic formulation for a flat mode-$n$ matrix unfolding of the PARAFAC decomposition:

$$\mathbf{Y}_{I_{n+1}\ldots I_N I_1 \ldots I_{n-1} \times I_n} = \left(\mathbf{A}^{(n+1)} \diamond \ldots \diamond \mathbf{A}^{(N)} \diamond \mathbf{A}^{(1)} \diamond \ldots \diamond \mathbf{A}^{(n-1)}\right) \mathbf{A}^{(n)T}. \tag{2.120}$$

Note the similarity between the Eqs.(2.89) and (2.120). The Kronecker product in the matrix unfolding of the Tucker model is replaced by the Khatri-Rao product in the matrix unfolding of the PARAFAC model since the matrices have the same number of columns, while the core tensor is replaced by the identity tensor.

*Uniqueness*

The uniqueness of the PARAFAC model was discussed in several works such as [59, 60, 61, 62], among others, but the most well-known result is attributed to Kruskal [59]. Kruskal derived conditions for essential uniqueness of third-order PARAFAC models and

Sidiropoulos *et al.* [63, 64] extended the results for an $N$-order tensor. PARAFAC decomposition is essentially unique, i.e., factor matrices can be estimated up to scaling and permutation ambiguities. This uniqueness property is true if the following sufficient condition is satisfied:

$$\sum_{n=1}^{N} k_{\mathbf{A}^{(n)}} \geq 2R + (N-1), \tag{2.121}$$

where $k_{\mathbf{A}^{(n)}}$ is the $k$-rank of $\mathbf{A}^{(n)}$. The condition (2.121) is sufficient but not necessary to guarantee essential uniqueness [46]. The following theorem is valid for any arbitrary tensor that satisfies a PARAFAC decomposition.

**Theorem 1.** *Consider the $N$-order tensor $\mathcal{Y} \in \mathbb{C}^{I_1 \times \ldots \times I_N}$ that satisfies a PARAFAC decomposition. If the sufficient condition (2.121) is satisfied, the factor matrices $\boldsymbol{A}^{(n)} \in \mathbb{C}^{I_n \times R}$, for $n \in \{1, N\}$, are unique up to permutation and scaling ambiguities, such that $\hat{\boldsymbol{A}}^{(n)} = \boldsymbol{A}^{(n)}\boldsymbol{\Pi}\boldsymbol{\Lambda}^{(n)}$, where $\boldsymbol{\Pi} \in \mathbb{C}^{R \times R}$ is the permutation matrix and $\boldsymbol{\Lambda}^{(n)} \in \mathbb{C}^{R \times R}$ are diagonal scaling matrices, with $\prod_{n=1}^{N} \boldsymbol{\Lambda}^{(n)} = \boldsymbol{I}_R$.*

#### 2.5.3.2 Normalized form of the PARAFAC decomposition

PARAFAC decomposition can also be defined in normalized form as [46]:

$$y_{i_1,\ldots,i_N} = \sum_{r=1}^{R} g_r \prod_{n=1}^{N} b_{i_n,r}^{(n)}, \tag{2.122}$$

with $g_r > 0$ and the column vectors $\mathbf{B}_{.r}^{(n)}$ are obtained by normalizing the columns $\mathbf{A}_{.r}^{(n)}$ as:

$$\mathbf{B}_{.r}^{(n)} = \frac{1}{\| \mathbf{A}_{.r}^{(n)} \|_F} \mathbf{A}_{.r}^{(n)}, \tag{2.123}$$

$$g_r = \prod_{n=1}^{N} \| \mathbf{A}_{.r}^{(n)} \|_F, \tag{2.124}$$

with $r \in \{1, R\}$ and $n \in \{1, N\}$. In this case, the identity tensor $\mathcal{I}_{N,R}$ in (2.119) is replaced by the diagonal tensor $\mathcal{G} \in \mathbb{C}^{R \times \ldots \times R}$ whose diagonal elements are equal to the scaling factors $g_r$:

$$\begin{cases} g_r & \text{if} \quad r_1 = \ldots = r_N = r, \quad r \in \{1, R\} \\ 0 & \text{otherwise} \end{cases}. \tag{2.125}$$

PARAFAC decomposition in normalized form can be seen as a Tucker model ($\mathcal{G}, \mathbf{B}^{(1)}$, ...,$\mathbf{B}^{(N)}$), where $\mathbf{g} = [g_1, ..., g_R]^T$ is the vector whose components are the weights $g_r$. The matrix unfolding then becomes:

$$\mathbf{Y}_{\mathbb{S}_1 \times \mathbb{S}_2} = \left( \diamond_{n \in \mathbb{S}_1} \mathbf{B}^{(n)} \right) \text{diag}(\mathbf{g}) \left( \diamond_{n \in \mathbb{S}_2} \mathbf{B}^{(n)} \right)^T, \tag{2.126}$$

where diag($\mathbf{g}$) is a diagonal matrix whose diagonal elements are the coefficients $g_r$.

The normalized form of the PARAFAC decomposition is unique up to scaling ambiguities $\lambda_r^{(n)}$ for each column of the factor matrices $\mathbf{B}^{(n)}$, satisfying $\prod_{n=1}^{N} \lambda_r^{(n)} = 1$, for every $r \in \{1, R\}$. To eliminate the permutation ambiguities of the columns, we can arrange them in such a way that they are associated with the factors $g_r$ in decreasing order ($g_1 \geq g_2 \geq ... \geq g_R$).

### 2.5.4 Estimation methods of the PARAFAC decomposition

Several PARAFAC fitting algorithms have been proposed in the literature. They can be classified into two categories: alternating algorithms and non-iterative algorithms. In the first category, a subset of parameters is updated at each step whereas, in the second category, the parameters are estimated in a closed-form way. The first category belongs to the alternating least squares (ALS) algorithm, the gradient descent method and Levenberg-Marquardt (LM) also called damped Gauss-Newton algorithm. The second category belongs to KRF, KronF and THOSVD algorithms. In this section, some iterative methods are presented to estimate the factor matrices in the PARAFAC model. These algorithms are ALS, gradient descent and Levenberg-Marquardt.

#### 2.5.4.1 Alternating least squares (ALS) method

The estimation of the three matrices of the PARAFAC decomposition is generally carried out by minimizing the following cost function deduced from Eq.(2.113):

$$\min_{\mathbf{A},\mathbf{B},\mathbf{C}} \| \mathcal{X} - \mathcal{I}_{3,R} \times_1 \mathbf{A} \times_2 \mathbf{B} \times_3 \mathbf{C} \|_F^2 . \tag{2.127}$$

The principles of ALS were introduced in 1933 by [65] and it is based on the idea of reducing the optimization problem to smaller sub-problems that are solved iteratively. ALS method replaces the optimization problem (2.127) with three LS sub-problems deduced from the matrix unfoldings (2.114)-(2.116), leading to the alternate minimization of the following LS criteria:

$$\min_{\mathbf{A}} \| \mathbf{X}_{I_3 I_2 \times I_1} - \left(\hat{\mathbf{C}}_{[i-1]} \diamond \hat{\mathbf{B}}_{[i-1]}\right) \mathbf{A}^T \|_F^2 \longrightarrow \hat{\mathbf{A}}_{[i]}, \tag{2.128}$$

$$\min_{\mathbf{B}} \| \mathbf{X}_{I_1 I_3 \times I_2} - \left(\hat{\mathbf{A}}_{[i]} \diamond \hat{\mathbf{C}}_{[i-1]}\right) \mathbf{B}^T \|_F^2 \longleftrightarrow \hat{\mathbf{B}}_{[i]}, \tag{2.129}$$

$$\min_{\mathbf{C}} \| \mathbf{X}_{I_2 I_1 \times I_3} - \left(\hat{\mathbf{B}}_{[i]} \diamond \hat{\mathbf{A}}_{[i]}\right) \mathbf{C}^T \|_F^2 \longleftrightarrow \hat{\mathbf{C}}_{[i]}. \tag{2.130}$$

The update equations at iteration $[i]$ are given by:

$$\hat{\mathbf{A}}_{[i]} = \left[ \left(\hat{\mathbf{C}}_{[i-1]} \diamond \hat{\mathbf{B}}_{[i-1]}\right)^{\dagger} \mathbf{X}_{I_3 I_2 \times I_1} \right]^T , \tag{2.131}$$

$$\hat{\mathbf{B}}_{[i]} = \left[ \left(\hat{\mathbf{A}}_{[i]} \diamond \hat{\mathbf{C}}_{[i-1]}\right)^{\dagger} \mathbf{X}_{I_1 I_3 \times I_2} \right]^T , \tag{2.132}$$

$$\hat{\mathbf{C}}_{[i]} = \left[ \left( \hat{\mathbf{B}}_{[i]} \diamond \hat{\mathbf{A}}_{[i]} \right)^{\dagger} \mathbf{X}_{I_3 \times I_2 I_1} \right]^T , \tag{2.133}$$

where $\left(\hat{\mathbf{C}} \diamond \hat{\mathbf{B}}\right)^{\dagger}$, $\left(\hat{\mathbf{A}} \diamond \hat{\mathbf{C}}\right)^{\dagger}$ and $\left(\hat{\mathbf{B}} \diamond \hat{\mathbf{A}}\right)^{\dagger}$ denote the pseudo-inverse of $\left(\hat{\mathbf{C}} \diamond \hat{\mathbf{B}}\right)$, $\left(\hat{\mathbf{A}} \diamond \hat{\mathbf{C}}\right)$ and $\left(\hat{\mathbf{B}} \diamond \hat{\mathbf{A}}\right)$, respectively. These matrices must have full column rank to ensure uniqueness of the LS estimates, which implies the following necessary condition: $R \leq \min\left(I_3 I_2, I_1 I_3, I_2 I_1\right)$. Taking into account property 3, the computation of the pseudo-inverse in ALS algorithm can be simplified as follows:

$$\begin{aligned} \left(\hat{\mathbf{C}}_{[i-1]} \diamond \hat{\mathbf{B}}_{[i-1]}\right)^{\dagger} &= \left[ \left(\hat{\mathbf{C}}_{[i-1]} \diamond \hat{\mathbf{B}}_{[i-1]}\right)^H \left(\hat{\mathbf{C}}_{[i-1]} \diamond \hat{\mathbf{B}}_{[i-1]}\right) \right]^{-1} \left(\hat{\mathbf{C}}_{[i-1]} \diamond \hat{\mathbf{B}}_{[i-1]}\right)^H \\ &= \left( \hat{\mathbf{C}}_{[i-1]}^H \hat{\mathbf{C}}_{[i-1]} \odot \hat{\mathbf{B}}_{[i-1]}^H \hat{\mathbf{B}}_{[i-1]} \right)^{-1} \left(\hat{\mathbf{C}}_{[i-1]} \diamond \hat{\mathbf{B}}_{[i-1]}\right)^H , \end{aligned} \tag{2.134}$$

$$\begin{aligned} \left(\hat{\mathbf{A}}_{[i]} \diamond \hat{\mathbf{C}}_{[i-1]}\right)^{\dagger} &= \left[ \left(\hat{\mathbf{A}}_{[i]} \diamond \hat{\mathbf{C}}_{[i-1]}\right)^H \left(\hat{\mathbf{A}}_{[i]} \diamond \hat{\mathbf{C}}_{[i-1]}\right) \right]^{-1} \left(\hat{\mathbf{A}}_{[i]} \diamond \hat{\mathbf{C}}_{[i-1]}\right)^H \\ &= \left( \hat{\mathbf{A}}_{[i]}^H \hat{\mathbf{A}}_{[i]} \odot \hat{\mathbf{C}}_{[i-1]}^H \hat{\mathbf{C}}_{[i-1]} \right)^{-1} \left(\hat{\mathbf{A}}_{[i]} \diamond \hat{\mathbf{C}}_{[i-1]}\right)^H , \end{aligned} \tag{2.135}$$

$$\begin{aligned} \left(\hat{\mathbf{B}}_{[i]} \diamond \hat{\mathbf{A}}_{[i]}\right)^{\dagger} &= \left[ \left(\hat{\mathbf{B}}_{[i]} \diamond \hat{\mathbf{A}}_{[i]}\right)^H \left(\hat{\mathbf{B}}_{[i]} \diamond \hat{\mathbf{A}}_{[i]}\right) \right]^{-1} \left(\hat{\mathbf{B}}_{[i]} \diamond \hat{\mathbf{A}}_{[i]}\right)^H \\ &= \left( \hat{\mathbf{B}}_{[i]}^H \hat{\mathbf{B}}_{[i]} \odot \hat{\mathbf{A}}_{[i]}^H \hat{\mathbf{A}}_{[i]} \right)^{-1} \left(\hat{\mathbf{B}}_{[i]} \diamond \hat{\mathbf{A}}_{[i]}\right)^H . \end{aligned} \tag{2.136}$$

This is equivalent to replacing the computation of pseudo-inverses of the matrices of size $I_3 I_2 \times R$, $I_1 I_3 \times R$, and $I_2 I_1 \times R$ calculating the inverses of the three matrices of size $R \times R$. For deciding the convergence of the ALS algorithm, we consider the error at the $[i]^{th}$ iteration deduced from (2.116) as:

$$error_{[i]} = \| \mathbf{X}_{I_1 I_2 \times I_3} - \left(\hat{\mathbf{B}}_{[i]} \diamond \hat{\mathbf{A}}_{[i]}\right) \hat{\mathbf{C}}_{[i]}^T \|_F^2 . \tag{2.137}$$

Convergence at the $[i]^{th}$ iteration is declared when this error does not significantly change between two successive iterations, i.e., $|error_{[i-1]} - error_{[i]}| \leq \delta$, where $\delta$ is a predefined threshold (e.g. $\delta = 10^{-6}$).

This algorithm has several advantages: it is easy to implement, ensures convergence and is simple to extend to higher-order matrices. The shortcomings are mainly in the occasional slowness of the convergence process in the presence of swamps [66] or high collinearity [67]. In addition, the loss function decreases almost linearly with iterations, while other methods can provide, at least in principle, superlinear or even quadratic convergence rate [68]. The ALS algorithm for the estimation of factor matrices is summarized in Table 4.

#### 2.5.4.2 Gradient descent algorithm

Let us consider the third-order tensor $\mathcal{X} \in \mathbb{C}^{I_1 \times I_2 \times I_3}$ modeled by the PARAFAC decomposition in Eq.(2.113) and the minimization problem as [69]:

$$\mathrm{Y} = \min_{\mathbf{A},\mathbf{B},\mathbf{C}} \| \mathcal{X} - \mathcal{I}_{3,R} \times_1 \mathbf{A} \times_2 \mathbf{B} \times_3 \mathbf{C} \|_F^2 . \tag{2.138}$$

Table 4 – ALS algorithm.

| **ALS algorithm for estimation of $\hat{\mathbf{A}}$, $\hat{\mathbf{B}}$ and $\hat{\mathbf{C}}$** |
|---|
| **Input:** tensor $\hat{\hat{\mathcal{X}}}$ |
| **Output:** Estimated matrices $\hat{\mathbf{A}}$, $\hat{\mathbf{B}}$ and $\hat{\mathbf{C}}$ |
| 1) Random initialization of $\mathbf{B}_{[0]}$, $\mathbf{C}_{[0]}$. |
| 2) Update the estimates of $\hat{\mathbf{A}}$, $\hat{\mathbf{B}}$ and $\hat{\mathbf{C}}$ using Eqs.(2.131)-(2.133) or Eqs.(2.134)-(2.136). |
| 3) Calculate the error (2.137) and $\lvert error_{[i-1]} - error_{[i]} \rvert$. |
| - **if** $\lvert error_{[i-1]} - error_{[i]} \rvert < \delta$ or $i =$ maximum number of iterations |
| - **stop** |
| - **else** $i \rightarrow i+1$; |
| $\hat{\mathbf{A}}$, $\hat{\mathbf{B}}$ and $\hat{\mathbf{C}}$ |
| **end** |

The goal of the Gradient descent algorithm is to minimize the Frobenius norm of the partial derivative of each unfolding of $\mathcal{X}$ with respect to matrix factors, which may be written as:

$$\mathrm{Y}\left(\mathbf{p}_{[i]}\right) = \| \mathbf{X}_{I_2 I_3 \times I_1} - \left(\mathbf{B}_{[i]} \diamond \mathbf{C}_{[i]}\right) \mathbf{A}_{[i]}^{T} \|_F^2 . \tag{2.139}$$

For the gradient descent the iteration is given by [69]:

$$\mathbf{p}_{[i]} = \mathbf{p}_{[i-1]} - \mu_{[i-1]} \mathbf{g}_{[i-1]}, \tag{2.140}$$

where $\mathbf{p}_{[i]}$ corresponds to the concatenation of vec $\left(\mathbf{A}_{[i]}\right)$, vec $\left(\mathbf{B}_{[i]}\right)$ and vec $\left(\mathbf{C}_{[i]}\right)$, $\mathbf{g}_{[i]}$ is the concatenation of the gradient of $\mathbf{X}_{I_2 I_3 \times I_1}$, $\mathbf{X}_{I_3 I_1 \times I_2}$ and $\mathbf{X}_{I_1 I_2 \times I_3}$ with respect to vec$(\mathbf{A}) \in \mathbb{C}^{RI_1}$, vec$(\mathbf{B}) \in \mathbb{C}^{RI_2}$ and vec$(\mathbf{C}) \in \mathbb{C}^{RI_3}$, respectively, and $\mu_{[i-1]}$ is a step size of the previous iteration that is varied as convergence progress. Even with a good strategy of variation of $\mu_{[i-1]}$, this algorithm has often very poor convergence properties. $\mathbf{p}_{[i]}$ and $\mathbf{g}_{[i]}$ are given by:

$$\mathbf{p}_{[i]} = \begin{bmatrix} \text{vec}\left(\mathbf{A}_{[i]}\right) \\ \text{vec}\left(\mathbf{B}_{[i]}\right) \\ \text{vec}\left(\mathbf{C}_{[i]}\right) \end{bmatrix} \quad \text{and} \quad \mathbf{g}_{[i]} = \begin{bmatrix} \mathbf{g}_{\mathbf{A}[i]} \\ \mathbf{g}_{\mathbf{B}[i]} \\ \mathbf{g}_{\mathbf{C}[i]} \end{bmatrix} . \tag{2.141}$$

And $\mathbf{g}_{\mathbf{A}[i]}$, $\mathbf{g}_{\mathbf{B}[i]}$ and $\mathbf{g}_{\mathbf{C}[i]}$ are given by [69]:

$$\mathbf{g}_{\mathbf{A}[i]} = \frac{\partial \left(\mathbf{X}_{I_2 I_3 \times I_1}\right)}{\partial \left(\text{vec}(\mathbf{A}[i])\right)}, \tag{2.142}$$

$$\mathbf{g}_{\mathbf{B}[i]} = \frac{\partial \left(\mathbf{X}_{I_3 I_1 \times I_2}\right)}{\partial \left(\text{vec}(\mathbf{B}[i])\right)}, \tag{2.143}$$

$$\mathbf{g}_{\mathbf{C}[i]} = \frac{\partial \left(\mathbf{X}_{I_1 I_2 \times I_3}\right)}{\partial \left(\text{vec}(\mathbf{C}[i])\right)}, \tag{2.144}$$

Such that:

$$\mathbf{g}_{\mathbf{A}[i]} = \left[\mathbf{I}_{\mathbf{A}} \otimes \left(\mathbf{C}_{[i-1]}^{T}\mathbf{C}_{[i-1]} \odot \mathbf{B}_{[i-1]}^{T}\mathbf{B}_{[i-1]}\right)\right] \text{vec}\left(\mathbf{A}^{T}\right) - \left[\mathbf{I}_{\mathbf{A}} \otimes \left(\mathbf{C}_{[i-1]} \diamond \mathbf{B}_{[i-1]}\right)\right]^{T} \text{vec}\left(\mathbf{X}_{I_2 I_3 \times I_1}\right), \tag{2.145}$$

$$\mathbf{g}_{\mathbf{B}[i]} = \left[\mathbf{I}_{\mathbf{B}} \otimes \left(\mathbf{A}_{[i]}^{T}\mathbf{A}_{[i]} \odot \mathbf{C}_{[i-1]}^{T}\mathbf{C}_{[i-1]}\right)\right] \text{vec}\left(\mathbf{B}^{T}\right) - \left[\mathbf{I}_{\mathbf{B}} \otimes \left(\mathbf{A}_{[i]} \diamond \mathbf{C}_{[i-1]}\right)\right]^{T} \text{vec}\left(\mathbf{X}_{I_3 I_1 \times I_2}\right), \tag{2.146}$$

$$\mathbf{g}_{\mathbf{C}[i]} = \left[\mathbf{I}_{\mathbf{C}} \otimes \left(\mathbf{B}_{[i]}^{T}\mathbf{B}_{[i]} \odot \mathbf{A}_{[i]}^{T}\mathbf{A}_{[i]}\right)\right] \text{vec}\left(\mathbf{C}^{T}\right) - \left[\mathbf{I}_{\mathbf{C}} \otimes \left(\mathbf{B}_{[i-1]} \diamond \mathbf{A}_{[i-1]}\right)\right]^{T} \text{vec}\left(\mathbf{X}_{I_1 I_2 \times I_3}\right), \tag{2.147}$$

The Gradient descent algorithm is summarized in Table 5.

Table 5 – Gradient descent algorithm.

**Gradient descent algorithm for estimation of $\hat{\mathbf{A}}$, $\hat{\mathbf{B}}$ and $\hat{\mathbf{C}}$**

**Input:** tensor $\hat{\hat{\mathcal{X}}}$
**Output:** Estimated matrices $\hat{\mathbf{A}}$, $\hat{\mathbf{B}}$ and $\hat{\mathbf{C}}$
1) Random initialization of $\mathbf{B}_{[0]}$, $\mathbf{C}_{[0]}$.
2) Update the estimates of $\hat{\mathbf{A}}$, $\hat{\mathbf{B}}$ and $\hat{\mathbf{C}}$ using Eqs.(2.131)-(2.133) or Eqs.(2.134)-(2.136).
3) Compute $\mathbf{p}_{[i]}$ as Eqs.(2.141) and (2.140).
4) Compute $\mathbf{g}_{[i]}$ as Eqs.(2.141)-(2.147).

- **if** $\Upsilon\left(\mathbf{p}_{[i]}\right) < \delta$
- **stop**
- **else** $i \rightarrow i + 1$;
4) Compute $\hat{\mathbf{A}}$, $\hat{\mathbf{B}}$ and $\hat{\mathbf{C}}$ from $\mathbf{p}_{[i]}$.
**end**

#### 2.5.4.3 Levenberg-Marquart algorithm

Damped Gauss-Newton algorithms, also known as Levenberg-Marquart algorithms, take into account the second derivative. This allows faster local convergence. An approximation using only first-order derivatives is given by the iteration below [70]:

$$\mathbf{p}_{[i]} = \mathbf{p}_{[i-1]} - \left[\mathbf{H}_{[i-1]} + \lambda_{[i-1]}^{2}\mathbf{I}\right]^{-1} \mathbf{g}_{[i-1]}, \tag{2.148}$$

where $\mathbf{H}_{[i-1]} = \mathbf{J}_{[i-1]}^{T}\mathbf{J}_{[i-1]}$ denotes the approximate Hessian, $\mathbf{J}_{[i-1]}$ is the Jacobian matrix $[\mathbf{J}_{\mathbf{A}}, \mathbf{J}_{\mathbf{B}}, \mathbf{J}_{\mathbf{C}}]$ at iteration $[i-1]$ with respect to vec($\mathbf{A}$), vec($\mathbf{B}$) and vec($\mathbf{C}$), respectively, and $\lambda_{[i-1]}^{2}$ is a positive regularization parameter. The compact forms of Jacobian matrices of each iteration are defined as:

$$\mathbf{J}_{\mathbf{A}[i]} = \mathbf{I}_{\mathbf{A}} \otimes \left(\mathbf{C}_{[i-1]} \diamond \mathbf{B}_{[i-1]}\right), \tag{2.149}$$

$$\mathbf{J}_{\mathbf{B}[i]} = \mathbf{\Pi}_1 \left[\mathbf{I}_{\mathbf{B}} \otimes \left(\mathbf{A}_{[i]} \diamond \mathbf{C}_{[i-1]}\right)\right], \tag{2.150}$$

$$\mathbf{J}_{\mathbf{C}[i]} = \mathbf{\Pi}_2 \left[\mathbf{I}_{\mathbf{C}} \otimes \left(\mathbf{B}_{[i]} \diamond \mathbf{A}_{[i]}\right)\right], \tag{2.151}$$

where $\mathbf{\Pi}_1$ and $\mathbf{\Pi}_2$ are permutation matrices that put the entries in the right order. There are several ways to calculate $\lambda^2_{[i-1]}$, and this has an important influence on convergence. Updates of $\mathbf{p}$ and $\lambda^2$ are controlled by the gain ratio $\gamma$ as:

$$\gamma = \mathrm{Y}_{[i-1]} - \mathrm{Y}_{[i]} \cdot \left(\hat{\mathrm{Y}}\left(\mathbf{0}\right) - \hat{\mathrm{Y}}\left(\Delta\mathbf{p}_{[i-1]}\right)\right)^{-1}, \tag{2.152}$$

where $\hat{\mathrm{Y}}\left(\Delta\mathbf{p}_{[i-1]}\right)$ is a second order approximation of $\mathrm{Y}\left(\mathbf{p}_{[i-1]} + \Delta\mathbf{p}_{[i-1]}\right)$. The Levenberg-Marquardt algorithm is summarized in Table 6.

Table 6 – Levenberg-Marquardt algorithm.

**Levenberg-Marquardt algorithm for estimation of $\hat{\mathbf{A}}$, $\hat{\mathbf{B}}$ and $\hat{\mathbf{C}}$**

**Input:** tensor $\hat{\hat{\mathcal{X}}}$
**Output:** Estimated matrices $\hat{\mathbf{A}}$, $\hat{\mathbf{B}}$ and $\hat{\mathbf{C}}$
1) Random initialization of $\mathbf{B}_{[0]}$, $\mathbf{C}_{[0]}$
2) Update the estimates $\hat{\mathbf{A}}$, $\hat{\mathbf{B}}$ and $\hat{\mathbf{C}}$ using Eqs.(2.131)-(2.133) or Eqs.(2.134)-(2.136).
3) Update the gradient using Eq.(2.141).
4) Update Jacobians using Eqs. (2.149)-(2.151).
3) Find the new direction as:

$$\Delta\mathbf{p}_{[i]} = -\left[\mathbf{J}^T_{[i]}\mathbf{J}_{[i]} + \lambda^2_{[i]}\mathbf{I}\right]^{-1}\mathbf{g}_{[i]}, \tag{2.153}$$

4) Compute $\mathbf{p}_{[i]}$ as Eq.(2.148).
5) Compute $\mathrm{Y}\left(\Delta\mathbf{p}_{[i]}\right)$ as Eq.(2.139).
6) Compute $\gamma$ as:

$$\gamma = \mathrm{Y}_{[i-1]} - \mathrm{Y}_{[i]} \cdot \left(\hat{\mathrm{Y}}\left(\mathbf{0}\right) - \hat{\mathrm{Y}}\left(\Delta\mathbf{p}_{[i-1]}\right)\right)^{-1}, \tag{2.154}$$

- **if** $\gamma \geq 0$, then $\mathbf{p}_{[i]}$ is accepted with:

$$\lambda^2_{[i]} = \lambda^2_{[i-1]} * \max\left(\frac{1}{3}, 1 - (2\gamma - 1)^3\right) \quad \text{and} \quad \nu = 2. \tag{2.155}$$

- **stop**
- **otherwise**, $\mathbf{p}_{[i]}$ is rejected, then

$$\lambda^2_{[i]} = \nu\lambda^2_{[i-1]} \quad \text{and} \quad \nu \leftarrow 2\nu. \tag{2.156}$$

7) Compute $\hat{\mathbf{A}}$, $\hat{\mathbf{B}}$ and $\hat{\mathbf{C}}$ from $\mathbf{p}_{[i]}$.
**end**

## 2.6 Chapter summary

This chapter has provided some fundamentals of multilinear algebra, tensor decompositions and algorithmic backgrounds in multilinear algebra. All content presented in this chapter provides the basic material that will be exploited throughout this thesis. In the first part of this chapter, some notations were introduced. In the second and third parts, we introduced some operations involving matrices, namely Kronecker and Khatri-Rao products, SVD, KronF and KRF algorithms and their generalizations GKronF and GKRF methods, respectively. In the fourth and fifth parts, we focused on presenting basic tensor operations, tensor decompositions and some algorithms to estimate factor matrices in tensor decompositions. These decompositions have been formulated in scalar, outer product and mode-$n$ product forms. In each case, the factorization of the tensor in matrix unfolding form has been defined and the uniqueness conditions have been presented. Most algorithms presented in this chapter are dedicated to estimate the factor matrices of PARAFAC decomposition as ALS, gradient descent, LM, among others. Tensor decompositions are very important in the contexts of application of this thesis, where they will be widely used in MIMO communication systems.

# 3 Semi-blind receivers for point-to-point MIMO System with MKRST Coding

*In this chapter, the first original contributions of this work are presented. First, a bibliographic review of existing tensor-based MIMO systems is presented in terms of coding. Then a particular case of the multiple Khatri-Rao space-time (MKRST) coding is considered, where the pre-coding matrix corresponds to a symbol matrix that is assumed known. MKRST coding provides extra diversity due to multiple Khatri-Rao products of symbol matrices. Based on this coding, a new point-to-point MIMO system is introduced. This system is modeled by the PARAFAC decomposition, in which the MKRST coding is applied to the source to code the signals to be transmitted.*

*By exploiting the tensor model of the received signals, five semi-blind receivers are derived to jointly estimate the channel and symbol matrices. The proposed receivers are semi-blind since we have no channel knowledge and one symbol matrix should be known, which contains pilot symbols. Monte Carlo simulation results illustrate the impact of design parameters on the system performance and the behavior of the proposed receivers in terms of symbol error rate (SER) and normalized mean square error (NMSE).*

## 3.1 Bibliographic review of tensor-based MIMO systems and codings

With the advance of the 5G wireless communication system, the development of 6G mobile network has attracted a great deal of attention in massive MIMO systems. 6G is expected to advance the current wireless technologies, providing considerably enhanced system performance. In terms of speed, 6G will likely use a higher frequency spectrum that should be about 100 to 1000 times faster than 5G to improve the data rate [11, 71]. More specifically, 6G networks will allow a hundred gigabits per second to terabit-per-second links by making use of multi-band high-spread spectrum [11, 72]. Massive MIMO is a core technology of 5G and will probably be the system that requests the most attention in the development of 6G. For massive MIMO, a very large number of antennas is used when spatially multiplexing several users, reducing the multi-user interference (MUI), or to compensate for the path loss when higher frequencies than microwaves are used, such as the millimeter-waves [10]. Massive MIMO systems provide performance gains in terms of

reliability and security over the existing MIMO communication systems [73, 74]. However, realizing many of these advantages in practice hinges on accurate estimation of the CSI, which affects the performance of beamforming and decoding accuracy at the receivers [75]. For that, it is necessary to propose received signal models and receivers that allow estimating the channel and its parameters with better precision.

During the last years, several tensor decompositions have been widely proposed for MIMO wireless communication systems due to their capacity to exploit multiple diversities. The main goal of diversity techniques is to exploit several copies of the information symbols to be recovered at the receiver. This enables the mitigation of fading in wireless links and hence, an increase of the reception reliability, which leads to a reduction of error rate [14, 76]. A way to impose diversity on the system is to apply coding techniques combined with tensor decompositions to transmit the information symbols. Tensor-based MIMO systems combined with matrix or tensor codings allow for improving link reliability as well as jointly estimating the channel and the transmitted symbols by means of semi-supervised or supervised receivers. They have the advantage of not requiring a priori channel knowledge, but only a few pilot symbols are needed to eliminate scaling ambiguities inherent to each particular tensor model. Moreover, tensor codings lead to natural tensor formulations of transmitted and received signals, and consequently to tensor system models [14].

For improving the error performance in parameter estimation, a key idea is to jointly exploit the system diversities. The diversity here corresponds to a set of techniques that aims to enhance the quality of received signals in communication systems, providing a wireless link improvement at a relatively low cost [77, 78]. When the diversity in MIMO systems is exploited, it means that redundancies in the signal are created by exploiting the random nature of the radio propagation in such a way that different and independent versions of the same signal reach the destination. There are many ways to obtain diversity [12, 30, 31]. For example, spatial diversity can be found in wireless MIMO systems and consists of transmitting independent data streams in parallel on multiple-transmit antennas and can be used for increasing the transmission rate. The benefit from spatial diversity comes from the redundancies in the transmitted signal, leading the receive antennas to possibly obtain uncorrelated faded versions of the same signal increasing the probability of effective reception of the transmitted information. Time diversity can be obtained by transmitting the same symbols or data streams over multiple blocks, each symbol period corresponding to a single channel use. The time spreading also can be obtained via coding where the information is coded and dispersed in the time domain in different periods so that different parts of the codewords experience roughly uncorrelated fading [63, 79, 80]. The frequency diversity can be provided by the channels as is the case with frequency-selective and time-selective channels, leading to frequency or multipath diversity and Doppler diversity, respectively.

Since the pioneering work [63], tensor models combined with coding schemes have

been extensively used to model wireless communication systems, such as the point-to-point MIMO communication systems [35, 55, 63, 81] and cooperative MIMO systems [17, 23, 33]. Tensor-based wireless communication systems can be classified according to the type of system (code-division multiple access (CDMA), direct sequence CDMA (DS-CDMA), OFDM, CDMA-OFDM, time division duplex (TDD), among others); type of coding (space-time (ST), space-time-frequency (STF), multiple Kronecker product (KronST, MKronST), multiple Khatri-rao product (KRST, MKRST), matrices/tensors); and type of tensor model: PARAFAC [63], PARATUCK-(2,4) [55], PARATUCK-2 [82], generalized PARATUCK [35], nested PARAFAC [16]. According to [55], also there are different ways of classifying coding schemes as the type of MIMO channel (flat fading/frequency selective/ time-varying MIMO channels); the amount of CSI knowledge at the transmitter; and design criteria to be optimized (i.e. tradeoffs to be achieved).

The use of these codings with tensor approaches for the design of MIMO wireless communication systems, mainly in cooperative MIMO systems, has led to the development of new supervised and semi-supervised receivers. Table 7 presents some coding schemes that are combined with tensor approaches to model received signals.

Table 7 – Presentation of different codings.

| **Codings** | **Transmission rate** | **Dimension of the received signal** | **received signal tensor** |
|---|---|---|---|
| KRST [20] | $R/P$ | $PN \times R$ | nested-PARAFAC |
| ST [82] | $R/P$ | $M \times N \times P$ | Paratuck-2 |
| STF [83] | $R/FP$ | $F \times M \times N \times P$ | generalized PARATUCK-2 |
| TST [55] | $R/P$ | $M \times N \times P \times J$ | PARATUCK-(2,4) |
| TSTF [35] | $R/PF$ | $M \times N \times F \times P \times J$ | generalized PARATUCK-(2,5) |
| STM [84] | $R/P$ | $M \times P \times N$ | block-PARAFAC |
| MKRST [33] | $\left(R\sum_{l=1}^{L} N_l\right) / \left(P\prod_{l=1}^{L} N_l\right)$ | $PN \times R$ | PARAFAC |
| MKronST [33] | $\left(\sum_{l=1}^{L} N_l R_l\right) / \left(P\prod_{l=1}^{L} N_l\right)$ | $PN \times R$ | PARAFAC |
| particular case of MKRST [81] | $\left(R\sum_{l=2}^{L} N_l\right) / \left(N_1\prod_{l=2}^{L} N_l\right)$ | $N \times R$ | PARAFAC |

Regarding Table 7, it is important to note that all these coded signals consider one symbol matrix associated with a coding tensor/matrix or an allocation tensor/matrix to transmit the symbols except for [33] and its particular case [81], that considers more than one symbol matrix to be transmitted. The combination of coding matrices/tensors or allocation matrices/tensors improves the space diversity because creates redundancy of each

transmitted symbol, improving the estimation at the receiver. The received signal model of the system depends on the coding used to encode the symbols. Depending on the system, it is necessary to know one symbol or even more to eliminate scaling ambiguities.

## 3.2 Proposed system model

Let us consider the point-to-point MIMO wireless communication system presented in Figure 8, where $\mathbf{H} \in \mathbb{C}^{K \times R}$ is the channel matrix with $K$ receive antennas and $R$ transmit antennas and $\mathbf{S} \in \mathbb{C}^{N \times R}$ consists in a multiple Khatri-Rao product of $L$ symbol matrices, where each symbol matrix being formed of $R$ data streams composed of $N_l$ symbols each, to be multiplexed by $R$ transmit antennas. The symbols are encoded at the transmitter. Sections 3.2.1 and 3.2.2 describe the coding used and the model of the received signals, respectively.

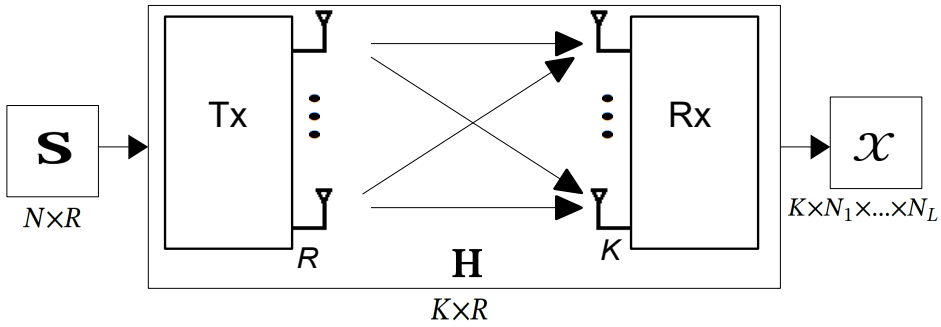


Figure 8 – Block diagram of the point-to-point MIMO systems.

### 3.2.1 MKRST coding

This section presents the coding used at the transmitter, which is called multiple Khatri-Rao space-time (MKRST) coding [33]. In this case, we consider a particular case of MKRST coding, where the pre-coding matrix corresponds to a symbol matrix that is assumed to be known. This coding provides extra diversity due to multiple Khatri-Rao products of the symbol matrices, by jointly adding time and space spreadings [81]. It consists in a multiple Khatri-Rao product of $L$ symbol matrices $\mathbf{S}^{(l)} \in \mathbb{C}^{N_l \times R}$, $l \in \{1, L\}$, each one being formed of $R$ data streams composed of $N_l$ symbols each:

$$\mathbf{S} = \diamond_{l=1}^{L} \mathbf{S}^{(l)} \triangleq \mathbf{S}^{(1)} \diamond \ldots \diamond \mathbf{S}^{(L)} \in \mathbb{C}^{N \times R}, \tag{3.1}$$

where $N = \prod_{l=1}^{L} N_l$. The scalar writing of (3.1) is as follow:

$$s_{n,r} = \prod_{l=1}^{L} s_{n_l,r}^{(l)}, \quad n \in \{1,N\}, \quad r \in \{1,R\}, \tag{3.2}$$

with $n = n_L^{(L)} + \left(n_{L-1}^{(L-1)} - 1\right) N_L + \cdots + \left(n_1^{(1)} - 1\right) \prod_{l=2}^{L} N_l$, where $n_l^{(l)} \in \{1, N_l\}$ denotes the index $n_l$ in $s_{n_l,r}^{(l)}$. This writing (3.2) highlights the way to compute each element of the multiple Khatri-Rao product matrix $\mathbf{S}$.

### 3.2.2 Point-to-point MIMO system

In the noise-free case, the received signals are obtained by transmitting the coded signal matrix (3.1) through the wireless channel $\mathbf{H} \in \mathbb{C}^{K \times R}$, which gives a standard system model as:

$$\mathbf{X} = \mathbf{H}\mathbf{S}^T \in \mathbb{C}^{K \times N}, \tag{3.3}$$

where $\mathbf{H}$ is the channel matrix drawn from a Gaussian distribution and $\mathbf{S}$ is the symbol matrix. The symbol matrix $\mathbf{S}$ is coded at the transmitter by the MKRST coding (3.1) which provides extra diversity due to the multiple Khatri-Rao product of the symbol matrices. The received signal in (3.3), can be written in a scalar form as:

$$x_{k,n} = \sum_{r=1}^{R} h_{k,r} s_{n,r}, \tag{3.4}$$

with $k \in \{1, K\}$, $r \in \{1, R\}$ and $n \in \{1, N\}$, such that $n = n_L^{(L)} + \left(n_{L-1}^{(L-1)} - 1\right) N_L + \cdots + \left(n_1^{(1)} - 1\right) \prod_{l=2}^{L} N_l$. Substituting (3.1) in (3.3), leads to the received signals written in terms of mode-1 unfolding:

$$\mathbf{X}_{K \times N_1 \ldots N_L} = \mathbf{H}(\mathbf{S}^{(1)} \diamond \ldots \diamond \mathbf{S}^{(L)})^T, \tag{3.5}$$

where $N = N_1 \ldots N_L$. The received signals form a tensor that satisfies a $(L+1)$-order PARAFAC model with rank $R$ given by:

$$\mathcal{X} = \mathcal{I}_{L+1,R} \times_1 \mathbf{H} \times_2 \mathbf{S}^{(1)} \times_3 \ldots \times_{L+1} \mathbf{S}^{(L)}, \tag{3.6}$$

where $\mathbf{S}^{(l)}$ for $l \in \{1, L\}$ are the symbol matrices coded by the MKRST coding and $\mathcal{X} \in \mathbb{C}^{K \times N_1 \times \ldots \times N_L}$. From (3.3)-(3.6), we can conclude that the tensor of received signals satisfies an $(L+1)$-order PARAFAC model, as illustrated by means of the blocks diagram in Figure 9. Note that the first block represents the transmitted symbols coded by the particular case of the MKRST coding, the second block is the channel matrix, the third block presents the received signal tensor and the fourth block corresponds to the estimated symbols and channel by using the proposed receivers presented in next sections.

Let us consider $\mathbf{S}^{(1)}$ known and $\mathbf{S}^{(c)} = \diamond_{l=2}^{L} \mathbf{S}^{(l)} \in \mathbb{C}^{N_c \times R}$ being the symbol matrices that we must estimate, with $N_c = \prod_{l=2}^{L} N_l$. Combining modes 3 to $L+1$ of $\mathcal{X}$ results in contracted form $\mathcal{X}_c \in \mathbb{C}^{K \times N_1 \times N_c}$ and the expression (3.6) can be rewritten as:

$$\mathcal{X}_c = \mathcal{I}_{3,R} \times_1 \mathbf{H} \times_2 \mathbf{S}^{(1)} \times_3 \mathbf{S}^{(c)}. \tag{3.7}$$

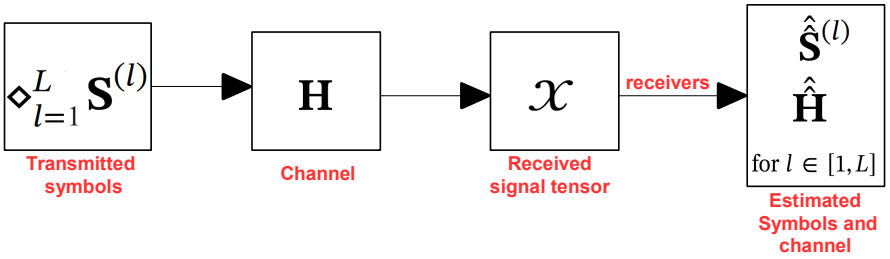


Figure 9 – Block diagram of the system represented by a $(L+1)$-order PARAFAC model.

Based on the contracted third-order PARAFAC model (3.7), it is easy to deduce the following matrix unfoldings of the tensor $\mathcal{X}$:

$$\mathbf{X}_{K\times N_1 N_c} = \mathbf{H}\left(\mathbf{S}^{(1)} \diamond \mathbf{S}^{(c)}\right)^T \in \mathbb{C}^{K\times N_1 N_c}, \tag{3.8}$$

$$\mathbf{X}_{N_1\times N_c K} = \mathbf{S}^{(1)}\left(\mathbf{S}^{(c)} \diamond \mathbf{H}\right)^T \in \mathbb{C}^{N_1\times N_c K}, \tag{3.9}$$

$$\mathbf{X}_{N_c\times K N_1} = \mathbf{S}^{(c)}\left(\mathbf{H} \diamond \mathbf{S}^{(1)}\right)^T \in \mathbb{C}^{N_c\times K N_1}. \tag{3.10}$$

For MKRST coding, five semi-blind receivers are presented for channel and symbol matrices estimation. The receivers are considered semi-blind since the symbol matrix $\mathbf{S}^{(1)}$ is assumed to be known at the receiver.

## 3.3 Semi-blind receivers

In this section, we exploit the tensor model of the point-to-point MIMO system presented in Subsection 3.2.2 to develop five semi-blind receivers to jointly estimate the symbol matrices and the channel. The first three receivers are closed-form solutions based on LS estimation of the Khatri-Rao products (KRF) and THOSVD methods. The last two receivers are iterative algorithms based on the ALS method. The estimation of the unknown parameters in a unique way is related to the uniqueness properties of the involved tensor methods. The PARAFAC model is unique up to scaling ambiguities when one of the matrices is known (see Theorem 1, Subsection 2.5.5). Here, we assume that the pilot symbol matrix $\mathbf{S}^{(1)}$ is known. Following, for the purpose of simplicity, the equations are derived from the noiseless case.

### 3.3.1 Receivers based on Khatri-Rao product

In this section, three semi-blind receivers are presented to estimate the channel and symbol matrices. From the 3-mode matrix unfolding (3.9) we deduce the LS estimation of the Khatri-Rao product as:

$$\left[\left(\mathbf{S}^{(1)}\right)^{\dagger}\mathbf{X}_{N_1\times N_c K}\right]^T = \mathbf{S}^{(c)} \diamond \mathbf{H} \in \mathbb{C}^{N_c K\times R}, \tag{3.11}$$

where $\left(\mathbf{S}^{(1)}\right)^{\dagger}$ is the pseudo-inverse of $\mathbf{S}^{(1)}$. Considering two symbol matrices being transmitted such that $\mathbf{S}^{(c)} = \mathbf{S}^{(2)} \diamond \mathbf{S}^{(3)} \in \mathbb{C}^{N_2 N_3 \times R}$, we have:

$$\mathbf{Z} = \mathbf{S}^{(2)} \diamond \mathbf{S}^{(3)} \diamond \mathbf{H} \in \mathbb{C}^{N_2 N_3 K \times R} = \left[\left(\mathbf{S}^{(1)}\right)^{\dagger} \mathbf{X}_{N_1 \times N_2 N_3 K}\right]^{T}. \tag{3.12}$$

where $N_c = N_2 N_3$. From Eq.(3.12) we can formulate four receivers based on the Khatri-Rao product. KRF, KRF-KRF, THOSVD and Rank-one ALS receivers are described in the next section.

*Identifiability condition and ambiguities relations*

For computing the pseudo-inverse in Eq.(3.11), one condition is required to ensure the uniqueness. $\mathbf{S}^{(1)}$ must be left-invertible, i.e., it must be full column rank,

$$R \leq N_1. \tag{3.13}$$

For KRF, KRF-KRF, THOSVD and rank-one ALS receivers presented in this section, the unknown parameters are affected by the following ambiguities:

$$\begin{cases} \hat{\mathbf{S}}^{(2)} = \mathbf{S}^{(2)}\mathbf{\Lambda}^{(2)}, \\ \hat{\mathbf{S}}^{(3)} = \mathbf{S}^{(3)}\mathbf{\Lambda}^{(3)}, \quad \mathbf{\Lambda}^{(2)}\mathbf{\Lambda}^{(3)}\mathbf{\Lambda}^{(H)} = \mathbf{I}_R, \\ \hat{\mathbf{H}} = \mathbf{H}\mathbf{\Lambda}^{(H)}. \end{cases} \tag{3.14}$$

The scaling ambiguities of $\hat{\mathbf{S}}^{(2)}$ and $\hat{\mathbf{S}}^{(3)}$ can be removed by assuming the prior knowledge of one row of $\mathbf{S}^{(2)}$ and $\mathbf{S}^{(3)}$, respectively, where the first row is formed by 1's. The elements of $\mathbf{\Lambda}^{(l)}$, with $l \in \{2, 3\}$ are:

$$\lambda_r^{(l)} = \hat{s}_{1r}^{(l)}, \tag{3.15}$$

where $\hat{s}_{1r}^{(l)}$ are the elements of the first row of $\hat{\mathbf{S}}^{(l)}$, for $r \in \{1, R\}$. The scaling matrix $\mathbf{\Lambda}^{(l)}$ corresponds to a matrix with the elements $\lambda_r^{(l)}$ on the main diagonal. Thus, to eliminate the scaling ambiguities on the estimated parameters, we use the following equations:

$$\hat{\hat{\mathbf{S}}}^{(l)} \rightarrow \hat{\mathbf{S}}^{(l)}\left(\mathbf{\Lambda}^{(l)}\right)^{-1}, \quad \hat{\hat{\mathbf{H}}} \rightarrow \hat{\mathbf{H}}\left(\mathbf{\Lambda}^{(2)}\mathbf{\Lambda}^{(3)}\right). \tag{3.16}$$

#### 3.3.1.1 KRF receivers

Based on the KRF algorithm (Table 2), we present two semi-blind receivers. The first one is based on the GKRF algorithm summarized in Subsection 2.3.3.1, and the second one is based on the KRF algorithm in two steps.

*KRF receiver*

The receiver proposed in this section uses the GKRF algorithm described in Subsection 2.3.3.1 to estimate the channel and symbol matrices in Eq.(3.12) as,

$$\mathbf{Z} = \mathbf{S}^{(2)} \diamond \mathbf{S}^{(3)} \diamond \mathbf{H} \in \mathbb{C}^{N_2 N_3 K \times R} = \left[ \left( \mathbf{S}^{(1)} \right)^{\dagger} \mathbf{X}_{N_1 \times N_2 N_3 K} \right]^{T}. \tag{3.17}$$

To estimate $\mathbf{S}^{(2)}$ and $\mathbf{H}$ we consider respectively:

$$\mathbf{Z} = \mathbf{S}^{(2)} \diamond \mathbf{B}^{(1)}, \tag{3.18}$$

$$\mathbf{Z} = \mathbf{B}^{(2)} \diamond \mathbf{H}, \tag{3.19}$$

Note that $\mathbf{B}^{(1)} = \mathbf{S}^{(3)} \diamond \mathbf{H}$ and $\mathbf{B}^{(2)} = \mathbf{S}^{(2)} \diamond \mathbf{S}^{(3)}$. To estimate $\mathbf{S}^{(2)}$ and $\mathbf{H}$ in (3.18) and (3.19), respectively, we apply the KRF algorithm described in Table 2. For estimating $\mathbf{S}^{(3)}$, we permute the rows of (3.12) as:

$$\mathbf{Z}_{\mathbf{S}^{(3)}} = \left( \mathbf{\Pi}_{N_3, N_2} \otimes \mathbf{I}_K \right) \mathbf{Z} = \mathbf{S}^{(3)} \diamond \mathbf{S}^{(2)} \diamond \mathbf{H}, \tag{3.20}$$

$$\mathbf{Z}_{\mathbf{S}^{(3)}} = \mathbf{S}^{(3)} \diamond \mathbf{B}^{(3)}, \tag{3.21}$$

where $\mathbf{B}^{(3)} = \mathbf{S}^{(2)} \diamond \mathbf{H}$ and $\mathbf{\Pi}_{N_3, N_2}$ is defined in expression (2.32). From (3.21) we apply again the KRF algorithm that allows us to estimate $\mathbf{S}^{(3)}$. The final estimated symbols are obtained after a projection onto the finite alphabet. The KRF receiver is summarized in Table 8.

Table 8 – KRF algorithm for estimating the channel and the symbol matrices.

| **KRF algorithm for estimating $\hat{\mathbf{S}}^{(2)}$, $\hat{\mathbf{S}}^{(3)}$ and $\hat{\mathbf{H}}$.** |
|---|
| **Input:** matrix $\mathcal{X}$, $\mathbf{S}^{(1)}$ and $R$. |
| **Output:** Estimated matrices $\hat{\mathbf{S}}^{(2)}$, $\hat{\mathbf{S}}^{(3)}$ and $\hat{\mathbf{H}}$. |
| 1) Calculate the LS estimate $\mathbf{Z}$ defined in (3.12). |
| 2) Estimate $\hat{\mathbf{S}}^{(2)}$ from (3.18) by means of the KRF algorithm in Table 2, where $\mathbf{S}^{(2)}$ corresponds to $\mathbf{D}$. |
| 3) Estimate $\hat{\mathbf{H}}$ from (3.19) by means of the KRF algorithm in Table 2, where $\mathbf{H}$ corresponds to $\mathbf{E}$. |
| 4) Permute the rows of (3.12) as (3.20). |
| 5) Estimate $\hat{\mathbf{S}}^{(3)}$ from (3.21) by means of the KRF algorithm in Table 2, where $\mathbf{S}^{(3)}$ corresponds to $\mathbf{D}$. |
| 6) Eliminate the scaling ambiguities using (3.15)-(3.16). |
| 7) Project the estimated symbols onto the finite alphabet. |

*KRF-KRF receiver*

The receiver proposed in this section uses the KRF algorithm summarized in Table 2 in two steps to estimate the channel and symbol matrices in Eq.(3.11). To estimate $\mathbf{S}^{(c)}$ and $\mathbf{H}$ consider:

$$\mathbf{Z} = \mathbf{S}^{(c)} \diamond \mathbf{H}. \tag{3.22}$$

First we apply KRF algorithm (Table 2) to estimate $\mathbf{S}^{(c)}$ and $\mathbf{H}$. After, in the second step we apply again the KRF algorithm to separate the symbol matrices $\mathbf{S}^{(2)}$ and $\mathbf{S}^{(3)}$, such that:

$$\mathbf{S}^{(c)} = \mathbf{S}^{(2)} \diamond \mathbf{S}^{(3)}. \tag{3.23}$$

Note that the KRF-KRF receiver has an error propagation that can affect the estimation of $\hat{\mathbf{S}}^{(2)}$, $\hat{\mathbf{S}}^{(3)}$. The KRF-KRF receiver is summarized in Table 9.

Table 9 – KRF-KRF algorithm for estimation of the channel and symbol matrices.

| **KRF-KRF algorithm for estimating $\hat{\mathbf{S}}^{(2)}$, $\hat{\mathbf{S}}^{(3)}$ and $\hat{\mathbf{H}}$.** |
|---|
| **Input:** matrix $\mathcal{X}$, $\mathbf{S}^{(1)}$ and $R$. |
| **Output:** Estimated matrices $\hat{\mathbf{S}}^{(2)}$, $\hat{\mathbf{S}}^{(3)}$ and $\hat{\mathbf{H}}$. |
| **Step 1) KRF algorithm** |
| 1) Calculate the LS estimate $\mathbf{Z}$ defined in (3.12). |
| 2) Estimate $\hat{\mathbf{S}}^{(c)}$ and $\hat{\mathbf{H}}$ by means of the KRF algorithm in Table 2. |
| **Step 2) KRF algorithm** |
| 3) From $\hat{\mathbf{S}}^{(c)}$, estimate $\hat{\mathbf{S}}^{(2)}$ and $\hat{\mathbf{S}}^{(3)}$ by means of the KRF algorithm in Table 2. |
| 4) Eliminate the scaling ambiguities using (3.15)-(3.16). |
| 5) Project the estimated symbols onto the finite alphabet. |

#### 3.3.1.2 THOSVD receiver

In this section the truncated HOSVD (THOSVD) algorithm is presented to directly and jointly estimate the channel and symbol matrices, using a closed-form solution based on the THOSVD algorithm. Let us consider Eq.(3.12) and Definition 2, $\mathbf{Z}$ can be defined as a Kronecker product in columns such as:

$$\mathbf{Z} = \left[ \begin{array}{ccc} \mathbf{S}^{(2)}_{.1} \otimes \mathbf{S}^{(3)}_{.1} \otimes \mathbf{H}_{.1} & \ldots & \mathbf{S}^{(2)}_{.R} \otimes \mathbf{S}^{(3)}_{.R} \otimes \mathbf{H}_{.R} \end{array} \right] \in \mathbb{C}^{N_2 N_3 K \times R}, \tag{3.24}$$

where $\mathbf{S}^{(2)}_{.r} \in \mathbb{C}^{N_2}$, $\mathbf{S}^{(3)}_{.r} \in \mathbb{C}^{N_3}$, $\mathbf{H}_{.r} \in \mathbb{C}^{K}$ represent the column vectors of the matrices $\mathbf{S}^{(2)}$, $\mathbf{S}^{(3)}$, $\mathbf{H}$, respectively, with $r \in \{1,R\}$. From Eq.(3.24) we define each column $r$ as a rank-one tensor such that:

$$\mathcal{Z}_r = \mathbf{S}^{(2)}_{.r} \circ \mathbf{S}^{(3)}_{.r} \circ \mathbf{H}_{.r} \in \mathbb{C}^{N_2 \times N_3 \times K}. \tag{3.25}$$

The factor matrices can be estimated by calculating the rank-one approximation for each column ($r = 1, ..., R$) through the THOSVD algorithm. It consists of taking the HOSVD on the Eq.(3.25), which corresponds to calculate the SVD of its matrix unfolding for each $r$ as:

$$[\mathbf{Z}_r]_{N_2 \times N_3 K} = \mathbf{U}^{(1)}_r \mathbf{\Sigma}^{(1)}_r \mathbf{V}^{(1)T}_r = \hat{\mathbf{S}}^{(2)}_{.r} \left( \mathbf{S}^{(3)}_{.r} \otimes \mathbf{H}_{.r} \right)^T, \tag{3.26}$$

$$[\mathbf{Z}_r]_{N_3\times KN_3} = \mathbf{U}_r^{(2)}\mathbf{\Sigma}_r^{(2)}\mathbf{V}_r^{(2)T} = \hat{\mathbf{S}}_{.r}^{(3)}\left(\mathbf{H}_{.r}\otimes\mathbf{S}_{.r}^{(2)}\right)^T, \tag{3.27}$$

$$[\mathbf{Z}_r]_{K\times N_2N_3} = \mathbf{U}_r^{(3)}\mathbf{\Sigma}_r^{(3)}\mathbf{V}_r^{(3)T} = \hat{\mathbf{H}}_{.r}\left(\mathbf{S}_{.r}^{(2)}\otimes\mathbf{S}_{.r}^{(3)}\right)^T. \tag{3.28}$$

Each column of each factor matrix corresponds to the first left singular vector calculated for each $n$-mode matrix unfolding of $r$ tensors $\mathcal{Z}_r$. The estimated matrices are constructed as:

$$\hat{\mathbf{S}}^{(2)} = \left[\begin{array}{ccc}\left(\mathbf{U}_1^{(1)}\right)_{.1} & \cdots & \left(\mathbf{U}_R^{(1)}\right)_{.1}\end{array}\right] \in \mathbb{C}^{N_2\times R}, \tag{3.29}$$

$$\hat{\mathbf{S}}^{(3)} = \left[\begin{array}{ccc}\left(\mathbf{U}_1^{(2)}\right)_{.1} & \cdots & \left(\mathbf{U}_R^{(2)}\right)_{.1}\end{array}\right] \in \mathbb{C}^{N_3\times R}, \tag{3.30}$$

$$\hat{\mathbf{H}} = \left[\begin{array}{ccc}\left(\mathbf{U}_1^{(3)}\right)_{.1} & \cdots & \left(\mathbf{U}_R^{(3)}\right)_{.1}\end{array}\right] \in \mathbb{C}^{K\times R}, \tag{3.31}$$

where $\left(\mathbf{U}_r^{(n)}\right)_{.1}$ is the dominant left singular vector for the $n$-mode matrix unfolding. Note that KRF and THOSVD are equivalent from a computation point of view. The difference lies in the fact that for the THOSVD receiver $\mathbf{Z}$ is reorganized as a tensor of rank-one $\mathcal{Z}_r$ for each $r$ to then estimate the matrices, while the KRF considers the matrix $\mathbf{Z}$ and the permutation between matrices to make the estimation. The THOSVD receiver is summarized in Table 10.

Table 10 – THOSVD algorithm for estimation of the channel and symbol matrices.

| **THOSVD algorithm for estimating $\hat{\mathbf{S}}^{(2)}$, $\hat{\mathbf{S}}^{(3)}$ and $\hat{\mathbf{H}}$.** |
|---|
| **Input:** matrix $\mathcal{X}$, $\mathbf{S}^{(1)}$ and $R$. |
| **Output:** Estimated matrices $\hat{\mathbf{S}}^{(2)}$, $\hat{\mathbf{S}}^{(3)}$ and $\hat{\mathbf{H}}$. |
| 1) Calculate the LS estimate $\mathbf{Z}$ defined in (3.12). |
| **for** $r \in \{1,R\}$ |
| 2) Build the rank-one tensor $\mathcal{Z}_r$ of size $N_2 \times N_3 \times K$ from $\mathbf{Z}$. |
| 3) Compute the SVD of each $n$-mode unfolding of $\mathcal{Z}_r$, and calculate the estimates $\hat{\mathbf{S}}^{(2)}$, $\hat{\mathbf{S}}^{(3)}$ and $\hat{\mathbf{H}}$ as Eqs.(3.29)-(3.31). |
| **end** |
| 4) Eliminate the scaling ambiguities using (3.15)-(3.16). |
| 5) Project the estimated symbols onto the finite alphabet. |

#### 3.3.1.3 Rank-one ALS receiver

In this section rank-one ALS algorithm is presented for the estimation of the channel $\mathbf{H}$ and symbol matrices $\mathbf{S}^{(2)}$ and $\mathbf{S}^{(3)}$. Rank-one ALS receiver is based on the ALS algorithm presented in Table 4. From Eq.(3.12), we define each column $r$ of $\mathbf{Z}$ as a rank-one tensor in Eq.(3.25) and estimate the matrices calculating the rank-one approximation for each column.

The factor matrices can be estimated through the rank-one ALS algorithm calculated for each tensor $\mathcal{Z}_r$. The optimization problem to be solved is:

$$\min_{\mathbf{S}^{(2)}_{.r},\mathbf{S}^{(3)}_{.r},\mathbf{H}_{.r}} \| \mathcal{Z}_r - \mathbf{S}^{(2)}_{.r} \circ \mathbf{S}^{(3)}_{.r} \circ \mathbf{H}_{.r} \|^2_F, \tag{3.32}$$

with respect to $\mathbf{S}^{(2)}_{.r}$, $\mathbf{S}^{(3)}_{.r}$, $\mathbf{H}_{.r}$, for $r \in \{1, R\}$. The rank-one ALS method replaces the optimization problem (3.32) with three LS sub-problems, leading to the alternate minimization of the following LS criteria:

$$\min_{\mathbf{H}_{.r} \in \mathbb{C}^K} \| [\mathbf{Z}_r]_{K \times N_2 N_3} - \mathbf{H}_{.r} \left( \hat{\mathbf{S}}^{(2)}_{.r[i-1]} \otimes \hat{\mathbf{S}}^{(3)}_{.r[i-1]} \right)^T \|^2_F \rightarrow \hat{\mathbf{H}}_{.r[i]}, \tag{3.33}$$

$$\min_{\mathbf{S}^{(2)}_{.r} \in \mathbb{C}^{N_2}} \| [\mathbf{Z}_r]_{N_2 \times N_3 K} - \mathbf{S}^{(2)}_{.r} \left( \hat{\mathbf{S}}^{(3)}_{.r[i-1]} \otimes \hat{\mathbf{H}}_{.r[i]} \right)^T \|^2_F \rightarrow \hat{\mathbf{S}}^{(2)}_{.r[i]}, \tag{3.34}$$

$$\min_{\mathbf{S}^{(3)}_{.r} \in \mathbb{C}^{N_3}} \| [\mathbf{Z}_r]_{N_3 \times K N_2} - \mathbf{S}^{(3)}_{.r} \left( \hat{\mathbf{H}}_{.r[i]} \otimes \hat{\mathbf{S}}^{(2)}_{.r[i]} \right)^T \|^2_F \rightarrow \hat{\mathbf{S}}^{(3)}_{.r[i]}, \tag{3.35}$$

where $[\mathbf{Z}_r]_{K \times N_2 N_3}$, $[\mathbf{Z}_r]_{N_2 \times N_3 K}$ and $[\mathbf{Z}_r]_{N_3 \times K N_2}$ are the 1-mode, 2-mode and 3-mode matrix unfolding of $\mathcal{Z}_r$. The rank-one ALS method solves the three LS sub-problems (3.33)-(3.35) for each $r$ to obtain the matrices $\hat{\mathbf{H}}$, $\hat{\mathbf{S}}^{(2)}$ and $\hat{\mathbf{S}}^{(3)}$. The updates are:

$$\hat{\mathbf{H}}_{.r[i]} = [\mathbf{Z}_r]_{K \times N_2 N_3} \left[ \left( \hat{\mathbf{S}}^{(2)}_{.r[i-1]} \otimes \hat{\mathbf{S}}^{(3)}_{.r[i-1]} \right)^T \right]^\dagger, \tag{3.36}$$

$$\hat{\mathbf{S}}^{(2)}_{.r[i]} = [\mathbf{Z}_r]_{N_2 \times N_3 K} \left[ \left( \hat{\mathbf{S}}^{(3)}_{.r[i-1]} \otimes \hat{\mathbf{H}}_{.r[i]} \right)^T \right]^\dagger, \tag{3.37}$$

$$\hat{\mathbf{S}}^{(3)}_{.r[i]} = [\mathbf{Z}_r]_{N_3 \times K N_2} \left[ \left( \hat{\mathbf{H}}_{.r[i]} \otimes \hat{\mathbf{S}}^{(2)}_{.r[i]} \right)^T \right]^\dagger. \tag{3.38}$$

For the updates we have:

$$\hat{\mathbf{H}}_{.r[i]} = [\mathbf{Z}_r]_{K \times N_2 N_3} \frac{\left( \hat{\mathbf{S}}^{(2)}_{.r[i-1]} \otimes \hat{\mathbf{S}}^{(3)}_{.r[i-1]} \right)^*}{\| \hat{\mathbf{S}}^{(2)}_{.r[i-1]} \|^2_2 \| \hat{\mathbf{S}}^{(3)}_{.r[i-1]} \|^2_2}, \tag{3.39}$$

$$\hat{\mathbf{S}}^{(2)}_{.r[i]} = [\mathbf{Z}_r]_{N_2 \times N_3 K} \frac{\left( \hat{\mathbf{S}}^{(3)}_{.r[i-1]} \otimes \hat{\mathbf{H}}_{.r[i]} \right)^*}{\| \hat{\mathbf{S}}^{(3)}_{.r[i-1]} \|^2_2 \| \hat{\mathbf{H}}_{.r[i]} \|^2_2}, \tag{3.40}$$

$$\hat{\mathbf{S}}^{(3)}_{.r[i]} = [\mathbf{Z}_r]_{N_3 \times K N_2} \frac{\left( \hat{\mathbf{H}}_{.r[i]} \otimes \hat{\mathbf{S}}^{(2)}_{.r[i]} \right)^*}{\| \hat{\mathbf{H}}_{.r[i]} \|^2_2 \| \hat{\mathbf{S}}^{(2)}_{.r[i]} \|^2_2}. \tag{3.41}$$

The error at the $[i]^{th}$ iteration is considered for deciding the convergence of the rank-one ALS algorithm:

$$err_{[i]} = \| \ [\mathbf{Z}_r]_{K\times N_2N_3} - \mathbf{H}_{.r[i]} \left( \hat{\mathbf{S}}^{(2)}_{.r[i]} \otimes \hat{\mathbf{S}}^{(3)}_{.r[i]} \right)^T \ \|^2_F \ . \tag{3.42}$$

Convergence at the $[i]^{th}$ iteration is declared when this error does not significantly change between two successive iterations, i.e., $|err_{[i-1]} - err_{[i]}| \leq \delta$, where $\delta$ is a predefined threshold.

*Proof.* For Eqs.(3.39)-(3.41) let us consider a full-row rank matrix $\mathbf{D} \in \mathbb{C}^{M\times N}$, its right pseudo-inverse is given by:

$$\mathbf{D}^{\dagger} = \mathbf{D}^H \left( \mathbf{D}\mathbf{D}^H \right)^{-1}. \tag{3.43}$$

Note that the Khatri-Rao product is the column-wise Kronecker product and since $\mathbf{D}_{.m}$ is a column vectors, we can rewrite Eq.(3.43) as:

$$\left[ (\mathbf{D}_{.m})^T \right]^{\dagger} = \mathbf{D}^*_{.m} \left( \mathbf{D}^T_{.m} \mathbf{D}^* \right)^{-1}. \tag{3.44}$$

By replacing $(\mathbf{D}_{.m})^T$ by $\left( \hat{\mathbf{S}}^{(2)}_{.r} \otimes \hat{\mathbf{S}}^{(3)}_{.r} \right)^T$ in Eq.(3.36):

$$\left[ (\hat{\mathbf{S}}^{(2)}_{.r} \otimes \hat{\mathbf{S}}^{(3)}_{.r})^T \right]^{\dagger} = \left( \hat{\mathbf{S}}^{(2)}_{.r} \otimes \hat{\mathbf{S}}^{(3)}_{.r} \right)^* \left[ (\hat{\mathbf{S}}^{(2)}_{.r} \otimes \hat{\mathbf{S}}^{(3)}_{.r})^T (\hat{\mathbf{S}}^{(2)}_{.r} \otimes \hat{\mathbf{S}}^{(3)}_{.r})^* \right]^{-1}. \tag{3.45}$$

Using properties 1 and 2 (Eqs.(2.3)-(2.4)) we have:

$$\begin{aligned} \left[ (\hat{\mathbf{S}}^{(2)}_{.r} \otimes \hat{\mathbf{S}}^{(3)}_{.r})^T \right]^{\dagger} &= \left( \hat{\mathbf{S}}^{(2)}_{.r} \otimes \hat{\mathbf{S}}^{(3)}_{.r} \right)^* \left[ (\hat{\mathbf{S}}^{(2)T}_{.r} \hat{\mathbf{S}}^{(2)*}_{.r}) \otimes (\hat{\mathbf{S}}^{(3)T}_{.r} \hat{\mathbf{S}}^{(3)*}_{.r}) \right]^{-1}, \\ &= \frac{\left( \hat{\mathbf{S}}^{(2)}_{.r} \otimes \hat{\mathbf{S}}^{(3)}_{.r} \right)^*}{\| \ \hat{\mathbf{S}}^{(2)}_{.r} \ \|^2_2 \| \ \hat{\mathbf{S}}^{(3)}_{.r} \ \|^2_2}. \end{aligned} \tag{3.46}$$

*Identifiability conditions and ambiguity relations*

As Rank-one ALS is based on Eq.(3.11), then only one condition is required to ensure the uniqueness, where $\mathbf{S}^{(1)}$ must be left-invertible, i.e., it must be full column rank,

$$R \leq N_1. \tag{3.47}$$

Note that the identifiability condition is always satisfied for a row. Moreover, for the factors estimated through the rank-one ALS receiver, there are implicit scaling ambiguities. The relation for the scaling ambiguities is similar to the relation presented for the KRF and THOSVD receivers in Eqs.(3.15)-(3.16). These ambiguities are eliminated by assuming a

priori knowledge of the first row of each matrix $\mathbf{S}^{(l)}$, for $l \in \{2,3\}$, where these rows are formed by 1's.

This process continues iteratively until some convergence criterion is satisfied. The rank-one ALS receiver is sub-optimal with respect to the ALS receiver presented in next section. The rank-one ALS receiver is summarized in Algorithm 11.

Table 11 – Rank-one ALS algorithm for estimation of the channel and symbol matrices.

**Rank-one ALS algorithm for estimating $\hat{\mathbf{S}}^{(2)}$, $\hat{\mathbf{S}}^{(3)}$ and $\hat{\mathbf{H}}$.**

**Input:** matrix $\mathcal{X}$, $\mathbf{S}^{(1)}$ and $R$.
**Output:** Estimated matrices $\hat{\mathbf{S}}^{(2)}$, $\hat{\mathbf{S}}^{(3)}$ and $\hat{\mathbf{H}}$.

1) Calculate the LS estimate $\mathbf{Z}$ defined in (3.12).
**for** $r \in \{1,R\}$
2) Build the rank-one tensor $\mathcal{Z}_r$ of size $N_2 \times N_3 \times K$ from $\mathbf{Z}_r$.
3) Initialization of $\mathbf{S}^{(2)}_{.r[0]}$ and $\mathbf{S}^{(3)}_{.r[0]}$ with symbols randomly drawn from the alphabet.
4) Update the estimates of $\mathbf{S}^{(2)}$, $\mathbf{S}^{(3)}$ and $\mathbf{H}$ using Eqs.(3.39)-(3.41).
5) Calculate the error (3.42) and $|err_{[i-1]} - err_{[i]}|$.
- **if** $|err_{[i-1]} - err_{[i]}| \leq \delta$ or $i =$ maximum number of iterations.
- **stop**
- **else** $i \rightarrow i+1$.
**end**
6) Eliminate the scaling ambiguities using (3.15)-(3.16).
7) Project the estimated symbols onto the finite alphabet.

#### 3.3.1.4 ALS receiver

The ALS algorithm is used to jointly estimate the symbol matrices ($\mathbf{S}^{(2)}$, $\mathbf{S}^{(3)}$) and the channel ($\mathbf{H}$) and results from the minimization of the following LS criteria:

$$\min_{\mathbf{S}^{(2)},\mathbf{S}^{(3)},\mathbf{H}} \| \mathcal{X} - \mathcal{I}_{4,R} \times_1 \mathbf{S}^{(1)} \times_2 \mathbf{S}^{(2)} \times_3 \mathbf{S}^{(3)} \times_4 \mathbf{H} \|_F^2, \tag{3.48}$$

where $\mathbf{S}^{(1)}$ is considered known. The ALS method replaces the optimization problem (3.48) with three LS sub-problems leading to the alternate minimization of the following LS criteria:

$$\min_{\mathbf{H}\in\mathbb{C}^{K\times R}} \| \mathbf{X}_{K\times N_1N_2N_3} - \mathbf{H}\left(\mathbf{S}^{(1)} \diamond \hat{\mathbf{S}}^{(2)}_{[i-1]} \diamond \hat{\mathbf{S}}^{(3)}_{[i-1]}\right)^T \|_F^2 \rightarrow \hat{\mathbf{H}}_{[i]}, \tag{3.49}$$

$$\min_{\mathbf{S}^{(2)}\in\mathbb{C}^{N_2\times R}} \| \mathbf{X}_{N_2\times N_3KN_1} - \mathbf{S}^{(2)}\left(\hat{\mathbf{S}}^{(3)}_{[i-1]} \diamond \hat{\mathbf{H}}_{[i]} \diamond \mathbf{S}^{(1)}\right)^T \|_F^2 \rightarrow \hat{\mathbf{S}}^{(2)}_{[i]}, \tag{3.50}$$

$$\min_{\mathbf{S}^{(3)}\in\mathbb{C}^{N_3\times R}} \| \mathbf{X}_{N_3\times KN_1N_2} - \mathbf{S}^{(3)}\left(\hat{\mathbf{H}}_{[i]} \diamond \mathbf{S}^{(1)} \diamond \mathbf{S}^{(2)}_{[i]}\right)^T \|_F^2 \rightarrow \hat{\mathbf{S}}^{(3)}_{[i]}. \tag{3.51}$$

The update equations at iteration $[i]$ are given by:

$$\hat{\mathbf{H}}_{[i]} = \mathbf{X}_{K\times N_1N_2N_3}\left[\left(\mathbf{S}^{(1)} \diamond \hat{\mathbf{S}}^{(2)}_{[i-1]} \diamond \hat{\mathbf{S}}^{(3)}_{[i-1]}\right)^T\right]^{\dagger}, \tag{3.52}$$

$$\hat{\mathbf{S}}^{(2)}_{[i]} = \mathbf{X}_{N_2\times N_3KN_1}\left[\left(\hat{\mathbf{S}}^{(3)}_{[i-1]} \diamond \hat{\mathbf{H}}_{[i]} \diamond \mathbf{S}^{(1)}\right)^T\right]^{\dagger}, \tag{3.53}$$

$$\hat{\mathbf{S}}^{(3)}_{[i]} = \mathbf{X}_{N_3\times KN_1N_2}\left[\left(\hat{\mathbf{H}}_{[i]} \diamond \mathbf{S}^{(1)} \diamond \hat{\mathbf{S}}^{(2)}_{[i]}\right)^T\right]^{\dagger}. \tag{3.54}$$

The error at the $[i]^{th}$ iteration is considered for deciding the convergence of the ALS algorithm:

$$err_{[i]} = \| \mathbf{X}_{K\times N_1N_2N_3} - \mathbf{H}_{[i]}\left(\mathbf{S}^{(1)} \diamond \hat{\mathbf{S}}^{(2)}_{[i]} \diamond \hat{\mathbf{S}}^{(3)}_{[i]}\right)^T \|^2_F . \tag{3.55}$$

Convergence at the $[i]^{th}$ iteration is declared when this error does not significantly change between two successive iterations, i.e., $|err_{[i-1]} - err_{[i]}| \leq \delta$, where $\delta$ is a predefined threshold.

*Identifiability conditions and ambiguity relations*

In the case of the ALS algorithm, for the uniqueness of the pseudo-inverse, the matrices $\left(\hat{\mathbf{S}}^{(3)} \diamond \hat{\mathbf{H}} \diamond \mathbf{S}^{(1)}\right)^T$, $\left(\hat{\mathbf{S}}^{(3)} \diamond \hat{\mathbf{H}} \diamond \mathbf{S}^{(1)}\right)^T$ and $\left(\hat{\mathbf{H}} \diamond \mathbf{S}^{(1)} \diamond \hat{\mathbf{S}}^{(2)}\right)^T$ must be full-row rank, i.e.,

$$R \leq \min\left(N_1N_2N_3, N_3KN_1, KN_1N_2\right). \tag{3.56}$$

For the scaling ambiguities, the relations are similar to the previous algorithms and they are presented in Eqs.(3.15)-(3.16). We assume a priori knowledge of the first row of matrices $\mathbf{S}^{(2)}$ and $\mathbf{S}^{(3)}$, where these rows are formed by $1's$. The ALS receiver is summarized in Table 12.

#### 3.3.1.5 Zero-forcing-KRF receiver with perfect channel knowledge

To evaluate the impact of the design parameters on the system performance, we use the zero-forcing (ZF)-KRF receiver, which assumes perfect channel knowledge. This algorithm is called ZF-KRF because it has a second step called KRF. At this step, symbol matrices are estimated using the KRF algorithm. The ZF-KRF receiver is derived from Eq.(3.10) and given by:

$$\mathbf{X}_{N_c\times KN_1} = \mathbf{S}^{(c)}\left(\mathbf{H} \diamond \mathbf{S}^{(1)}\right)^T \in \mathbb{C}^{N_c\times KN_1}, \tag{3.57}$$

where $\mathbf{S}^{(c)} = \mathbf{S}^{(2)} \diamond \mathbf{S}^{(3)}$. The LS estimate of $\mathbf{S}^{(c)}$ is obtained using (3.10), with $\mathbf{H}$ replaced by the true channel $\mathbf{H}$, which gives:

$$\widehat{\mathbf{S}^{(2)} \diamond \mathbf{S}^{(3)}} = \mathbf{X}_{N_c\times KN_1}\left[\left(\mathbf{H} \diamond \mathbf{S}^{(1)}\right)^T\right]^{\dagger}. \tag{3.58}$$

Table 12 – ALS algorithm for estimation of the channel and symbol matrices.

**ALS algorithm for estimating $\hat{\mathbf{S}}^{(2)}$, $\hat{\mathbf{S}}^{(3)}$ and $\hat{\mathbf{H}}$.**

**Input:** matrix $\mathcal{X}$, $\mathbf{S}^{(1)}$ and $R$.

**Output:** Estimated matrices $\hat{\mathbf{S}}^{(2)}$, $\hat{\mathbf{S}}^{(3)}$ and $\hat{\mathbf{H}}$.

$i = 0$

1) Initialization of $\mathbf{S}^{(2)}_{[0]}$ and $\mathbf{S}^{(3)}_{[0]}$ with symbols randomly drawn from the alphabet and $s^{(l)}_{1r} = 1$, for $l \in \{2, 3\}$.

2) Update the estimates of $\mathbf{S}^{(2)}$, $\mathbf{S}^{(3)}$ and $\mathbf{H}$ using Eqs.(3.52)-(3.54).

3) Calculate the error (3.55) and $|err_{[i-1]} - err_{[i]}|$.

- **if** $|err_{[i-1]} - err_{[i]}| \leq \delta$ or $i =$ maximum number of iterations.
- **stop**
- **else** $i \rightarrow i + 1$.

4) Eliminate the scaling ambiguities using (3.15)-(3.16).

5) Project the estimated symbols onto the finite alphabet.

Then, the symbol matrices $\mathbf{S}^{(2)}$ and $\mathbf{S}^{(3)}$ are estimated using the KRF algorithm summarized in Table 2.

*Identifiability conditions and ambiguities relations*

In the case of the ZF-KRF receiver, for the uniqueness of the pseudo-inverse, $\left(\mathbf{H} \diamond \mathbf{S}^{(1)}\right)^T$ must be full row rank,i.e.,

$$R \leq N_1 K. \tag{3.59}$$

The relations for the scaling ambiguities are similar to the previous algorithms presented in Eqs.(3.15)-(3.16). To find the scaling ambiguities, we assume a priori knowledge of the first row of the symbol matrix $\mathbf{S}^{(2)}$, where this row is formed by $1'$s.

Table 13 summarizes the necessary conditions for parameter identifiability with each receiver. Note that the identifiability conditions of the KRF, KRF-KRF, THOSVD and rank-one ALS receivers are the same because these receivers consider Eq.(3.12) to estimate the symbol and channel matrices. Regarding the ALS algorithm note that the identifiability conditions differ because the ALS receiver considers the LS criteria (3.48) to estimate the symbol and channel matrices such that $\mathbf{S}^{(c)}$ is replaced by the Khatri-rao product of $\mathbf{S}^{(2)}$ and $\mathbf{S}^{(3)}$. In both receivers the symbol matrix $\mathbf{S}^{(1)}$ is considered known.

Table 13 – Identifiability conditions for the receivers.

| **Receiver** | **Identifiability conditions** |
|---|---|
| KRF | $R \leq N_1$ |
| KRF-KRF | $R \leq N_1$ |
| THOSVD | $R \leq N_1$ |
| Rank-one ALS | $R \leq N_1$ |
| ALS | $R \leq \min(N_1N_2N_3, N_3KN_1, KN_1N_2)$ |
| ZF-KRF | $R \leq N_1K$ |

### 3.3.2 Computational complexity

In this section, we compare the computational complexity of the proposed semi-blind receivers in terms of FLOPS (Floating-point Operations Per Second), considering the most expensive matrix operation is the SVD whose complexity is $O(IJ\min(I,J))$ for a matrix $\mathbf{A} \in \mathbb{C}^{I\times J}$. The complexities are evaluated taking the identifiability conditions into account.

Computing the HOSVD of an $N$-order tensor $\mathcal{X} \in \mathbb{C}^{I_1\times\ldots\times I_N}$ requires $N$ SVDs of $I_n \times I_{n+1}\ldots I_N I_1\ldots I_{n-1}$ matrices, for $n \in \{1,N\}$, inducing the following overall computational complexity $O\left((\sum_{n=1}^{N} I_n)\prod_{q=1}^{N} I_q\right)$ if $I_n \leq \prod_{q\neq n}^{N} I_q$. In particular, the complexity of the KRF algorithm described in section 2.3.3 for estimating the symbol matrices and the channel is $O\left(KR(\sum_{l=1}^{L} N_l)\prod_{q=1}^{L} N_q\right)$. To compute the PARAFAC decomposition of an $N$-order tensor $\mathcal{X}$ of size $I_1 \times \ldots \times I_N$ and assumed to be of rank $R$, using the ALS algorithm, requires to compute $N$ LS estimates, which needs to pseudo inverse $\prod_{q\neq n}^{N} I_q \times R$ matrices, for $n \in \{1,N\}$, and induces the overall computational complexity $O\left(R^2\sum_{n=1}^{N}(\prod_{q\neq n}^{N} I_q)\right)$, at each iteration. See [69] for more details.

In Table 14, the computational complexities of the receivers are compared, i.e., the KRF, KRF-KRF, THOSVD, Rank-one ALS and ALS algorithms. The complexity of the KRF, KRF-KRF and THOSVD is lower than that of the Rank-one ALS and ALS because they must be multiplied by the number of iterations needed for convergence, which explains why the computation time with the closed-form solutions (KRF, KRF-KRF and THOSVD algorithm) is generally lower than with the iterative Rank-one ALS and ALS algorithms.

Table 14 – Computational complexity of the KRF, KRF-KRF, THOSVD, Rank-one ALS and ALS receivers.

| **Algorithms** | **Computational complexity** |
|---|---|
| KRF | $O\left(R^2N_1\right) + O\left(2R(\sum_{l=2}^{L} N_l)\prod_{q=2}^{L} N_q K\right)$ |
| KRF-KRF | $O\left(R^2N_1\right) + O\left(RN_1K\right) + O\left(R(\sum_{l=2}^{L} N_l)\prod_{q=2}^{L} N_q\right)$ |
| THOSVD | $O\left(R^2N_1\right) + O\left(\left((\sum_{l=2}^{L} N_l)\prod_{q=2}^{L} N_q\right)^2 K\right) + O\left(KR(\sum_{l=2}^{L} N_l)\prod_{q=2}^{L} N_q\right)$ |
| Rank-one ALS | $O\left(R^2N_1\right) + O\left(R(\sum_{l=2}^{L} N_l)\prod_{q=2}^{L} N_q + N_3K + KN_2\right)$ |
| ALS | $O\left(R(N_1^3((\sum_{l=2}^{L} N_l)\prod_{q=2}^{L} N_q)^3 + N_1^3N_3^3K^3 + N_1^3N_2^3K^3)\right)$ |

## 3.4 Simulation results

In this section, we evaluate the performance of the proposed point-to-point MIMO system and associated receivers. First, in Section 3.4.1, the simulations and the considered performance criteria are presented. In Section 3.4.2, the impact of design parameters on symbol error rate (SER) is studied considering the ZF-KRF receiver. Finally, in Section 3.4.3 the proposed semi-blind receivers are compared in terms of SER and channel normalized mean square error (NMSE).

### 3.4.1 General description of the simulations

The noisy received signals tensor $\mathcal{Y}$ is simulated as:

$$\mathcal{Y} = \mathcal{X}_c + \alpha\mathcal{V} \in \mathbb{C}^{N_c \times N_1 \times K}, \tag{3.60}$$

where $\mathcal{X}_c$ contains the noise-free received signals obtained by means of (3.7), and $\mathcal{V}$ is the additive noise tensor whose entries are zero-mean circularly-symmetric complex-valued Gaussian random variables, with unit variance, and $\alpha$ allows to fix the signal-noise ratio (SNR) calculated as:

$$SNR = 20\log\frac{\| \mathcal{X}_c \|_F}{\alpha \| \mathcal{V} \|_F}, \tag{3.61}$$

which gives $\alpha = \dfrac{\| \mathcal{X}_c \|_F}{\| \mathcal{V} \|_F} 10^{SNR/20}$. At each Monte Carlo run, the entries of the channel $\mathbf{H} \in \mathbb{C}^{K \times R}$ are drawn from a Gaussian distribution with variance $\dfrac{1}{R}$ and the symbols of $\mathbf{S}^{(l)} \in \mathbb{C}^{N_l \times R}$, for $l \in \{1, 3\}$ are randomly generated from the 64-QAM (quadrature amplitude modulation) alphabet with a uniform distribution. As mentioned before, the symbol matrix $\mathbf{S}^{(1)} \in \mathbb{C}^{N_1 \times R}$ is assumed known throughout the simulations. The number of transmit antennas $R$, the number of receive antennas $K$ and the number of symbols per data stream $N_l$, with $l \in \{2, 3\}$ are varied to evaluate the performance. The performance criteria, plotted versus SNR, are

calculated as:

$$NMSE(\mathbf{H}) = \frac{1}{M}\sum_{m=1}^{M}\frac{\| \hat{\mathbf{H}}_m - \mathbf{H}_m \|_F^2}{\| \mathbf{H}_m \|_F^2}, \tag{3.62}$$

where $\hat{\mathbf{H}}_m$ is the channel matrix $\mathbf{H}_m$ estimated at the $m^{th}$ run. The SER and NMSE are calculated by averaging the results over $M = 10^4$ Monte Carlo runs, after truncating the 5% worse and 5% better values to eliminate the influence of ill-convergence and outliers.

The transmission rate $T$ in bits per channel is given by [76]:

$$T = \frac{n_s}{n_{p_s}}\log_2(\mu), \tag{3.63}$$

where $n_s$ corresponds to the number of unknown symbols in the matrix $\mathbf{S}$, $n_{p_s}$ is the number of symbol periods and $\mu$ denotes the number of constellation points. Then, the transmission rate is:

$$T = \frac{R\left(\sum_{l=2}^{L} N_l - L\right)}{N_1 \prod_{l=2}^{L} N_l}\log_2(\mu). \tag{3.64}$$

Note that increasing the number of data streams/transmit antennas $R$ in the symbol matrix $\mathbf{S}^{(l)}$ induces an increase in transmission rate $T$, while increasing the number of unknown symbols $N_l$ induces a decrease in transmission rate.

For bit rate note that as the number of symbols increases, more data bits are transmitted per symbol. For example, 32-QAM is a QAM scheme with 32 symbols, and 64-QAM is a scheme with 64 symbols. 64-QAM conveys 6 bits per symbol (as $64 = 2^6$), so achieving twice the data rate of 8-QAM for the same symbol rate. The bit rate is given by:

$$B = \frac{T}{T_B} \tag{3.65}$$

where $T$ corresponds to the transmission rate in Eq. (3.64) that represents the number of bits transmitted according to the modulation and $T_B$ is the bit time in seconds. Then,

$$B = \frac{R\left(\sum_{l=2}^{L} N_l - L\right)}{N_1 \prod_{l=2}^{L} N_l}\log_2(\mu)\frac{1}{T_B}. \tag{3.66}$$

### 3.4.2 Impact of design parameters

In this section, we evaluate the SER performance of the proposed system under perfect channel knowledge. In this case, the ZF-KRF receiver is applied to estimate the transmitted symbols by means of Eq.(3.58). The design parameters used for the simulations are provided in Table 15 and the corresponding transmission rates are given in Table 16.

Figure 10 shows the impact on the SER for different numbers of symbols per data stream: $N_2 = N_3 \in \{4, 8, 12\}$. Note that SER(S) corresponds to the mean of the SERs calculated for each symbol matrix. From these simulation results, it can be concluded that the

Table 15 – Parameters for the simulations.

| **Figures** | **Impact of** | **Parameters** |
|---|---|---|
| Figure 10 | **numbers of symbols per data stream** | $N_1 = K = 4; R = 2\, N_2 = N_3 \in \{4, 8, 12\}$ |
| Figure 11 | **numbers of data stream and transmit antennas** | $N_1 = 10; K = 4; N_2 = N_3 = 8; N_1 = R \in \{4, 6, 8\}$ |
| Figure 12 | **numbers of receive antennas** | $N_1 = 4, R = 2; N_2 = N_3 = 8; K \in \{4, 6, 8\}$ |
| Figure 13 | **different configurations for $N_2$ and $N_3$** | $N_1 = 4, R = 2; K = 6; N_2 = 4; N_3 = 12$ |
| Figure 14 | **$m$-QAM** | $N_1 = 4\, R = 2; K = 4; N_2 = N_3 = 8; m \in \{4, 8, 16, 32, 64\}$ |
| Figures 15-16 | **Comparison of the proposed semi-blind receivers** | $N_1 = 4, R = 2; K = 4; N_2 = N_3 = 8$ |

SER is improved when the number of symbols increases, which implies an increase in coding diversity, since $N_2N_3$ is a dimension of the contracted form $\mathcal{Y}_c$ of the data tensor, which is not the case for $R$. As the number of symbols increases, the transmission rate decreases as shown in Table 16.

Table 16 – Transmission rates for different configurations.

| **Figures** | **Parameters** | **Transmission rate (bits per channel)** |
|---|---|---|
| Figure 10 | $N_2 = N_3 \in \{4, 8, 12\}$ | $T = 1.125; 0.656; 0.458$ |
| Figure 11 | $R \in \{4, 6, 8\}$ | $T = 0.525; 0.787; 1.05$ |
| Figure 12 | $K \in \{4, 6, 8\}$ | $T = 0.656$ |
| Figure 13 | $N_2 = 4; N_3 = 12$ | $T = 0.875$ |
| Figure 14 | $m \in \{4, 8, 16, 32, 64\}$ | $T = 0.218; 0.328; 0.437; 0.546; 0.656$ |
| Figures 15-16 | Comparison of the proposed semi-blind receivers | $T = 2.906$ |

Figure 11 compares the SER for three different data stream numbers/ transmit antenna numbers: $R \in \{4, 6, 8\}$. Note that increasing $R$ implies an increase of the number of symbols to be estimated, without increasing the number of data in the tensor $\mathcal{Y}_c$ for performing the symbol estimation, thus inducing a degradation of the SER, while the transmission rate increases (Table 16).

Figure 12 shows the impact on the SER for different numbers of receive antennas: $K \in \{4, 6, 8\}$. From these simulation results, it can be concluded that the SER is improved when the number of receive antennas increases, which implies an increase of coding diversity since $K$ is a dimension of the contracted form $\mathcal{Y}_c$ of the data tensor, while the transmission rate remains the same as shown in Table 16.

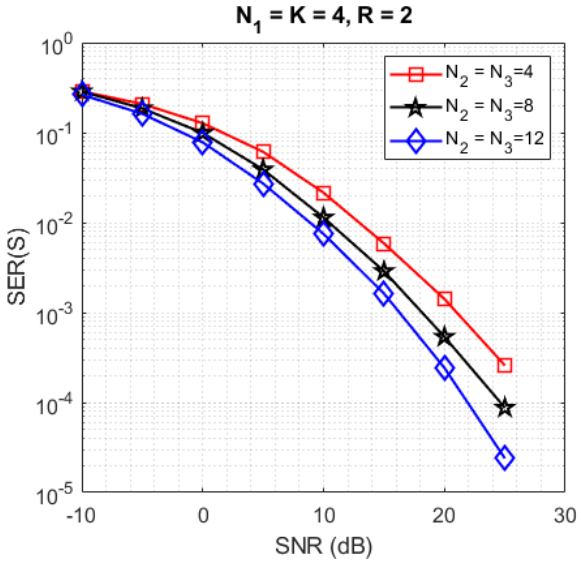


Figure 10 – Impact of numbers of symbols per data stream.

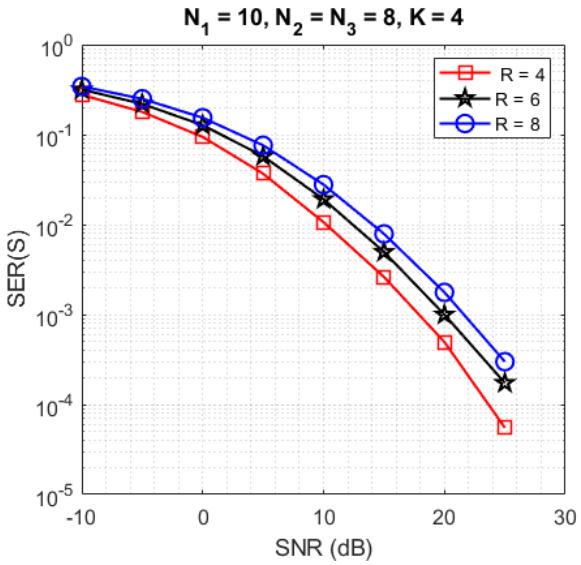


Figure 11 – Impact of numbers of data streams and transmit antennas.

In Figure 13, the simulation results compare the $\text{SER}_{global}$ with the individual SERs for $\mathbf{S}^{(2)}$ and $\mathbf{S}^{(3)}$, when $N_2 = 4$, $N_3 = 12$ and $R = 2$. For this configuration, the Khatri-Rao product between $\mathbf{S}^{(2)}$ and $\mathbf{S}^{(3)}$ induces a greater diversity for $\mathbf{S}^{(2)}$ than for $\mathbf{S}^{(3)}$, due to the fact that each symbol of $\mathbf{S}^{(2)}$ is repeated 12 times while each symbol of $\mathbf{S}^{(3)}$ is repeated only 4 times. That implies a SER smaller for $\mathbf{S}^{(2)}$ than for $\mathbf{S}^{(3)}$.

Figure 14 compares the SER obtained with five different modulations $m$-QAM, $m \in \{4, 8, 16, 32, 64\}$. As expected, the SER performance is better when the 4-QAM is considered, because decoding with 4-QAM is easier than with the other modulations. On the other hand, the transmission rate for 4-QAM (see Table 16) is less than 64-QAM, because 4-QAM has a lower diversity of elements.

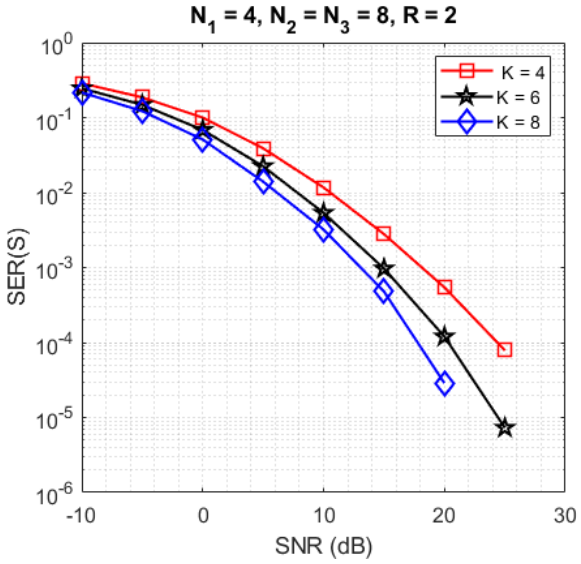


Figure 12 – Impact of numbers of receive antennas.

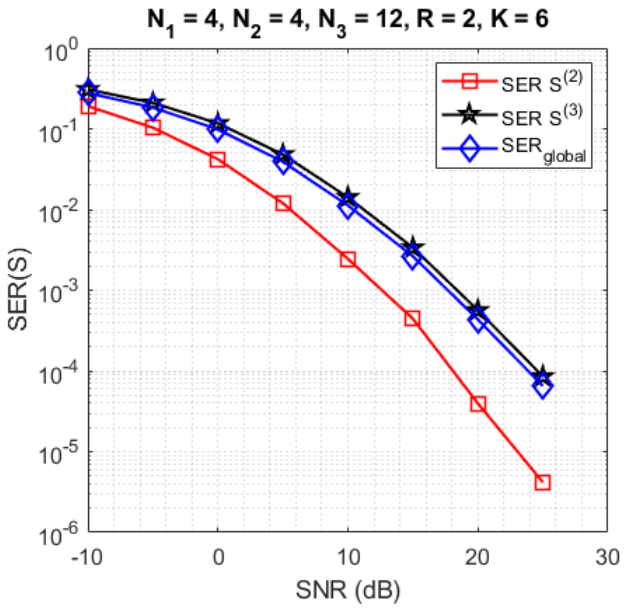


Figure 13 – Impact on the SER of individual symbol matrices.

### 3.4.3 Comparison of the proposed semi-blind receivers

In the next experiments, we compare the SER and NMSE obtained with the proposed semi-blind and ZF-KRF receivers. First, the results are presented in terms of SER (Figure 15), then, we compare the performance of semi-blind receivers in terms of channel NMSE (Figure 16). For these simulations, the design parameters are fixed with the following values: $N_2 = N_3 = 8$, $N_1 = K = 4$, and $R = 2$.

From Figure 15, we can conclude that the THOSVD, KRF and KRF-KRF provide a better SER performance related to ALS receiver. That is due to the closed-form solution of these receivers allowing to jointly estimate the channel and symbol matrices, while the ALS is an iterative algorithm. Comparing the THOSVD, KRF and KRF-KRF solutions to

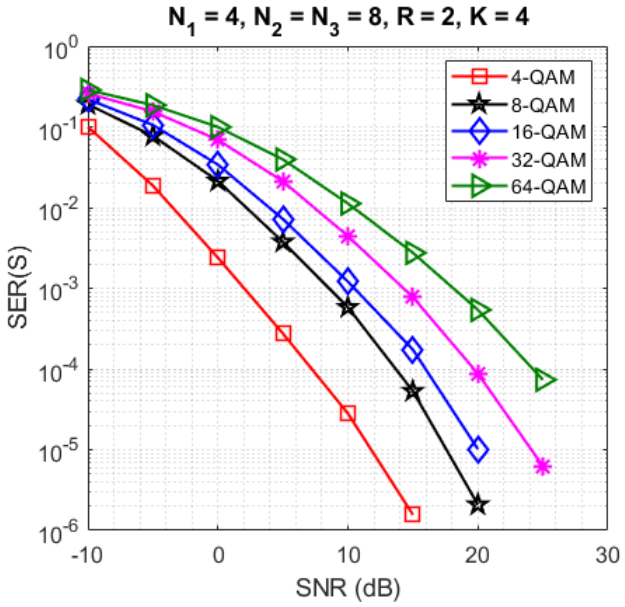


Figure 14 – Impact of modulation ($m$-QAM).

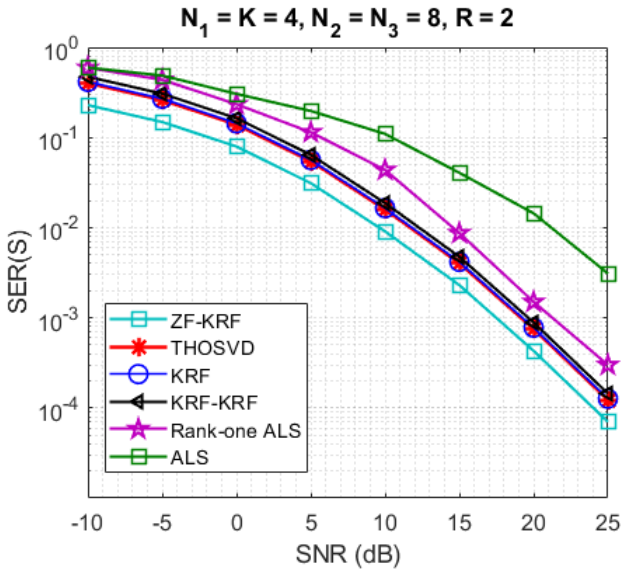


Figure 15 – SER comparison with KRF, KRF-KRF, Rank-one ALS, THOSVD, ALS and ZF receivers.

the Rank-one ALS receiver, note that the SER performance for the three receivers is a little better than for Rank-one ALS. This is because these algorithms have all closed-form steps, while the Rank-one ALS algorithm only has the first step in a closed form where the second is iterative. Considering rank-one ALS and ALS algorithms, note that the first is better than the second one because in this receiver the problem is solved for each vector and not for each matrix as for the ALS algorithm.

In Figure 16, the channel NMSE results are plotted. The results presented demonstrate that KRF, KRF-KRF and THOSVD receivers have the best performance among all receivers. This happens because these three receivers are closed-form, while rank-one ALS and ALS algorithms are iterative. Note that the KRF and THOSVD have better performance than

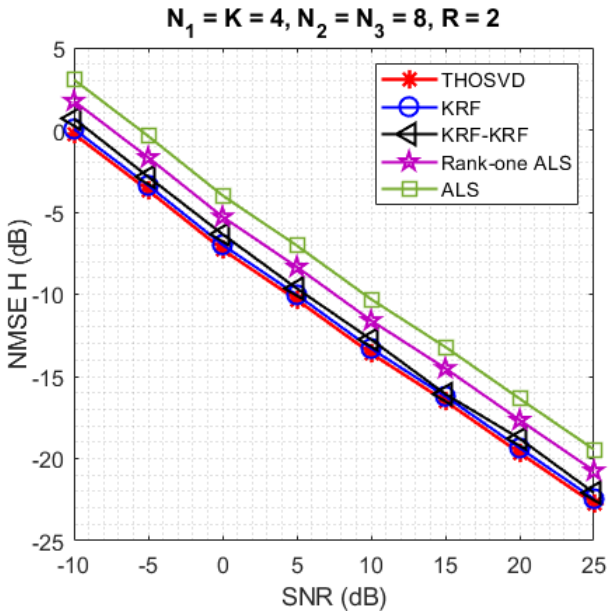


Figure 16 – Channel NMSE comparison with KRF, KRF-KRF, Rank-one ALS, THOSVD and ALS receivers.

KRF-KRF due to the propagation error implicit in KRF-KRF algorithm. And rank-one ALS receiver has better performance than the ALS receiver. This is because, in rank-one ALS, the problem is more subdivided into smaller sub-problems where the matrices are estimated column by column on each iteration, while the ALS estimates the complete matrices on each iteration.

In Table 14, a comparison of the complexities of KRF, KRF-KRF, THOSVD, rank-one ALS and ALS receivers is provided. Based on this table we can define the ratios $O_1$, $O_2$, $O_3$, $O_4$, $O_5$ and $O_6$, which expresses how many times one algorithm is more computationally demanding than another algorithm, such that:

- $O_1 = \frac{O_{KRF}}{O_{KRF-KRF}}$: expresses how many times KRF algorithm is more computationally demanding than KRF-KRF algorithm;
- $O_2 = \frac{O_{THOSVD}}{O_{KRF}}$: expresses how many times THOSVD algorithm is more computationally demanding than KRF algorithm;
- $O_3 = \frac{O_{THOSVD}}{O_{rank-oneALS}}$: expresses how many times THOSVD algorithm is more computationally demanding than rank-one ALS algorithm;
- $O_4 = \frac{O_{rank-oneALS}}{O_{KRF}}$: expresses how many times rank-one ALS algorithm is more computationally demanding than KRF algorithm;
- $O_5 = \frac{O_{ALS}}{O_{THOSVD}}$: expresses how many times ALS algorithm is more computationally demanding than THOSVD algorithm;

- $O_6 = \dfrac{O_{ALS}}{O_{rank-oneALS}}$: expresses how many times ALS algorithm is more computationally demanding than rank-one ALS algorithm.

Each ratio above can be defined as:

$$O_1 = \frac{O_{KRF}}{O_{KRF-KRF}} = \frac{R^2N_1 + 2R(\sum_{l=2}^{L} N_l)\prod_{q=2}^{L} N_q K}{R^2N_1 + RN_1K + R(\sum_{l=2}^{L} N_l)\prod_{q=2}^{L} N_q}, \tag{3.67}$$

$$O_2 = \frac{O_{THOSVD}}{O_{KRF}} = \frac{R^2N_1 + \left((\sum_{l=2}^{L} N_l)\prod_{q=2}^{L} N_q\right)^2 K + KR(\sum_{l=2}^{L} N_l)\prod_{q=2}^{L} N_q}{R^2N_1 + 2R(\sum_{l=2}^{L} N_l)\prod_{q=2}^{L} N_q K}, \tag{3.68}$$

$$O_3 = \frac{O_{THOSVD}}{O_{rank-oneALS}} = \frac{R^2N_1 + \left((\sum_{l=2}^{L} N_l)\prod_{q=2}^{L} N_q\right)^2 K + KR(\sum_{l=2}^{L} N_l)\prod_{q=2}^{L} N_q}{R^2N_1 + i_1\left(R(\sum_{l=2}^{L} N_l)\prod_{q=2}^{L} N_q + N_3K + KN_2\right)}, \tag{3.69}$$

$$O_4 = \frac{O_{rank-oneALS}}{O_{KRF}} = \frac{R^2N_1 + i_1\left(R(\sum_{l=2}^{L} N_l)\prod_{q=2}^{L} N_q + N_3K + KN_2\right)}{R^2N_1 + 2R(\sum_{l=2}^{L} N_l)\prod_{q=2}^{L} N_q K}, \tag{3.70}$$

$$O_5 = \frac{O_{ALS}}{O_{THOSVD}} = \frac{i_2\left(R(N_1^3((\sum_{l=2}^{L} N_l)\prod_{q=2}^{L} N_q)^3 + N_1^3N_3^3K^3 + N_1^3N_2^3K^3)\right)}{R^2N_1 + \left((\sum_{l=2}^{L} N_l)\prod_{q=2}^{L} N_q\right)^2 K + KR(\sum_{l=2}^{L} N_l)\prod_{q=2}^{L} N_q}, \tag{3.71}$$

$$O_6 = \frac{O_{ALS}}{O_{rank-oneALS}} = \frac{i_2\left(R(N_1^3((\sum_{l=2}^{L} N_l)\prod_{q=2}^{L} N_q)^3 + N_1^3N_3^3K^3 + N_1^3N_2^3K^3)\right)}{R^2N_1 + i_1\left(R(\sum_{l=2}^{L} N_l)\prod_{q=2}^{L} N_q + N_3K + KN_2\right)}. \tag{3.72}$$

where $i_1$ and $i_2$ are the average numbers of iterations for convergence of the rank-one ALS and ALS algorithms, respectively. Figure 17 shows the complexity ratios $O_1$, $O_2$, $O_3$ and $O_4$, while Figure 18 presents the complexity ratios $O_5$ and $O_6$. In both figures, the complexity ratios are calculated using average values for $i_1$ and $i_2$ obtained from all the Monte Carlo runs and considering the variation of the number of data streams/ transmit antennas $R \in \{4,12\}$. From Figures 17 and 18, we can note that even as the number of data streams/ transmit antennas increases, the complexities considered in $O_1$, $O_4$, $O_5$ and $O_6$ are linear, while the complexities considered in $O_2$ and $O_3$ decreases as $R$ increases. Also note that the complexity ratios $O_5$ and $O_6$ present the highest complexity ratios and is due that they are in a separate figure. The KRF-KRF is much less computationally demanding than the other algorithms because besides being a closed-form algorithm, also divides the problems into two steps to estimate separately the channel and symbol matrices, unlike the other algorithms, such that $O_{ALS} >> O_{THOSVD} >> O_{KRF} >> O_{rank-oneALS} >> O_{KRF-KRF}$.

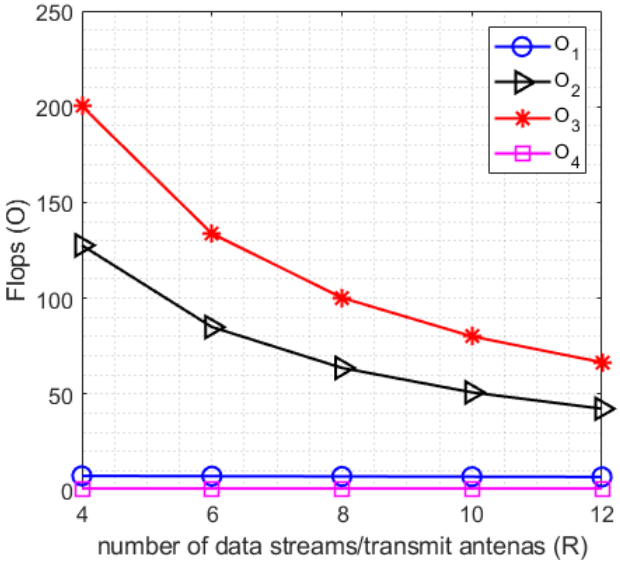


Figure 17 – Complexity ratio of KRF, KRF-KRF, Rank-one ALS and THOSVD receivers.

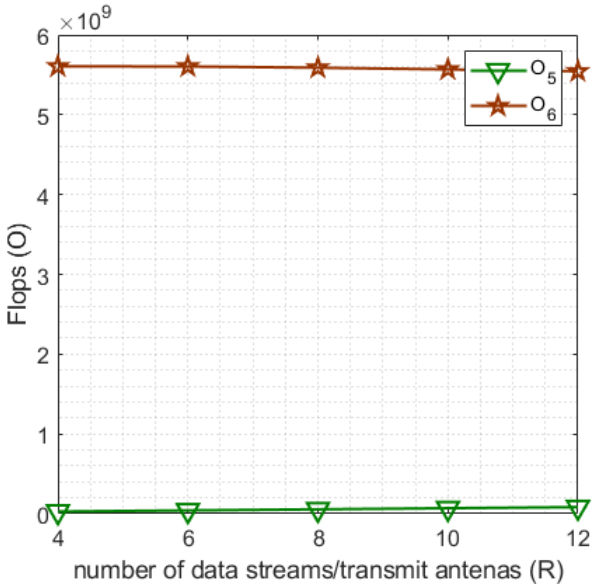


Figure 18 – Complexity ratio of Rank-one ALS, THOSVD and ALS receivers.

## 3.5 Chapter summary

In this chapter, we have presented a particular case of MKRST coding where the pre-coding matrix corresponds to a symbol matrix that is assumed known. Based on the coded symbols, a new received signal model is proposed. This coding provides extra space diversity through the multiple Khatri-Rao product of the symbol matrices. On the other hand, there is a decrease in the transmission rate, as shown. The contributions of this chapter extend previous works in different ways, either by using new coding, by extending to a newly received signal tensor, or by different estimation algorithms.

By exploiting the proposed received signal tensor model, we have derived five semi-

blind receivers and the identifiability conditions for each receiver. These receivers are based on closed-form and iterative algorithms. They allow to jointly estimate the channel and the symbol matrices without channel knowledge since one symbol matrix $\mathbf{S}^{(1)}$ is known. Besides, for the symbol estimation, a ZF receiver was considered to evaluate the impact of design parameters on the performance of the systems.

Simulation results have shown the performance of the proposed receivers for the new point-to-point MIMO system. The receivers are efficient in jointly estimating the channel and the symbol matrices, especially when they are based on closed-form solutions. The results for MKRST coding demonstrate that an increase in the number of data streams or the number of receiver antennas significantly improves the performance in terms of SER.

# 4 Semi-blind receivers for two-hop MIMO relay communication system with TSTF-MSMKron Coding

*In this chapter, first a bibliographic overview of multi-hop MIMO relay systems is presented. Then one of the main original contributions of this thesis is introduced. In particular, a new coding scheme based on multiple Kronecker products of symbol matrices called multiple symbol matrices Kronecker (MSMKron) coding is presented. MSMKron coding does not have a pre-coding matrix but provides extra diversity due to multiple Kronecker products of symbol matrices. Associated with the MSMKron coding is applied a TSTF coding at each hop, namely TSTF-MSMKron. Based on TSTF-MSMKron coding, a new two-hop OFDM-CDMA MIMO system is presented by the generalized Tucker decomposition, in which the source and relay use the proposed coding to code the signals to be transmitted. The protocol is the decode-forward (DF), where the signals are transmitted, estimated and retransmitted at the relay.*

*By exploiting the tensor model of the received signals and assuming the codings tensors known at each hop, two semi-blind receivers are derived to jointly estimate the transmitted symbols and the channels. The proposed receivers are semi-blind since we have no channel knowledge and only one symbol of each symbol matrix should be known. For each receiver, the identifiability conditions and computational complexities are established. Note that unlike almost all relay systems existing in the literature that use the AF protocol, the proposed two-hop system uses the DF protocol at the relay, which greatly facilitates its generalization to the multi-hop case.*

*Monte Carlo simulation results are provided to illustrate the performance of the TSTF-MSMKron coding, the impact of design parameters on the system performance and the behavior of the proposed receivers in terms of SER and NMSE.*

## 4.1 Overview on multi-hop MIMO systems

Cooperative MIMO systems were introduced by Meulen in 1971 [85], in which a cooperative channel was used to transmit information from the source to the destination. These systems are based on the exploitation of users or fixed stations as retransmitters (relays) of the signal coming from other users. On the other hand, all the involved nodes can be used as relays of the signal transmitted by the source. The repetition of the signal sent by the source through the relay allows the extension of the coverage area, amplifying the signal power that arrives at the destination, yielding significant gains in the capacity and

performance of the system [22].

Relaying protocols are techniques that define how the relays process the signal to be retransmitted. In literature, many relay processing protocols can be found in [86, 87]. The protocols can be divided into fixed and selective relaying schemes [87]. For the fixed relaying schemes the protocol used at the relay node is independent of the quality of the channel. For selective relaying schemes, the SNR (signal-noise ratio) of the received signal at the relay node is taken into account. In selective relaying schemes, a single relay or multiple relays are selected to collaborate on information transmission, where the relay selection could be based on distance information or instantaneous channel gains [88]. Most existing results on these schemes focus on the multiplexing diversity tradeoff analysis, where a fixed power level is assumed at the source and relays [89]. Fixed relaying schemes protocols are namely amplify-and-forward (AF) and decode-and-forward (DF). For AF protocol, also known as a non-regenerative protocol, the relay receives the signal from the source and amplifies it. This protocol is attractive for systems that consider constant channels, due to its simplicity. The use of the AF protocol is more frequent in cases when the relay is closer to the destination than the source to compensate for the fading. DF protocol, known as a regenerative protocol, consists of decoding the signal at the relay, and re-transmit to the destination. It is possible to apply coding at the relay node before retransmitting the signal [87, 90].

Cooperative MIMO systems provide spatial diversity and spatial multiplexing due to the use of multiple antennas to transmit and receive signals at each node of the systems. However, individual channel estimation in a cooperative MIMO system is a fundamental problem to solve, since the reliability of the system greatly depends on the accuracy of channel state information (CSI) in each hop [91]. During the last two decades, tensor models have been widely used for designing wireless communication systems [14, 15]. In the context of cooperative systems, some works are dedicated to the use of a training sequence for estimating the channels in a supervised way, as in [92, 93]. Such supervised systems are bandwidth-consuming, which explains the development of semi-blind receivers to jointly estimate the transmitted information symbols and the channels, i.e., without the use of training sequences, such as in the case for the systems briefly introduced below.

Many works combine cooperative MIMO systems with different space/time/frequency codings to increase system diversity and obtain better performance in terms of channel and symbol estimation. Among the used codings, one can mention the Khatri–Rao space–time (KRST) coding [20, 94, 21, 45], the multiple Khatri–Rao and Kronecker space–time (MKRST and MKronST) codings [33, 19], the TST [55, 95, 49] and TSTF codings [35]. Depending on the coding chosen for the relay system, different tensor models are obtained for the signals received at the relay and destination nodes. An exploitation of these models makes it possible to derive two families of receivers. One is made up of the most common receivers based on iterative algorithms such as ALS or the LM method. The other is composed

of closed-form algorithms based on SVD calculation, such as Khatri–Rao and Kronecker factorization algorithms, which are denoted KRF and KronF respectively. In Table 17, the tensor-based MIMO cooperative systems of the above cited references are compared in terms of the number of hops, coding, tensor model, and receiver, with the proposed MIMO relay system, which is referenced as “Proposed” in Table 17.

Table 17 – Tensor-based MIMO cooperative systems.

| Ref. | System Types | Codings | Tensor Models | Receivers |
|---|---|---|---|---|
| [94] | two-hop | KRST | PARAFAC/ PARATUCK | ALS |
| [20] | two-hop | KRST | nested PARAFAC | ALS |
| [21] | two-hop | KRST | nested PARAFAC | KRF |
| [17] | two-hop | TST | nested Tucker | ALS-KronF |
| [33] | two-hop | MKRST/MKronST | nested PARAFAC | KRF/KronF |
| [95] | two-hop | TST | coupled nested Tucker | KronF |
| [49] | three-hop | TST + PARAFAC | nested Tucker | coupled SVD/ALS |
| [25] | three-hop | KRST | nested PARAFAC | ALS/KRF |
| [23] | multi-hop | TST | high-order nested Tucker | KronF |
| [45] | multi-hop | KRST | nested PARAFAC | KRF |
| Proposed [91] | two-hop | TSTF-MSMKron | generalized Tucker | ALS-KronF/THOSVD |

Note that all systems presented in Table 17 consider an AF protocol at the relays except the system in [33] for which the AF protocol is compared with the DF and EF ones, showing that the use of these last two protocols allows significantly improving the SER performance at the cost of an additional computational complexity at the relay. From a coding point of view, the KRST coding was first used in [94, 20, 21] for a two-hop system and then in [45] for a multi-hop system. In [25], KRST coding is combined with a rotation coding matrix for a three-hop system. The TST coding initially proposed in [55], in the context of point-to-point systems, was used for a two-hop system in [17], leading to a new tensor model called nested Tucker decomposition and then for a multi-hop system in [23]. In this last reference, a new tensor model based on the nested Tucker decomposition was introduced. In [95], TST coding is used in a two-hop multi-relay system where the relays directly and sequentially communicate with the destination node. The sequential transmission from the relays to the destination leads to a new coupled nested Tucker model. In [49], TST coding

is combined with a PARAFAC coding structure for a two-half-duplex relay system. Two new codings, denoted MKRST and MKronST, were proposed in [33] for a two-hop system, leading to a nested PARAFAC model for the tensor of signals received at the destination which is exploited to develop closed-form semi-blind receivers for joint symbol and channel estimation.

An important difference between the systems in Table 17 and the system presented here concerns the a priori information needed to eliminate scaling ambiguities. Thus, the proposed system only requires a priori knowledge of one symbol of the symbol matrices, whereas all the systems in Table 17 also require knowledge of one entry or of one row of the channel matrices, which is a much more restrictive assumption [91]. Based on that, this chapter proposes a new two-hop OFDM-CDMA MIMO relay system that combines a TSTF coding with a MSMKron at the source and relay nodes. This new coding scheme, called TSTF-MSMKron coding, can be viewed as a generalization of the codings proposed in [33, 35], with the aim of increasing the diversity gain [91].

## 4.2 System model

### 4.2.1 Presentation of the proposed two-hop system

Consider a two-hop MIMO OFDM-CDMA system, as illustrated in Figure 19 and presented in [91]. This system is equipped with $M_S$, $M_R$ and $M_D$ antennas at the source, relay and destination nodes, respectively. The source-relay ($\mathcal{H}^{(SR)} \in \mathbb{C}^{M_R \times M_S \times F}$) and relay-destination ($\mathcal{H}^{(RD)} \in \mathbb{C}^{M_D \times M_R \times F}$) channels are assumed to be flat Rayleigh fading, which is represented by third-order tensors whose coefficients are zero-mean circularly symmetric complex Gaussian i.i.d. (independent and identically distributed) random variables, constant during at least $P$ transmission blocks.

The DF protocol is considered at the relay, and the transmission occurs in two hops. During the first one, the coded symbols are transmitted by the source to the relay via the channel $\mathcal{H}^{(SR)}$ and decoded at the relay. During the second one, the estimated symbols are re-encoded and then re-transmitted by the relay to the destination via the channel $\mathcal{H}^{(RD)}$. Each symbol matrix $\mathbf{S}^{(l)} = [s^{(l)}_{n_l,r_l}] \in \mathbb{C}^{N_l \times R_l}$, with $r_l \in \{1, R_l\}$, $n_l \in \{1, N_l\}$, for $l \in \{1, L\}$, is composed of $R_l$ data streams, each one containing $N_l$ information symbols. The transmission protocol is detailed in the next section which defines the TSTF-MSMKron coding. Then, in sections 4.2.3 and 4.2.4, the tensors of signals received at the relay and the destination will be described, respectively.

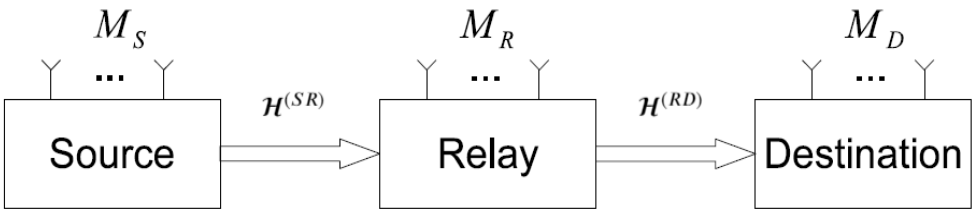


Figure 19 – Block diagram of the two-hop MIMO relay system.

### 4.2.2 TSTF-MSMKron coding

In the proposed system, the coding at the source node is composed of two steps. During the first one, a multiple Kronecker product of $L$ symbol matrices is calculated as:

$$\mathbf{S} = \otimes_{l=1}^{L} \mathbf{S}^{(l)} \triangleq \mathbf{S}^{(1)} \otimes \ldots \otimes \mathbf{S}^{(L)} \in \mathbb{C}^{N \times R}, \tag{4.1}$$

where $N = \prod_{l=1}^{L} N_l$, and $R = \prod_{l=1}^{L} R_l$. The scalar form of (4.1) is:

$$s_{n,r} = \prod_{l=1}^{L} s_{n_l,r_l}^{(l)}, \;\; n \in \{1,N\}, \;\; r \in \{1,R\}, \tag{4.2}$$

with $n = n_L^{(L)} + \left(n_{L-1}^{(L-1)} - 1\right) N_L + \cdots + \left(n_1^{(1)} - 1\right) \prod_{l=2}^{L} N_l$, and $r = r_L^{(L)} + \left(r_{L-1}^{(L-1)} - 1\right) R_L + \cdots + \left(r_1^{(1)} - 1\right) \prod_{l=2}^{L} R_l$, where $n_l^{(l)} \in \{1, N_l\}$, and $r_l^{(l)} \in \{1, R_l\}$ denote the indices $n_l$ and $r_l$ in $s_{n_l,r_l}^{(n)}$. This operation, called MSMKron coding, corresponds to a simplified version of the MKronST coding [33] without a known precoding matrix. This coding is called multiple symbol matrices Kronecker (MSMKron) coding and induces time and code spreadings of each symbol $s_{n_l,r_l}^{(l)}$ due to the multiple Kronecker product of the symbol matrix $\mathbf{S}^{(l)}$ with the other matrices $\mathbf{S}^{(l')}$ ,$l' = 1, ..., L$ and $l' \neq l$.

The transmission being composed of $P$ time-slots means each symbol $s_{n_l,r_l}^{(l)}$ is repeated $P\Big(\prod_{\substack{l'=1 \\ l' \neq l}}^{L} N_{l'}\Big)\Big(\prod_{\substack{l'=1 \\ l' \neq l}}^{L} R_{l'}\Big)$ times, which implies an increase of time and code diversities when increasing the dimensions $N_l$ and $R_l$, respectively.

During the second step, the MSMKron coding is combined with a tensor space-time-frequency (TSTF) coding [35] carried out by means of the $(L+3)$-order tensor $\mathcal{G}^{(S)} \in \mathbb{C}^{M_S \times R_1 \times \ldots \times R_L \times F \times P}$ in such a way that the tensor of signals coded at the source satisfies an $(L+3)$-order Tucker model given by:

$$\mathcal{V}^{(S)} = \mathcal{G}^{(S)} \times_1 \mathbf{I}_{M_S} \times_2 \mathbf{S}^{(1)} \times_3 \ldots \times_{L+1} \mathbf{S}^{(L)} \times_{L+2} \mathbf{I}_F \times_{L+3} \mathbf{I}_P \in \mathbb{C}^{M_S \times N_1 \times \ldots \times N_L \times F \times P}. \tag{4.3}$$

Note that the core tensor of this decomposition is the coding tensor $\mathcal{G}^{(S)}$. In scalar notation, the coded signals transmitted by the $m_S^{th}$ antenna at the source, using the $f^{th}$

subcarrier, during the $p^{th}$ time slot are given by:

$$v^{(S)}_{m_S,n_1,\ldots,n_L,f,p} = \sum_{r_1=1}^{R_1} \cdots \sum_{r_L=1}^{R_L} g^{(S)}_{m_S,r_1,\ldots,r_L,f,p} \prod_{l=1}^{L} s^{(l)}_{n_l,r_l}, \tag{4.4}$$

where $m_S \in \{1,M_S\}$, $f \in \{1,F\}$, $p \in \{1,P\}$. The TSTF-MSMKron coding increases space-time-frequency diversity, as will be illustrated in the simulations.

### 4.2.3 Tensor of signals received at the relay

In the noise-free case and assuming a flat Rayleigh fading propagation channel, the signal $x^{(SR)}_{m_R,n_1,\ldots,n_L,f,p}$ received at the $m_R^{th}$ antenna of the relay, during the $n_l^{th}$ symbol period of the $p^{th}$ block and associated with the $f^{th}$ subcarrier, is given by:

$$x^{(SR)}_{m_R,n_1,\ldots,n_L,f,p} = \sum_{m_S=1}^{M_S} h^{(SR)}_{m_R,m_S,f} v^{(S)}_{m_S,n_1,\ldots,n_L,f,p}, \tag{4.5}$$

where $m_R \in \{1,M_R\}$ and $h^{(SR)}_{m_R,m_S,f}$ is an entry of the channel $\mathcal{H}^{(SR)} \in \mathbb{C}^{M_R \times M_S \times F}$. In terms of mode-$n$ products, we have:

$$\mathcal{X}^{(SR)} = \mathcal{V}^{(S)} \times_1 \mathcal{H}^{(SR)} \in \mathbb{C}^{M_R \times N_1 \times \ldots \times N_L \times F \times P}. \tag{4.6}$$

Note that the transmission via channel $\mathcal{H}^{(SR)}$ can be interpreted as a mode-1 linear transformation applied to the tensor $\mathcal{V}^{(S)}$ of coded signals. Substituting (4.4) into (4.5) gives the signal received at the relay written in a scalar form as:

$$x^{(SR)}_{m_R,n_1,\ldots,n_L,f,p} = \sum_{m_S=1}^{M_S} \sum_{r_1=1}^{R_1} \cdots \sum_{r_L=1}^{R_L} g^{(S)}_{m_S,r_1,\ldots,r_L,f,p} h^{(SR)}_{m_R,m_S,f} \prod_{l=1}^{L} s^{(l)}_{n_l,r_l}. \tag{4.7}$$

The signals received at the relay form the tensor $\mathcal{X}^{(SR)}$ that satisfies a generalized Tucker-$(L+1, L+3)$ model given by:

$$\mathcal{X}^{(SR)} = \mathcal{G}^{(S)} \times_1 \mathcal{H}^{(SR)} \times_2 \mathbf{S}^{(1)} \times_3 \ldots \times_{L+1} \mathbf{S}^{(L)} \times_{L+2} \mathbf{I}_F \times_{L+3} \mathbf{I}_P, \tag{4.8}$$

where $\mathbf{S}^{(l)}$ represents the symbol matrices encoded by the TSTF-MSMKron coding for $l \in \{1, L\}$ and $\mathcal{G}^{(S)}$ is the core tensor of the Tucker model. As it is well known, knowledge of the core tensor implies the uniqueness of this model. Combining modes 2 to $L+1$ of tensors $\mathcal{G}^{(S)}$ and $\mathcal{X}^{(SR)}$ results in contracted forms $\mathcal{G}^{(S)}_c \in \mathbb{C}^{M_S \times R \times F \times P}$ and $\mathcal{X}^{(SR)}_c \in \mathbb{C}^{M_R \times N \times F \times P}$, and Eq.(4.8) can be rewritten as:

$$\mathcal{X}^{(SR)}_c = \mathcal{G}^{(S)}_c \times_1 \mathcal{H}^{(SR)} \times_2 \mathbf{S} \times_3 \mathbf{I}_F \times_4 \mathbf{I}_P. \tag{4.9}$$

From the Tucker model (4.9), it is easy to deduce the following matrix unfoldings of the tensor $\mathcal{X}^{(SR)}$:

$$\mathbf{X}^{(SR)}_{FPN \times M_R} = (\mathbf{I}_{FP} \otimes \mathbf{S})\, \mathbf{G}^{(S)}_{FPR \times FM_S} \mathbf{H}^{(SR)}_{FM_S \times M_R} \in \mathbb{C}^{FPN \times M_R}, \tag{4.10}$$

$$\mathbf{X}^{(SR)}_{PFM_R\times N} = \left(\mathbf{I}_P \otimes \text{bdiag}\left(\mathbf{H}^{(SR)}_{..f}\right)\right)\mathbf{G}^{(S)}_{PFM_S\times R}\mathbf{S}^T \in \mathbb{C}^{PFM_R\times N}, \tag{4.11}$$

$$\mathbf{X}^{(SR)}_{M_RN\times FP} = \left(\mathbf{H}^{(SR)}_{M_R\times FM_S} \otimes \mathbf{S}\right)\mathbf{G}^{(S)}_{FM_SR\times FP} \in \mathbb{C}^{M_RN\times FP}, \tag{4.12}$$

with $\mathbf{H}^{(SR)}_{..f} \in \mathbb{C}^{M_R\times M_S}$ and bdiag(.) previously defined in the notation. Note that the identity matrix $\mathbf{I}_{FP} \in \mathbb{R}^{FP\times FP}$ in (4.10) is associated with $FP$ repetitions of the symbol matrices inducing time-frequency diversity for the system.

The block structure of the matrix unfoldings $\mathbf{G}^{(S)}_{FPR\times FM_S}$ and $\mathbf{G}^{(S)}_{FM_SR\times FP}$ in Eqs.(4.10) and (4.12), respectively, is defined as follows:

$$\mathbf{G}^{(S)}_{FPR\times FM_S} = \text{bdiag}\left[\begin{array}{ccc}\text{vec}(\mathcal{G}^{(S)}_{1..f.}) & \ldots & \text{vec}(\mathcal{G}^{(S)}_{M_S..f.})\end{array}\right] = \text{bdiag}\left(\left[\mathbf{G}^{(S)}_{PR\times M_S}\right]_f\right), \tag{4.13}$$

$$\mathbf{G}^{(S)}_{FM_SR\times FP} = \text{bdiag}\left[\begin{array}{ccc}\text{vec}(\mathcal{G}^{(S)}_{...f1}) & \ldots & \text{vec}(\mathcal{G}^{(S)}_{...fP})\end{array}\right] = \text{bdiag}\left(\left[\mathbf{G}^{(S)}_{M_SR\times P}\right]_f\right). \tag{4.14}$$

$\mathbf{G}^{(S)}_{FPR\times FM_S}$ in Eq.(4.13) is a block-diagonal matrix, formed of $F$ diagonal blocks of dimension $PR \times M_S$, each block being formed of $M_S$ column vectors corresponding to a vectorized form of the tensor slice $\mathcal{G}^{(S)}_{m_S..f.}$ of size $R_1 \times \ldots \times R_L \times P$, for $m_S \in \{1, M_S\}$, such that $\text{vec}(\mathcal{G}^{(S)}_{m_S..f.}) \in \mathbb{C}^{PR}$. Similarly, $\mathbf{G}^{(S)}_{FM_SR\times FP}$ in (4.14) is a block-diagonal matrix whose diagonal blocks are of dimension $M_SR \times P$, with $\text{vec}(\mathcal{G}^{(S)}_{...fp}) \in \mathbb{C}^{M_SR}$.

To illustrate the matrix unfolding (4.14), consider the case where $R = P = M_S = F = 2$, leading to the following matrix:

$$\mathbf{G}^{(S)}_{FM_SR\times FP} = \begin{bmatrix} g^{(S)}_{1111} & g^{(S)}_{1112} & 0 & 0 \\ g^{(S)}_{2111} & g^{(S)}_{2112} & 0 & 0 \\ g^{(S)}_{1211} & g^{(S)}_{1212} & 0 & 0 \\ g^{(S)}_{2211} & g^{(S)}_{2212} & 0 & 0 \\ 0 & 0 & g^{(S)}_{1121} & g^{(S)}_{1122} \\ 0 & 0 & g^{(S)}_{2121} & g^{(S)}_{2122} \\ 0 & 0 & g^{(S)}_{1221} & g^{(S)}_{1222} \\ 0 & 0 & g^{(S)}_{2221} & g^{(S)}_{2222} \end{bmatrix}. \tag{4.15}$$

### 4.2.4 Tensor of signals received at the destination

With the DF protocol, the symbols received at the relay are first decoded by means of one of the receivers described in Section 4.3, leading to the estimated symbol matrices $\hat{\mathbf{S}}^{(l)}$, which are also written as $\mathbf{S}^{(l)}_R$. The estimated symbols are then re-encoded at the relay using a TSTF-MSMKron coding, with the tensor coding $\mathcal{G}^{(R)} \in \mathbb{C}^{M_R\times R_1\times\ldots\times R_L\times F\times P}$. The re-encoded signals are transmitted by the relay to the destination via the channel $\mathcal{H}^{(RD)} \in \mathbb{C}^{M_D\times M_R\times F}$. The signals received at the destination are similar to the signals received at the relay, defined by Eqs. (4.7) and (4.8), with the following correspondences:

$$\left(\mathcal{G}^{(S)}, \mathcal{H}^{(SR)}, \mathbf{S}^{(l)}\right) \leftrightarrow \left(\mathcal{G}^{(R)}, \mathcal{H}^{(RD)}, \mathbf{S}^{(l)}_R\right), \tag{4.16}$$

$$(M_R, M_S) \leftrightarrow (M_D, M_R), \tag{4.17}$$

Similar to (4.7), in the noiseless case, the signal received at the $m_D^{th}$ antenna of the destination node, during the $n_l^{th}$ symbol period of the $p^{th}$ time block and associated with the $f^{th}$ subcarrier, is given by:

$$x^{(RD)}_{m_D,n_1,\ldots,n_L,f,p} = \sum_{m_R=1}^{M_R} \sum_{r_1=1}^{R_1} \cdots \sum_{r_L=1}^{R_L} g^{(R)}_{m_R,r_1,\ldots,r_L,f,p} h^{(RD)}_{m_D,m_R,f} \prod_{l=1}^{L} [s_R^{(l)}]_{n_l,r_l}, \tag{4.18}$$

and the generalized Tucker-$(L+1, L+3)$ model (4.7) becomes:

$$\mathcal{X}^{(RD)} = \mathcal{G}^{(R)} \times_1 \mathcal{H}^{(RD)} \times_2 \mathbf{S}_R^{(1)} \times_3 \ldots \times_{L+1} \mathbf{S}_R^{(L)} \times_{L+2} \mathbf{I}_F \times_{L+3} \mathbf{I}_P, \tag{4.19}$$

where $\mathcal{X}^{(RD)} \in \mathbb{C}^{M_D \times N_1 \times \ldots \times N_L \times F \times P}$. Matrix unfoldings of this tensor can be deduced from (4.10)-(4.12) using the correspondences (4.16)-(4.17) with $\mathbf{G}^{(R)}_{PFM_R \times R}$, $\mathbf{G}^{(R)}_{FPR \times FM_R}$ and $\mathbf{G}^{(R)}_{FM_R R \times FP}$ instead of $\mathbf{G}^{(S)}_{PFM_S \times R}$, $\mathbf{G}^{(S)}_{FPR \times FM_S}$ and $\mathbf{G}^{(S)}_{FM_S R \times FP}$, respectively.

Combining the modes 2 to $L+1$ of tensors $\mathcal{G}^{(R)}$ and $\mathcal{X}^{(RD)}$ results in contracted forms $\mathcal{G}_c^{(R)} \in \mathbb{C}^{M_R \times R \times F \times P}$ and $\mathcal{X}_c^{(RD)} \in \mathbb{C}^{M_D \times N \times F \times P}$, and Eq.(4.8) can be rewritten as:

$$\mathcal{X}_c^{(RD)} = \mathcal{G}_c^{(R)} \times_1 \mathcal{H}^{(RD)} \times_2 \mathbf{S}_R \times_3 \mathbf{I}_F \times_4 \mathbf{I}_P. \tag{4.20}$$

From the Tucker model (4.20), it is easy to deduce the following matrix unfoldings of the tensor $\mathcal{X}^{(RD)}$:

$$\mathbf{X}^{(RD)}_{FPN \times M_D} = (\mathbf{I}_{FP} \otimes \mathbf{S}_R)\, \mathbf{G}^{(S)}_{FPR \times FM_R} \mathbf{H}^{(RD)}_{FM_R \times M_D} \in \mathbb{C}^{FPN \times M_D}, \tag{4.21}$$

$$\mathbf{X}^{(RD)}_{PFM_D \times N} = \left(\mathbf{I}_P \otimes \text{bdiag}\left(\mathbf{H}^{(RD)}_{..f}\right)\right) \mathbf{G}^{(R)}_{PFM_R \times R} \mathbf{S}_R^T \in \mathbb{C}^{PFM_D \times N}, \tag{4.22}$$

$$\mathbf{X}^{(RD)}_{M_D N \times FP} = \left(\mathbf{H}^{(RD)}_{M_D \times FM_R} \otimes \mathbf{S}_R\right) \mathbf{G}^{(R)}_{FM_R R \times FP} \in \mathbb{C}^{M_D N \times FP}, \tag{4.23}$$

with $\mathbf{H}^{(RD)}_{..f} \in \mathbb{C}^{M_D \times M_R}$, and bdiag(.) previously defined in the notation. The proposed OFDM-CDMA relaying system is illustrated by means of the block diagram in Figure 20. The system design parameters and the definitions of the system matrices and tensors are summarized in Tables 18 and 19, respectively.

Table 18 – System design parameters.

| System design parameters | Definitions |
|---|---|
| $L$ | number of symbol matrices |
| $R_l$ | number of data streams in $\mathbf{S}^{(l)}$ |
| $N_l$ | number of symbols in the $R_l^{th}$ data stream |
| $F$ | number of subcarriers |
| $P$ | number of time blocks |
| $M_S$ | number of antennas at the source |
| $M_R$ | number of antennas at the relay |
| $M_D$ | number of antennas at the destination |

Table 19 – System matrices and tensors.

| **Symbol matrices** |
|---|
| $\mathbf{S}^{(l)} \in \mathbb{C}^{N_l \times R_l}$, for $l \in \{1, L\}$ |
| $\mathbf{S} = \mathbf{S}^{(1)} \otimes ... \otimes \mathbf{S}^{(L)} \in \mathbb{C}^{N \times R}$ |
| $N = \prod_{l=1}^{L} N_l$, $R = \prod_{l=1}^{L} R_l$ |
| **Channel tensors** |
| $\mathcal{H}^{(SR)} \in \mathbb{C}^{M_R \times M_S \times F}$ |
| $\mathcal{H}^{(RD)} \in \mathbb{C}^{M_D \times M_R \times F}$ |
| **Space-time-frequency coding tensors** |
| $\mathcal{G}^{(S)} \in \mathbb{C}^{M_S \times R_1 \times ... \times R_L \times F \times P}$ |
| $\mathcal{G}^{(R)} \in \mathbb{C}^{M_R \times R_1 \times ... \times R_L \times F \times P}$ |
| **Received signals tensors** |
| $\mathcal{X}^{(SR)} \in \mathbb{C}^{M_R \times R_1 \times ... \times R_L \times F \times P}$ |
| $\mathcal{X}^{(RD)} \in \mathbb{C}^{M_D \times R_1 \times ... \times R_L \times F \times P}$ |

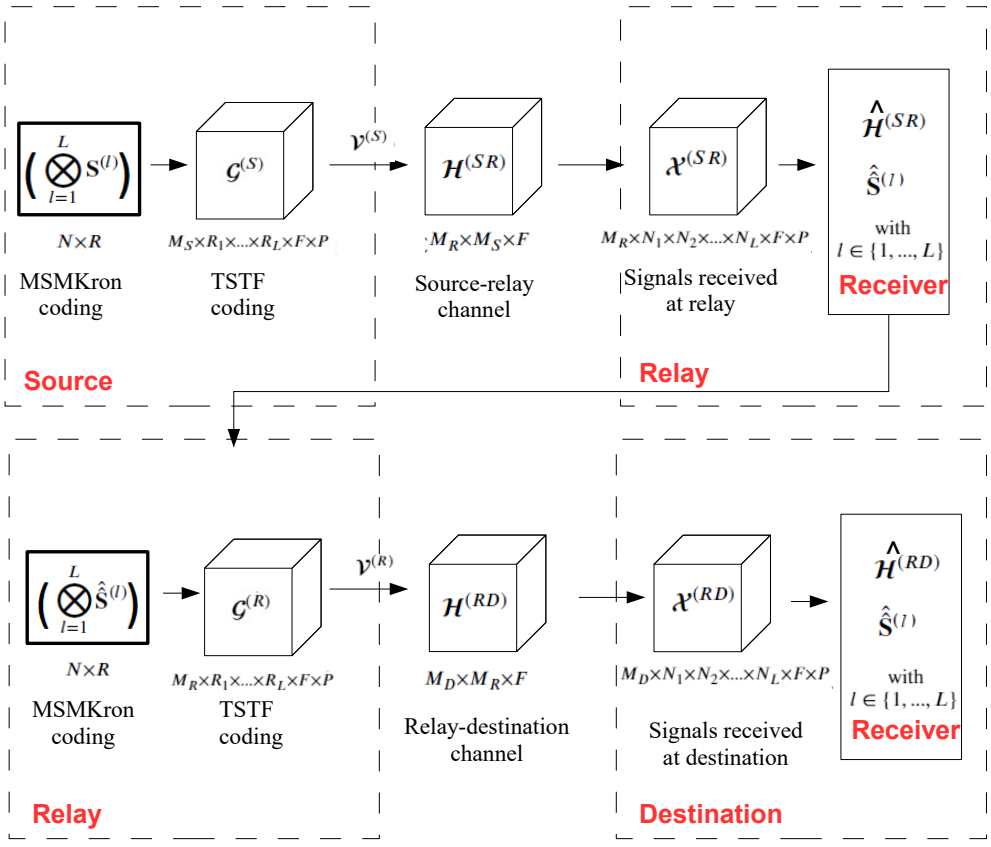


Figure 20 – Block diagram of the proposed two-hop MIMO OFDM-CDMA communication system.

### 4.2.5 Comparison with other MIMO systems using coding tensors

In Table 20, we present several tensor-based MIMO systems using coding in a unified way. From this Table, we can conclude that:

- The proposed TSTF-MSMKron coding extends the TSTF coding presented in [35], combining TSTF and MSMKron codings and not considering allocation tensors. MSMKron coding adds diversity to the system by the multiple Kronecker products of the symbol matrices.
- The TSTF-MSMKron coding can be viewed as a CDMA extension of the STF coding in [83], where the STF uses only a bi-dimensional coding.
- The TSTF-MSMKron coding can also be viewed as an OFDM extension of the TST system [55] with a combination of a TSTF with the MSMKron instead of a third-order tensor coding.

Table 20 – Comparison of tensor-based systems.

| Coding | Channel | Coding | Tensor model | Ref. |
|---|---|---|---|---|
| **TSTF-MSMKron** | $\mathcal{H} \in \mathbb{C}^{M_R \times M_S \times F}$<br>$\mathcal{H} \in \mathbb{C}^{M_R \times M_S \times F}$ | $\mathcal{G} \in \mathbb{C}^{M_S \times R \times F \times P}$<br>$\mathbf{S} = \otimes_{l=1}^{L} \mathbf{S}^{(l)} \in \mathbb{C}^{N \times R}$ | generalized Tucker-$(L+1,L+3)$ | proposed system [91] |
| **TSTF** | $\mathcal{H} \in \mathbb{C}^{M_R \times M_S \times F}$ | $\mathcal{W} \in \mathbb{C}^{M_S \times R \times F \times P \times J}$ | generalized PARATUCK-(2,5) | [35] |
| **STF** | $\mathbf{H} \in \mathbb{C}^{M_R \times M_S}$ | $\mathbf{W} \in \mathbb{C}^{M_S \times R}$ | generalized PARATUCK-(2,4) | [83] |
| **TST** | $\mathbf{H} \in \mathbb{C}^{M_R \times M_S}$ | $\mathcal{W} \in \mathbb{C}^{M_S \times R \times J}$ | PARATUCK-(2,4) | [55] |
| **ST** | $\mathbf{H} \in \mathbb{C}^{M_R \times M_S}$ | $\mathbf{W} \in \mathbb{C}^{M_S \times R}$ | PARATUCK-2 | [96] |

## 4.3 Semi-blind receivers

In this section, as in [91], two semi-blind receivers are proposed to estimate the channel tensors and symbol matrices at the relay and destination nodes. We assume that the coding tensors $\mathcal{G}^{(S)}$ and $\mathcal{G}^{(R)}$ are known. We also assume that one symbol of each symbol matrix is known to eliminate scalar ambiguities. The symbol matrices $\mathbf{S}^{(l)}$ and the channel tensor $\mathcal{H}^{(SR)}$ are estimated at the relay, while the symbol matrices $\mathbf{S}_R^{(l)}$ and the channel tensor $\mathcal{H}^{(RD)}$ are estimated at the destination. The proposed receivers are detailed for the relay. The same receivers can be derived for the destination, using the correspondences (4.16) and (4.17). The first one is based on the ALS algorithm to estimate the channel and the Kronecker product of symbol matrices, which is followed by the KronF method to separate the symbol matrices, while the second one is a closed-form solution allowing to jointly estimate the channel and the symbol matrices through the THOSVD algorithm.

### 4.3.1 Bi-ALS-KronF receiver

In the first step, the bi-alternating least squares (Bi-ALS) algorithm is used to jointly estimate the MSMKron product $\mathbf{S}$ and the channel tensor $\mathcal{H}^{(SR)}$. Then, the KronF algorithm is applied to separate the symbol matrices. The Bi-ALS algorithm results from the minimization of the following cost function deduced from Eq.(4.9) [91] :

$$\min_{\mathbf{S},\mathcal{H}^{(SR)}} \| \mathcal{X}_c^{(SR)} - \mathcal{G}_c^{(S)} \times_1 \mathcal{H}^{(SR)} \times_2 \mathbf{S} \times_3 \mathbf{I}_F \times_4 \mathbf{I}_P \|_F^2, \tag{4.24}$$

The Bi-ALS method replaces the optimization problem (4.24) by two LS sub-problems deduced from the matrix unfoldings (4.10) and (4.11), leading to the alternate minimization of the following LS criteria:

$$\min_{\mathbf{H}^{(SR)}_{FM_S\times M_R}} \| \mathbf{X}^{(SR)}_{FPN\times M_R} - \left[ \left( \mathbf{I}_{FP} \otimes \hat{\mathbf{S}}_{[i-1]} \right) \mathbf{G}^{(S)}_{FPR\times FM_S} \right] \mathbf{H}^{(SR)}_{FM_S\times M_R} \|_F^2 \longrightarrow \hat{\mathbf{H}}^{(SR)}_{FM_S\times M_R[i]}, \tag{4.25}$$

$$\min_{\mathbf{S}} \| \mathbf{X}^{(SR)}_{PFM_R\times N} - \left( \mathbf{I}_P \otimes \text{bdiag}\left( \hat{\mathbf{H}}^{(SR)}_{..f[i]} \right) \right) \mathbf{G}^{(S)}_{PFM_S\times R} \mathbf{S}^T \|_F^2 \longrightarrow \hat{\mathbf{S}}^T_{[i]}. \tag{4.26}$$

The update equations at iteration $[i]$ are given by:

$$\hat{\mathbf{H}}^{(SR)}_{FM_S\times M_R[i]} = \left[ \left( \mathbf{I}_{FP} \otimes \hat{\mathbf{S}}_{[i-1]} \right) \mathbf{G}^{(S)}_{FPR\times FM_S} \right]^{\dagger} \mathbf{X}^{(SR)}_{FPN\times M_R}, \tag{4.27}$$

$$\hat{\mathbf{S}}^T_{[i]} = \left[ \left( \mathbf{I}_P \otimes \text{bdiag}\left( \hat{\mathbf{H}}^{(SR)}_{..f[i]} \right) \right) \mathbf{G}^{(S)}_{PFM_S\times R} \right]^{\dagger} \mathbf{X}^{(SR)}_{PFM_R\times N}. \tag{4.28}$$

To simplify the computation of the estimate $\hat{\mathbf{H}}^{(SR)}_{FM_S\times M_R}$ in Eq.(4.27), we assume that the matrices $\left[ \mathbf{G}^{(S)}_{PR\times M_S} \right]_f$ and $\mathbf{S}$ have full column rank, which implies: $M_S \leq PR$ and $R \leq N$, respectively. Moreover, to simplify the computation of $\hat{\mathbf{S}}$ in Eq.(4.28), we assume that the unfolding $\mathbf{G}^{(S)}_{PFM_S\times R}$ is chosen as a full column rank truncated DFT matrix, which allows us to replace its pseudo-inverse by its transconjugate, implying the necessary condition: $R \leq PFM_S$. We also assume that $\mathcal{H}^{(SR)}_{..f}$ has full column rank, implying $M_S \leq M_R$. Exploiting these assumptions and substituting the unfolding $\mathbf{G}^{(S)}_{FPR\times FM_S}$ by Eq.(4.13) simplifies the LS estimates (4.27) and (4.28) as:

$$\hat{\mathbf{H}}^{(SR)}_{FM_S\times M_R[i]} = \text{bdiag}\left( \left[ \mathbf{G}^{(S)}_{PR\times M_S} \right]_f^{\dagger} \right) \left( \mathbf{I}_{FP} \otimes \hat{\mathbf{S}}^{\dagger}_{[i-1]} \right) \mathbf{X}^{(SR)}_{FPN\times M_R}, \tag{4.29}$$

$$\hat{\mathbf{S}}^T_{[i]} = \left( \mathbf{G}^{(S)}_{PFM_S\times R} \right)^H \left( \mathbf{I}_P \otimes \text{bdiag}\left( \hat{\mathbf{H}}^{(SR)\dagger}_{..f[i]} \right) \right) \mathbf{X}^{(SR)}_{PFM_R\times N}. \tag{4.30}$$

The Bi-ALS algorithms (4.29) and (4.30) are simplified versions of (4.27) and (4.28) in terms of pseudo-inverses computation at the price of additional constraints on the design parameters.

The error at the $[i]^{th}$ iteration, deduced from (4.10), is considered for deciding the convergence of the Bi-ALS algorithm:

$$err[i] = \| \mathbf{X}^{(SR)}_{FPN\times M_R} - \left(\mathbf{I}_{FP} \otimes \hat{\mathbf{S}}_{[i]}\right) \mathbf{G}^{(S)}_{FPR\times FM_S} \hat{\mathbf{H}}^{(SR)}_{FM_S\times M_R[i]} \|^2_F \, . \tag{4.31}$$

Convergence at the $[i]^{th}$ iteration is declared when this error does not significantly change between two successive iterations, i.e., $|err[i-1]-err[i]| \leq \epsilon$, where $\epsilon$ is a predefined threshold. Then, the symbol matrices $\mathbf{S}^{(l)}$ are then estimated by means of the KronF algorithm presented in Table 1, minimizing the following LS cost function:

$$\min_{\mathbf{S}^{(l)}, l\in\{1,L\}} \| \hat{\mathbf{S}} - \mathbf{S}^{(1)} \otimes \ldots \otimes \mathbf{S}^{(L)} \|^2_F \, . \tag{4.32}$$

After applying the KronF algorithm, the estimated symbol matrix $\hat{\mathbf{S}}^{(l)}$ is obtained by unvectorizing $\hat{\mathbf{s}}^{(l)}$ as:

$$\hat{\mathbf{S}}^{(l)} = \text{unvec}\left(\hat{\mathbf{s}}^{(l)}\right) \in \mathbb{C}^{N_l\times R_l}, \tag{4.33}$$

As mentioned previously, the Bi-ALS-KronF receiver at the destination can be deduced from the one at the relay, using the correspondences (4.16) and (4.17), to estimate the channel $\mathcal{H}^{(RD)} \in \mathbb{C}^{M_D\times M_R\times F}$ and the symbol matrices denoted $\mathbf{S}^{(l)}_R \in \mathbb{C}^{N_l\times R_l}$. To eliminate the scaling ambiguities in the second hop, we use the same relation (4.37) for the KronF algorithm. At each hop, the estimated symbols are obtained after a projection onto the symbol alphabet. The Bi-ALS-KronF algorithm is summarized in table 21.

*Identifiability conditions and ambiguity relations*

In the case of the Bi-ALS step, for the uniqueness of the pseudo-inverse, it is necessary that the matrices $\left[(\mathbf{I}_{FP} \otimes \mathbf{S})\, \mathbf{G}^{(S)}_{FPR\times FM_S}\right]$ and $\left[\left(\mathbf{I}_P \otimes \text{bdiag}\left(\mathbf{H}^{(SR)}_{..f}\right)\right) \mathbf{G}^{(S)}_{PFM_S\times R}\right]$ be full column rank to ensure uniqueness of the LS estimates, which implies the following necessary conditions:

$$M_S \leq PN \quad \text{and} \quad R \leq PFM_R. \tag{4.34}$$

In the case of the Bi-ALS-KronF algorithm, since the core tensor $\mathcal{G}^{(S)}$ is assumed to be known, there is no permutation ambiguity, and the generalized Tucker model (4.9) is unique up to scalar scaling ambiguities. The LS estimates $\hat{\hat{\mathbf{H}}}^{(SR)}_{FM_S\times M_R}$ and $\hat{\hat{\mathbf{S}}}$, at convergence, after correcting the ambiguities are given by:

$$\hat{\hat{\mathbf{S}}} = \hat{\mathbf{S}}\left(\lambda^{(S)}\right)^{-1}, \quad \hat{\hat{\mathbf{H}}}^{(SR)}_{FM_S\times M_R} = \hat{\mathbf{H}}^{(SR)}_{FM_S\times M_R}\left(\lambda^{(H)}\right)^{-1}, \text{ with } \lambda^{(S)}\lambda^{(H)} = 1. \tag{4.35}$$

For eliminating the scaling ambiguities in Bi-ALS step, it is sufficient to assume that one element of $\mathbf{S}$ is known a priori, e.g., $s_{11} = 1$. Under this assumption, $\lambda^{(S)}$ is calculated as:

$$\lambda^{(S)} = \hat{s}_{11}. \tag{4.36}$$

Considering the KronF step, we assume $s_{11}^{(l)} = 1$ and the scalar ambiguity is corrected by:

$$\hat{\mathbf{S}}^{(l)} = \hat{\mathbf{S}}^{(l)} \left(\hat{s}_{11}^{(l)}\right)^{-1}. \tag{4.37}$$

Table 21 – Bi-ALS-KronF receiver for estimation of the channels and symbol matrices.

**Bi-ALS-KronF receiver for estimating symbol matrices $\mathbf{S}^{(l)}$ and the channels $\mathcal{H}^{(SR)}$ and $\mathcal{H}^{(RD)}$.**

**Input:** tensors $\mathcal{X}^{(SR)}$, $\mathcal{X}^{(RD)}$, $\mathcal{G}^{(S)}$, $\mathcal{G}^{(R)}$
**Output:** Estimated symbol matrices and channels
**First hop: source - relay**
**- Step 1: Bi-ALS algorithm**
$it = 0$
1) Initialization of $\mathbf{S}^{(l)}[0]$ with symbols randomly drawn from the alphabet and $s_{11}^{(l)} = 1$, for $l \in \{1, L\}$.
2) Update the estimates of $\mathbf{H}^{(SR)}_{FM_S \times M_R}$ and $\mathbf{S}$ using Eqs.(4.27) and (4.28) or (4.29) and (4.30).
3) Calculate the error (4.31) and $|err[i-1] - err[i]|$.
-**if** $|err[i-1] - err[i]| \leq \epsilon$ or $it =$ maximum number of iterations
- **stop**
- **else** $it \rightarrow i + 1$;
4) Eliminate the scaling ambiguities using Eq.(4.35).

**- Step 2: KronF algorithm**
5) Build the rank-one tensor: $\hat{\hat{\mathcal{S}}} = \text{reshape}\left(\hat{\hat{\mathbf{S}}}, [R_1 N_1, ..., R_L N_L]\right)$.
6) Estimate each vector $\hat{\mathbf{s}}^{(l)}$ by means of the KronF algorithm recalled in Table 1, and unvectorize it using Eq.(4.33).
7) Eliminate the scaling ambiguities using Eq.(4.37).
8) Project the estimated symbols onto the symbol alphabet.

**Second hop: relay - destination**
**- Step 1: Bi-ALS algorithm**
- Apply the stages 1) to 4) of the first hop, using the correspondences (4.16) and (4.17).

**- Step 2: KronF algorithm**
- Apply the stages 5) to 8) of the first hop, using the correspondences (4.16) and (4.17).

### 4.3.2 THOSVD-based receiver

The THOSVD-based receiver is proposed to jointly estimate the channels and the symbol matrices. This closed-form solution can be viewed as a generalization of the KronF algorithm used to separate the symbol matrices. The difference is that we can now simultaneously estimate all the matrices $\left(\mathbf{H}^{(SR)}_{M_R \times FM_S}, \mathbf{S}^{(1)}, ..., \mathbf{S}^{(L)}\right)$. From the matrix unfolding (4.12),

with $\mathbf{S}$ and $\mathbf{G}^{(S)}_{FM_SR\times FP}$ replaced by their expressions (4.1) and (4.14), we deduce the following LS estimate of the multiple Kronecker product:

$$\mathbf{Z}^{(SR)} \triangleq \mathbf{H}^{(SR)}_{M_R\times FM_S} \widehat{\otimes \mathbf{S}^{(1)}} \otimes \ldots \otimes \mathbf{S}^{(L)} = \mathbf{X}^{(SR)}_{M_RN\times FP} \left[\text{bdiag}\left(\left[\mathbf{G}^{(S)}_{M_SR\times P}\right]^{\dagger}_{f}\right)\right], \tag{4.38}$$

with $\mathbf{Z}^{(SR)} \in \mathbb{C}^{M_RN\times FM_SR}$. The matrices $\mathbf{S}^{(l)}$ and $\mathbf{H}^{(SR)}_{M_R\times FM_S}$ are jointly estimated by means of the rank-one approximation-based KronF algorithm, described in Table 1. The THOSVD receiver at the destination is deduced from the one at the relay, using the correspondences (4.16) and (4.17), to estimate the channel $\mathcal{H}^{(RD)}$ and the symbol matrices $\mathbf{S}^{(l)}_R$. The THOSVD receiver is summarized in Table 22.

*Identifiability conditions and ambiguity relations*

In the case of the THOSVD algorithm, for the uniqueness of the pseudo-inverse, it is necessary that the unfolding $\left[\mathbf{G}^{(S)}_{M_SR\times P}\right]_f$ be full row rank for ensuring the uniqueness of this LS estimate, which induces the necessary condition:

$$M_SR \leq P. \tag{4.39}$$

For the scaling ambiguities, we assume a priori knowledge of the first element of the matrices $\mathbf{S}^{(l)}$, for $l \in \{1, L\}$, e.g., $s_{11} = 1$. Under this assumption, $\lambda^{(l)}$ is calculated as:

$$\lambda^{(l)} = \hat{s}^{(l)}_{11}, \lambda^{(H)} = \left(\prod_{l=1} L\hat{s}^{(l)}_{11}\right)^{-1}. \tag{4.40}$$

Table 22 – THOSVD receiver for estimation of the channels and symbol matrices.

**THOSVD receiver for estimating symbol matrices $\mathbf{S}^{(l)}$ and the channels $\mathcal{H}^{(SR)}$ and $\mathcal{H}^{(RD)}$.**

**Input:** tensors $\mathcal{X}^{(SR)}$, $\mathcal{X}^{(RD)}$, $\mathcal{G}^{(S)}$, $\mathcal{G}^{(R)}$
**Output:** Estimated symbol matrices and channels
**First hop: source - relay**
1) Calculate the LS estimate $\mathbf{Z}^{(SR)}$ defined in (4.38).
2) Build the rank-one tensor $\mathcal{Z}^{(SR)}$ of size $R_1N_1 \times \ldots \times R_LN_L \times FM_SM_R$ from $\mathbf{Z}^{(SR)}$.
3) Compute the SVD of each mode-$n$ unfolding of $\mathcal{Z}^{(SR)}$, and calculate the estimates $\hat{\mathbf{s}}^{(l)} = \text{vec}\left(\hat{\mathbf{S}}^{(l)}\right)$ and $\hat{\mathbf{h}}^{(SR)} = \text{vec}\left(\hat{\mathbf{H}}^{(SR)}_{M_R\times FM_S}\right)$ as the first left singular vector of each mode-$n$ unfolding.
4) Unvectorize $\hat{\mathbf{s}}^{(l)}$ and $\hat{\mathbf{h}}^{(SR)}$ to obtain the estimates $\hat{\mathbf{S}}^{(l)}$ and $\hat{\mathbf{H}}^{(SR)}_{M_R\times FM_S}$.
5) Eliminate the scaling ambiguities.
6) Project the estimated symbols onto the symbol alphabet.

**Second hop: relay - destination**
- Apply the stages 1) to 6) of the first hop, using the correspondences (4.16) and (4.17).

### 4.3.3 Zero-forcing (ZF)-KronF receiver

To evaluate the impact of the design parameters on the system performance, we use the zero-forcing (ZF)-KronF receiver, which assumes perfect channel knowledge. The LS estimate of $\mathbf{S}$ is obtained using (4.28) or (4.30), with $\mathbf{H}^{(SR)}_{..f[i]}$ replaced by the true channel slice $\mathbf{H}^{(SR)}_{..f}$, which gives:

$$\hat{\mathbf{S}}^{T}_{ZF} = \left[\left(\mathbf{I}_P \otimes \text{bdiag}\left(\mathbf{H}^{(SR)}_{..f}\right)\right)\mathbf{G}^{(S)}_{PFM_S\times R}\right]^{\dagger}\mathbf{X}^{(SR)}_{PFM_R\times N}, \tag{4.41}$$

or

$$\hat{\mathbf{S}}^{T}_{ZF} = \left(\mathbf{G}^{(S)}_{PFM_S\times R}\right)^{H}\left(\mathbf{I}_P \otimes \text{bdiag}\left(\mathbf{H}^{(SR)\dagger}_{..f}\right)\right)\mathbf{X}^{(SR)}_{PFM_R\times N}. \tag{4.42}$$

As for the Bi-ALS algorithm, the use of (4.41) or (4.42) implies the following necessary conditions: $R \leq PFM_R$ or $R \leq PFM_S$, and $M_S \leq M_R$. Then, the symbol matrices $\mathbf{S}^{(l)}$ are estimated using the KronF algorithm as in the second step of the Bi-ALS-KronF receiver. For the second hop, the ZF-KronF receiver is similar to the one in the first hop with the correspondences (4.16) and (4.17), $\mathbf{H}^{(RD)}_{..f}$ considered known and the matrix unfolding $\mathbf{G}^{(R)}_{PFM_R\times R}$ chosen as a truncated DFT matrix. The uniqueness of the ZF solution for the second hop implies the necessary conditions: $R \leq PFM_D$ or $R \leq PFM_R$, and $M_R \leq M_D$.

Table 23 – Identifiability conditions for the receivers.

| **Receiver** | **Identifiability conditions (First hop)** | **Identifiability conditions (Second hop)** |
|---|---|---|
| Bi-ALS-KronF (4.27) and (4.28) | $R \leq PFM_R$; $M_S \leq PN$ | $R \leq PFM_D$; $M_R \leq PN$ |
| Bi-ALS-KronF (4.29) and (4.30) | $M_S \leq \min(PR, M_R)$; $R \leq \min(N, PFM_S)$ | $M_R \leq \min(PR, M_D)$; $R \leq \min(N, PFM_R)$ |
| THOSVD | $M_S R \leq P$; | $M_R R \leq P$ |
| ZF-KronF (4.41) | $R \leq PFM_R$ | $R \leq PFM_D$ |
| ZF-KronF (4.42) | $R \leq PFM_S$; $M_S \leq M_R$ | $R \leq PFM_R$; $M_R \leq M_D$ |

Table 23 summarizes the necessary conditions for parameter identifiability with each receiver. Comparing the identifiability conditions for the Bi-ALS-KronF algorithm (4.29) and (4.30) with the ones for the Bi-ALS-KronF algorithms (4.27) and (4.28), we can deduce some implications. Indeed, for the estimate (4.29), the conditions $M_S \leq PR$ and $R \leq N$ imply $M_S \leq PN$, i.e., the identifiability condition for the LS solution (4.27). For the estimate (4.30), the conditions $R \leq PFM_S$ and $M_S \leq M_R$ imply $R \leq PFM_R$, i.e., the identifiability condition for the LS solution (4.28). In other words, if the identifiability conditions for (4.29) and (4.30) are satisfied, then the ones for the Bi-ALS algorithm (4.27) and (4.28) are automatically satisfied. Note also that $R \leq PFM_S$ and $M_S \leq PR$ imply $R \leq P^2FR$, which is always satisfied. Therefore, the condition $M_S \leq PR$ can be discarded.

| Algorithms | Computational Complexity |
|---|---|
| Bi-ALS-KonF (4.27) and (4.28) | $O\left(F^3M_S^2PN\right)+O\left(R^2PFM_R\right)+O\left(\left(\sum_{l=1}^{L}N_lR_l\right)\prod_{q=1}^{L}N_qR_q\right)$ |
| Bi-ALS-KonF (4.29) and (4.30) | $O\left(M_S^2PR\right)+O\left(R^2N\right)+O\left(F^3M_R^2M_S\right)+O\left(\left(\sum_{l=1}^{L}N_lR_l\right)\prod_{q=1}^{L}N_qR_q\right)$ |
| THOSVD | $O\left(P^2FM_SR\right)+O\left(F^2M_S^2M_R\right)+O\left(FM_SM_R(\sum_{l=1}^{L}N_lR_l)\prod_{q=1}^{L}N_qR_q\right)$ |

Table 24 – Computational complexity of the Bi-ALS-KronF and THOSVD algorithms at the first hop.

We can also conclude that the THOSVD receiver is more restrictive than the Bi-ALS receivers in the sense that a higher value of $P$ is required, implying a reduction in the transmission rate. As the ZF-KronF receiver (4.42) only estimates the symbol matrices, its identifiability conditions are a subset of those of the second Bi-ALS-KronF receiver.

## 4.4 Computational complexity

In this section, we compare the computational complexity of the proposed semi-blind receivers THOSVD and Bi-ALS-KronF by evaluating the cost of SVD calculation, which is the most expensive matrix operation. Note that for a matrix of dimensions $I \times J$, the complexity of SVD computation of $O(IJ\min(I,J))$. The complexities are evaluated by taking the identifiability conditions into account.

The complexity of the HOSVD algorithm for an $N$-th-order tensor $\mathcal{X} \in \mathbb{R}^{I_1\times\ldots\times I_N}$ is of the order of $O\left((\sum_{n=1}^{N}I_n)\prod_{q=1}^{N}I_q\right)$ if $I_n \leq \prod_{q\neq n}^{N}I_q$, requiring to compute $N$ SVDs of $I_n \times I_{n+1}\ldots I_N I_1\ldots I_{n-1}$ matrices for $n \in \{1,N\}$. The ALS algorithm requires, at each iteration, the overall computational complexity $O\left(R^2\sum_{n=1}^{N}(\prod_{q\neq n}^{N}I_q)\right)$ to compute the PARAFAC decomposition of an $N$-order tensor $\mathcal{X} \in \mathbb{C}^{I_1\times\ldots\times I_N}$ assumed to be of rank $R$. This algorithm requires calculating $N$ LS estimates, which need to pseudo-inverse $\prod_{q\neq n}^{N}I_q \times R$ matrices, for $n \in \{1,N\}$. For estimating the $L$ symbol matrices from their Kronecker product, the KronF algorithm has a complexity of $O\left((\sum_{l=1}^{L}(N_lR_l)\prod_{q=1}^{L}N_qR_q\right)$ flops.

In Table 24, the computational complexities of the Bi-ALS-KronF and THOSVD receivers are compared for the first hop. The computational complexities for the second hop can be easily derived using the correspondences (4.17) between the dimensions.

Note that, simplifying the pseudo-inverses in (4.27) and (4.28) results in less computational complexity for the Bi-ALS-KronF (4.29) and (4.30). Regarding the computational complexity of the closed-form THOSVD receiver, it is generally lower than the one of the iterative Bi-ALS algorithms, which depends on the number of iterations needed for convergence.

## 4.5 Simulation results

In this section, we evaluate the performance of the proposed two-hop OFDM-CDMA MIMO system and the associated receivers. First, in Section 4.5.1, we describe the simulations and present the considered performance criteria. In Section 4.5.2, we study the impact of design parameters on the SER, using the ZF-KronF receiver. Finally, in Section 4.5.3, the proposed semi-blind receivers are compared in terms of SER and channel NMSE.

### 4.5.1 Description of the simulations

The noisy signals received at each hop, $\mathcal{Y}^{(SR)}$ and $\mathcal{Y}^{(RD)}$, respectively, are simulated as:

$$\mathcal{Y}^{(SR)} = \mathcal{X}^{(SR)} + \alpha^{(SR)}\mathcal{N}^{(SR)} \in \mathbb{C}^{M_R \times N_1 \times \ldots \times N_L \times F \times P}, \tag{4.43}$$

$$\mathcal{Y}^{(RD)} = \mathcal{X}^{(RD)} + \alpha^{(RD)}\mathcal{N}^{(RD)} \in \mathbb{C}^{M_D \times N_1 \times \ldots \times N_L \times F \times P}, \tag{4.44}$$

where $\mathcal{N}^{(SR)} \in \mathbb{C}^{M_R \times N_1 \times \ldots \times N_L \times F \times P}$ and $\mathcal{N}^{(RD)} \in \mathbb{C}^{M_D \times N_1 \times \ldots \times N_L \times F \times P}$ are additive white Gaussian noise (AWGN) tensors whose entries are zero-mean circularly-symmetric complex-valued Gaussian random variables, the tensors $\mathcal{X}^{(SR)}$ and $\mathcal{X}^{(RD)}$ contain the noise-free received signals obtained by means of Eqs.(4.8) and (4.19), respectively, and $\alpha^{(SR)}$ and $\alpha^{(RD)}$ allow fixing the SNR calculated as:

$$\text{SNR}^{(SR)} = 20 \log \left( \frac{\| \mathcal{X}^{(SR)} \|_F}{\alpha^{(SR)} \| \mathcal{N}^{(SR)} \|_F} \right), \tag{4.45}$$

$$\text{SNR}^{(RD)} = 20 \log \left( \frac{\| \mathcal{X}^{(RD)} \|_F}{\alpha^{(RD)} \| \mathcal{N}^{(RD)} \|_F} \right), \tag{4.46}$$

which gives $\alpha^{(SR)} = \frac{\|\mathcal{X}^{(SR)}\|_F}{\|\mathcal{N}^{(SR)}\|_F} 10^{-\text{SNR}/20}$ and $\alpha^{(RD)} = \frac{\|\mathcal{X}^{(RD)}\|_F}{\|\mathcal{N}^{(RD)}\|_F} 10^{-\text{SNR}/20}$. Note that the SNRs at the relay and destination nodes are chosen equal in the simulations. The channel tensors $\mathcal{H}^{(SR)}$ and $\mathcal{H}^{(RD)}$ have i.i.d. complex Gaussian entries. The symbols of $\mathbf{S}^{(l)}$ are randomly generated from the 64-QAM alphabet with a uniform distribution, for $l \in \{1, 2\}$. It is worth mentioning that our proposed coding scheme and semi-blind receivers are not dependent on a specific choice for the modulation format as presented in [97, 98]. The proposed system may operate with any modulation, although the resulting SER performance and transmission rate will be affected by this choice. For instance, increasing the modulation cardinality of $M$-PSK (phase-shift keying) or $M$-QAM type constellations (under the same total transmit power constraint) would result in a higher transmission rate at the cost of an SER performance degradation. In this work, we have adopted 64-QAM since it offers a good trade-off between SER performance and transmission rate.

As mentioned before, the coding tensors are designed for each Monte Carlo run, in such a way that, their matrix unfoldings $\mathbf{G}^{(S)}_{PFM_S \times R}$ and $\mathbf{G}^{(R)}_{PFM_R \times R}$ are truncated DFT matrices.

The performance criteria, plotted versus SNR $\in \{-10, 20\}$ dB, are calculated as:

$$\text{NMSE}(\mathcal{Z}) = \frac{1}{K}\sum_{k=1}^{K}\frac{\| \hat{\mathcal{Z}}_k - \mathcal{Z}_k \|_F^2}{\| \mathcal{Z}_k \|_F^2}, \tag{4.47}$$

where $\hat{\mathcal{Z}}_k$ is the tensor $\mathcal{Z}_k$ estimated at the $k^{th}$ run, with $\mathcal{Z}_k \in \{\mathcal{H}_k^{(SR)}, \mathcal{H}_k^{(RD)}\}$. The SER and NMSE are calculated by averaging the results over $K = 5 \times 10^4$ Monte Carlo runs, after truncating the 5% worse and 5% better values to eliminate the influence of ill-convergence and outliers.

The transmission rate $T$ in bits per channel is given by [76]:

$$T = \frac{\sum_{l=1}^{L} N_l R_l - L}{FP\prod_{l=1}^{L} N_l}\log_2(\mu), \tag{4.48}$$

where $\sum_{l=1}^{L} N_l R_l$ corresponds to the total number of transmitted symbols, $L$ is the number of symbols assumed to be a priori known for ambiguity suppression, and $\mu$ denotes the number of constellation points. Note that increasing the number $N_l$ of symbols in the symbol matrix $\mathbf{S}^{(l)}$ induces an increase of coding diversity and a lower transmission rate $T$, while an increase of the number $P$ of repetitions implies a decrease of $T$.

For bit rate note that as the number of symbols increases, more data bits are transmitted per symbol, and we have a greater diversity of symbols. For example, 64-QAM is a QAM scheme with 64 symbols, and 256-QAM is a scheme with 256 symbols. 256-QAM conveys 8 bits per symbol (as $256 = 2^8$), so achieving twice the data rate of 16-QAM for the same symbol rate. The bit rate is given by:

$$B = \frac{T}{T_B} \tag{4.49}$$

where $T$ corresponds to the transmission rate in Eq. (4.48) that represents the number of bits transmitted according to the modulation and $T_B$ is the bit time in seconds. Then,

$$B = \frac{\sum_{l=1}^{L} N_l R_l - L}{FP\prod_{l=1}^{L} N_l}\log_2(\mu)\,\frac{1}{T_B}. \tag{4.50}$$

### 4.5.2 Impact of design parameters

In this section, we evaluate the SER performance of the proposed system under perfect channel knowledge. In this case, we use the ZF-KronF receiver to estimate the transmitted symbol matrices by means of Eq. (4.42). The results presented in Figs. 22-27 were obtained for both hops, but due to lack of place, some SER results are shown only for the relay. All parameters used for the simulations are provided in Table 25. Note that the default values of these parameters are chosen equal to two. The corresponding transmission rates are given in Table 26.

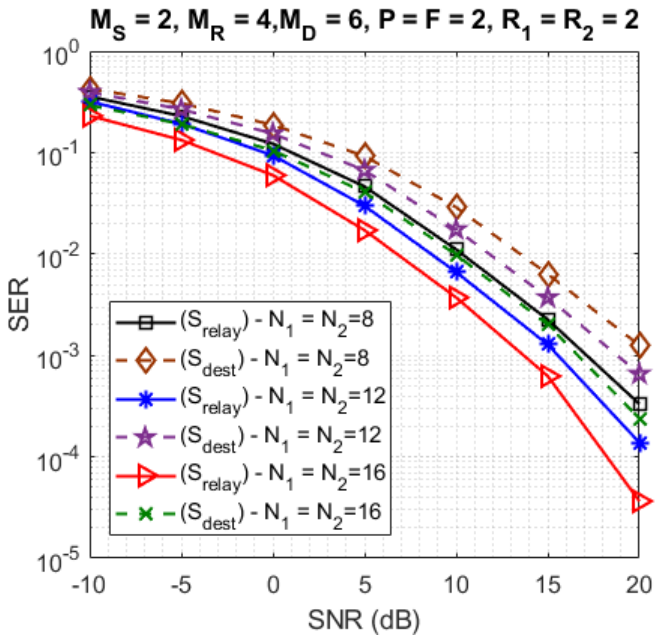


Figure 21 – Impact of numbers of symbols per data stream.

Figure 21 shows the impact on the SER for different numbers of symbols per data stream: $N_1 = N_2 \in \{8, 12, 16\}$, where $\mathbf{S}_{relay}$ and $\mathbf{S}_{dest}$ denote the SER at the relay and the destination, respectively. From these simulation results, it can be concluded that the SER is improved when the numbers of symbols increase, which implies an increase of coding diversity, since $N = N_1 N_2$ is a dimension of the contracted form $\mathcal{Y}_c^{(SR)}$ and $\mathcal{Y}_c^{(RD)}$ of the data tensors, which is not the case for $R = R_1 R_2$. On the other hand, the transmission rate decreases as shown in Table 26. In addition, note that the SER at the relay is better than the one at the destination. This happens because, with the DF protocol, the symbols are estimated and decoded before they are retransmitted by the relay to the destination, which induces a propagation error due to the decoding.

Table 25 – Parameters for the simulations.

| Figures | Impact of | Parameters |
|---|---|---|
| Figure 21 | **Number of symbols per data stream** | $(M_S, M_R, M_D) = (2, 4, 6)$; $F = 2$;$P = 2$; $R_1 = R_2 = 2$; $N_1 = N_2 \in \{8, 12, 16\}$ |
| Figure 22 | **Number of data streams** | $(M_S, M_R, M_D) = (2, 4, 6)$; $F = 4$; $P = 12$; $N_1 = N_2 = 4$; $R_1 = R_2 \in \{4, 6, 8\}$ |
| Figure 23 | **Different configurations for $N_1$ and $N_2$** | $(M_S, M_R, M_D) = (2, 4, 6)$; $P = F = 2$; $R_1 = R_2 = 2$; $N_1 = 4$; $N_2 = 12$ |
| Figure 24 | **Different configurations for** (F, P) | $(M_S, M_R, M_D) = (2, 4, 6)$; $N_1 = N_2 = 4$; $R_1 = R_2 = 2$; (F, P) $\in \{(2,2), (4,2), (8,2), (2,4), (2,8)\}$ |
| Figure 25 | **Number of symbol matrices** | **L = 2**: $N_1 = N_2 = 4$; $R_1 = R_2 = 4$; $F = 8$; $P = 12$; $(M_S, M_R, M_D) = (8, 8, 9)$<br>**L = 3**: $N_1 = N_2 = 4$; $N_3 = 1$; $R_1 = 4$; $R_2 = 2$; $R_3 = 9$; $F = 8$; $P = 12$; $(M_S, M_R, M_D) = (8, 8, 9)$<br>**L = 5**: $N_1 = N_2 = N_3 = N_4 = 2$; $N_5 = 1$; $R_1 = R_2 = R_3 = R_4 = 4$; $R_5 = 3$; $F = 8$; $P = 12$; $(M_S, M_R, M_D) = (8, 8, 9)$ |
| Figure 26 | **Different antenna configurations** | $N_1 = N_2 = 4$; $R_1 = R_2 = 2$; $F = 2$; $P = 4$; $(M_S,M_R,M_D) \in \{(2,4,6), (4,2,6), (2,2,4),(2,6,6)\}$ |
| Figure 27 | **Comparison of the TSTF-MSMKron and TSTF codings** | $(M_S, M_R, M_D) = (2, 4, 6)$; $N_1 = N_2 = 2$; $R_1 = 3$; $R_2 = 4$; $F = 2$; $P = 4$; $N = 2$; $R = 7$ |
| Figures 28-30 | **Comparison of the proposed semi-blind receivers** | $(M_S, M_R, M_D) = (2, 4, 4)$; $N_1 = N_2 = 4$; $R_1 = R_2 = 2$; $P = 18$; $F = 2$ |

Figures 22 to 27 present the SER obtained at the relay ($\mathbf{S}_{relay}$). Figure 22 compares the SER for three different data stream numbers: $R_1 = R_2 \in \{4, 6, 8\}$. From this figure, it can be concluded that increasing $R_1$ and $R_2$ implies an increase of the number of symbols to be estimated without increasing the number of data in the tensor $\mathcal{Y}^{(SR)}$ for performing the symbol estimation, thus inducing a degradation of the SER, while the transmission rate increases (see Table 26).

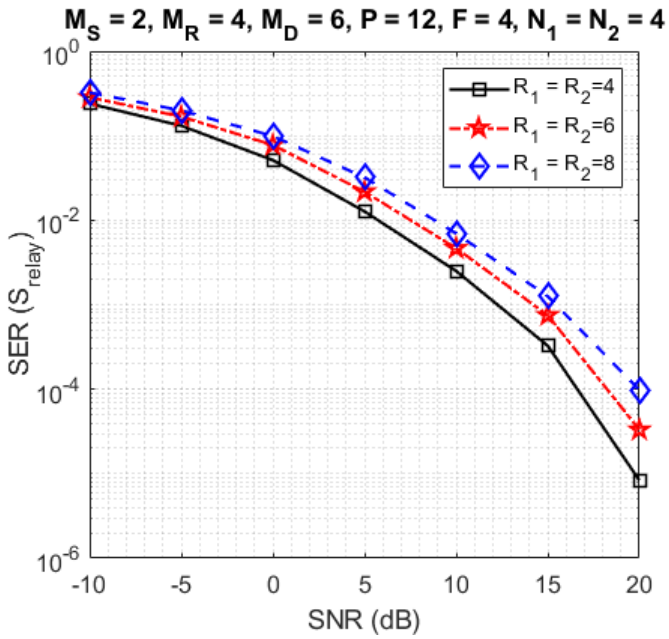


Figure 22 – Impact of data stream numbers.

Table 26 – Transmission rate for different configurations

| **Figures** | **Parameters** | **Transmission Rate (bits per channel)** |
|---|---|---|
| Figure 21 | $N_1 = N_2 \in \{8, 12, 16\}$ | T = 0.703; 0.479; 0.363 |
| Figure 22 | $R_1 = R_2 \in \{4, 6, 8\}$ | T = 0.234; 0.359; 0.484 |
| Figure 23 | $N_1 = 4; N_2 = 12$ | T = 0.812 |
| Figure 24 | $(F,P) \in \{(2,2), (4,2), (8,2), (2,4), (2,8)\}$ | T = 1.312; 0.656; 0.328; 0.656; 0.328 |
| Figure 25 | $L \in \{2,3,5\}$ | T = 0.117 |
| Figure 26 | $(M_S,M_R,M_D) \in \{(2,4,6), (4,2,6), (2,2,4), (2,6,6)\}$ | T = 0.656 |
| Figure 27 | Comparison of the TSTF-MSMKron and TSTF codings | T = 2.25; $T_S = 5.25$ |
| Figs. 28-30 | Comparison of the proposed semi-blind receivers | T = 0.145 |

In Figure 23, the simulation results compare the $\text{SER}_{global}$ with the individual SERs for $\mathbf{S}^{(1)}$ and $\mathbf{S}^{(2)}$, when $N_1 = 4$, $N_2 = 12$ and $R_1 = R_2 = 2$. For this configuration, the Kronecker product between $\mathbf{S}^{(1)}$ and $\mathbf{S}^{(2)}$ induces a greater diversity for $\mathbf{S}^{(1)}$ than for $\mathbf{S}^{(2)}$, due to the fact that each symbol of $\mathbf{S}^{(1)}$ is repeated $12R_2$ times while each symbol of $\mathbf{S}^{(2)}$ is repeated only $4R_1$ times. That implies a SER smaller for $\mathbf{S}^{(1)}$ than for $\mathbf{S}^{(2)}$.

Figure 24 presents the results considering different configurations for the numbers of subcarriers ($F$) and time blocks ($P$). Note that a performance improvement is obtained when $F$ and/or $P$ are/is increased due to an increase of frequency and/or time diversities. On the other hand, the transmission rate decreases. We can also remark that for the same

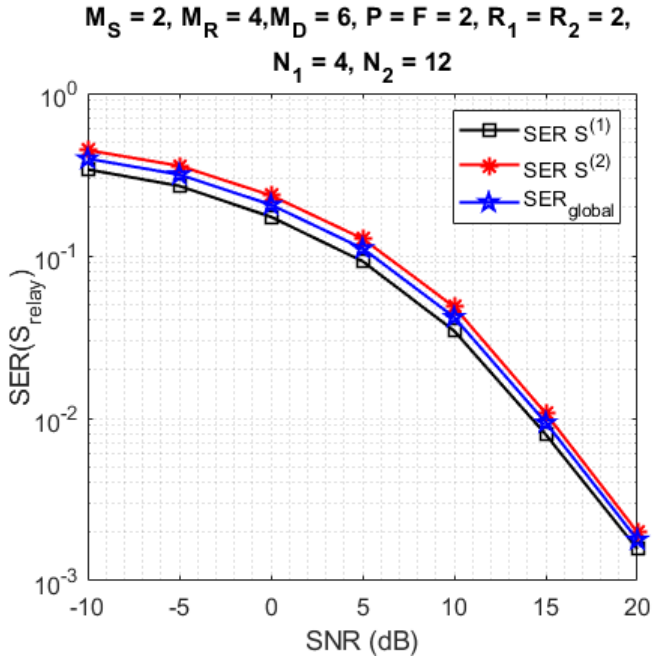


Figure 23 – Impact on the SER of individual symbol matrices.

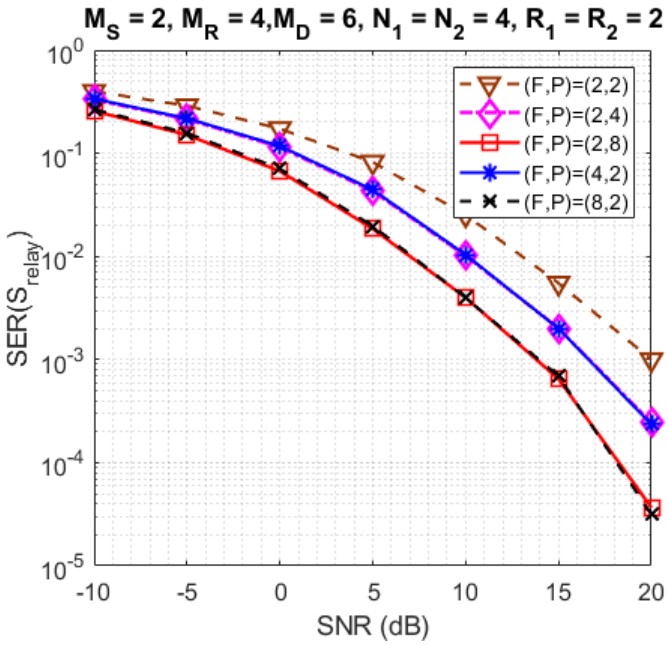


Figure 24 – Impact of different configurations of ($F$,$P$).

value of the product $FP = 8$ or $FP = 16$, the diversity gain is the same, implying very close SERs, which illustrates the symmetric role played by the frequency and time diversities in the SER performance.

In Figure 25, we compare the SER for different numbers of symbol matrices ($L \in \{2, 3, 5\}$). The design parameters have been chosen so that the transmission rate is the same for the three values of $L$. The TSTF-MSMKron scheme with $L = 5$ provides the best SER performance in comparison with $L \in \{2, 3\}$. These results corroborate the coding gain provided by the Kronecker product of symbol matrices.

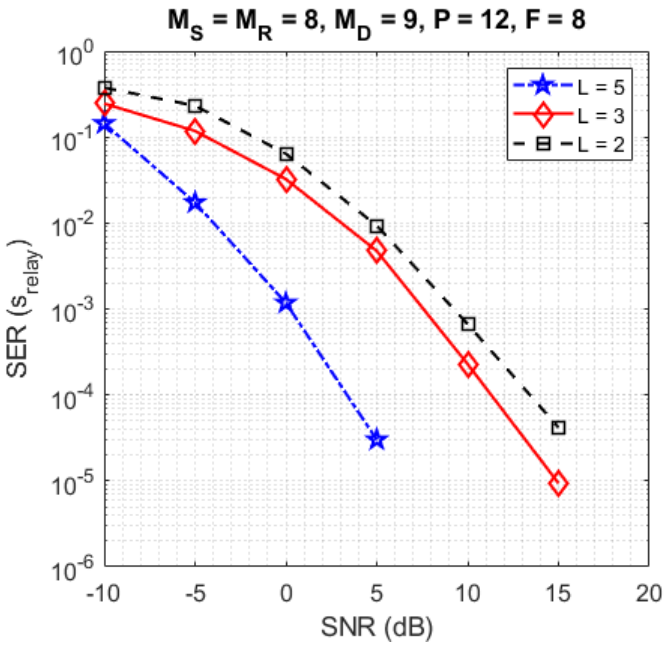


Figure 25 – Impact of $L$ on the SER.

In Figure 26, the SERs are plotted for different configurations of antenna numbers $(M_S, M_R, M_D) \in \{(2,4,6), (2,4,2), (4,2,6)\}$. Comparing these configurations, we note that the best SER is obtained when $M_D > M_R > M_S$. For the configuration (4,2,6), the SER is not good in both at the relay and the destination, because the identifiability condition $(M_S \leq M_R)$ at the relay is not satisfied. For the configuration (2,4,2), the SER at the relay is similar to the one for the configuration (2,4,6) because the antenna numbers $(M_S, M_R)$ are the same for both configurations, but the SER at the destination is not good because the identifiability condition $(M_R \leq M_D)$ at the destination is not satisfied for the configuration (2,4,2), which is not the case of the configuration (2,4,6). With this last configuration, we note that the SER at the relay is better than the one at the destination.

In Figure 27, the proposed TSTF-MSMKron coding is compared with the TSTF coding, i.e., using a single symbol matrix $\mathbf{S} \in \mathbb{C}^{N \times R}$ instead of a multiple Kronecker product of symbol matrices. With the TSTF coding, the symbol matrix is estimated using Eq. (4.28), and the transmission rate is given by:

$$T_{\mathbf{S}} = \frac{R}{FP} \log_2(\mu). \tag{4.51}$$

For both codings, the number (14) of transmitted symbols is the same. See the design parameters in Table 25.

As expected, from Figure 27, we conclude that the TSTF-MSMKron coding gives a better SER than the TSTF coding thanks to a greater coding diversity brought by the Kronecker product of symbol matrices. In counterpart, the transmission rate with the TSTF-MSMKron coding is smaller than the one with the TSTF coding. See Table 26.

We can draw the following conclusions about the new TSTF-MSMKron coding based

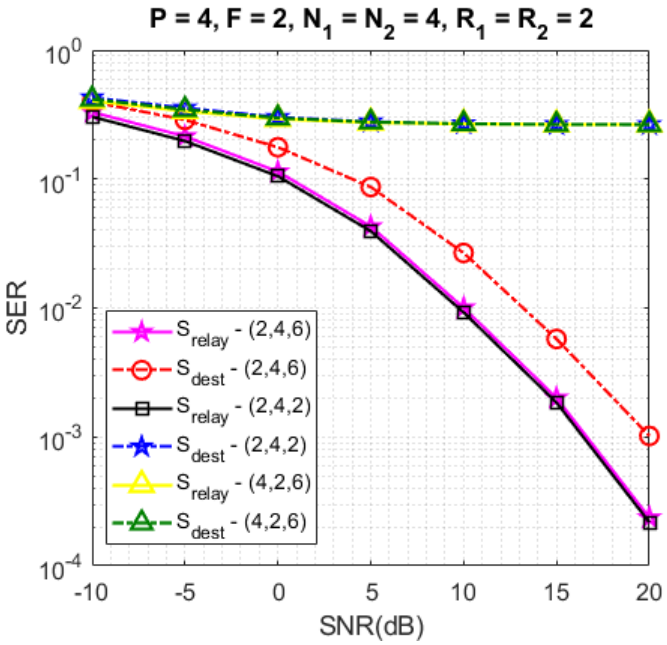


Figure 26 – Impact of different numbers of antennas.

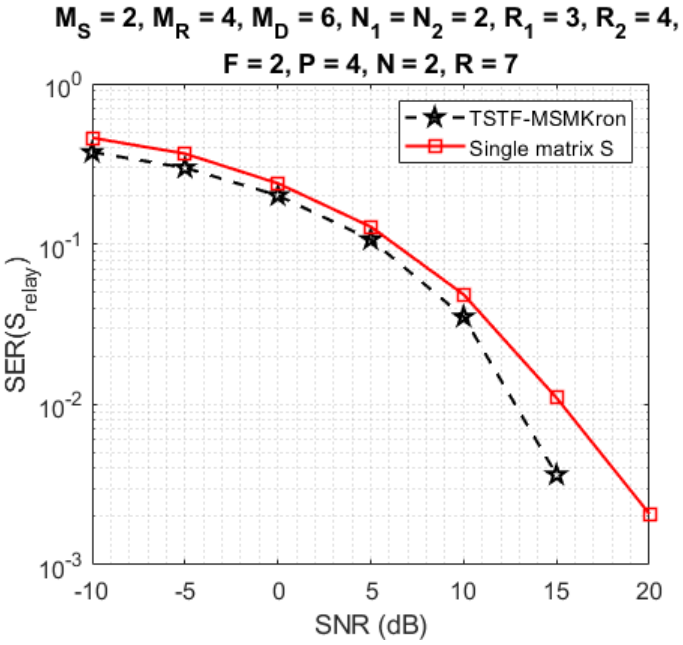


Figure 27 – Comparison of the TSTF-MSMKron and TSTF codings.

on analyzing the above presented experimental results:

- space diversity is provided by both the relay/destination antennas $(M_R, M_D)$ and the coding tensors $(\mathcal{G}^{(S)}, \mathcal{G}^{(R)})$ via the source/relay antennas $(M_S, M_R)$, respectively, implying an increase of the dimensions of the received signals tensor at each hop, and a greater redundancy in the transmitted symbols, respectively;
- time and frequency diversities are provided by the transmission in $P$ blocks and $F$ subcarries which implies a repetition of transmitted symbols and an increase of the number of received signals;
- coding diversity is introduced by the TSTF-MSMKron coding which creates redundancy of each transmitted symbol while increasing the number of received signals via the dimensions $N_l$ of the received signals tensor.

Space, time, frequency and coding diversities are highlighted in the expressions (4.7) and (4.18) of received signals at each hop, respectively, owing the sums on source/relay antennas due to the tensor coding, and on the numbers of symbols contained in each data stream, as resulting from cross-multiplications between symbols provided by multiple Kronecker products which define the MSMKron coding.

### 4.5.3 Comparison of THOSVD and Bi-ALS-KronF receivers

In the next experiments, we compare the SERs obtained with the proposed semi-blind and ZF-KronF receivers. First, the results are presented in terms of SER at the relay ($\mathbf{S}_{relay}$ - Figure 28) and the destination ($\mathbf{S}_{dest.}$ - Figure 29). Then, we compare the performance of semi-blind receivers, in terms of channel NMSE at each hop (Figure 30). For these simulations, the design parameters are fixed with the following values: $M_S = 2$, $M_R = M_D = 4$, $N_1 = N_2 = 4$, $R_1 = R_2 = 2$, $P = 18$, and $F = 2$.

From Figures 28 and 29, we can conclude that the THOSVD receiver provides a better SER performance than the Bi-ALS-KronF receiver. That is due to the closed form of the THOSVD receiver allowing to jointly estimate the channel and symbol matrices, while the Bi-ALS-KronF receiver is composed of two steps, one iterative and one closed-form. On the other hand, the THOSVD receiver is more constraining in terms of identifiability conditions ($M_S R \leq P$) than the Bi-ALS-KronF receiver, inducing a reduction of the transmission rate, as can be seen in Table 26. It can also be noted that the SER at the relay is better than the one at the destination due to error propagation caused by decoding at the relay. As expected, the ZF-KronF receiver provides the best SER due to a priori knowledge of the channels.

In Figure 30, the channel NMSE results obtained at each hop are plotted. Note that the THOSVD receiver gives better results than the Bi-ALS-KronF one. As for the SER, this

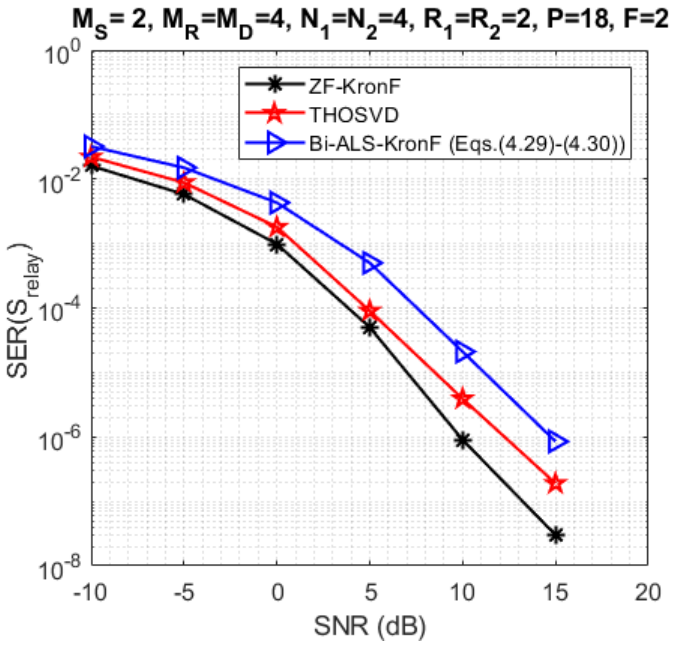


Figure 28 – SER comparison with THOSVD, Bi-ALS-KronF Eqs.(4.29)-(4.30) and ZF receivers at the relay.

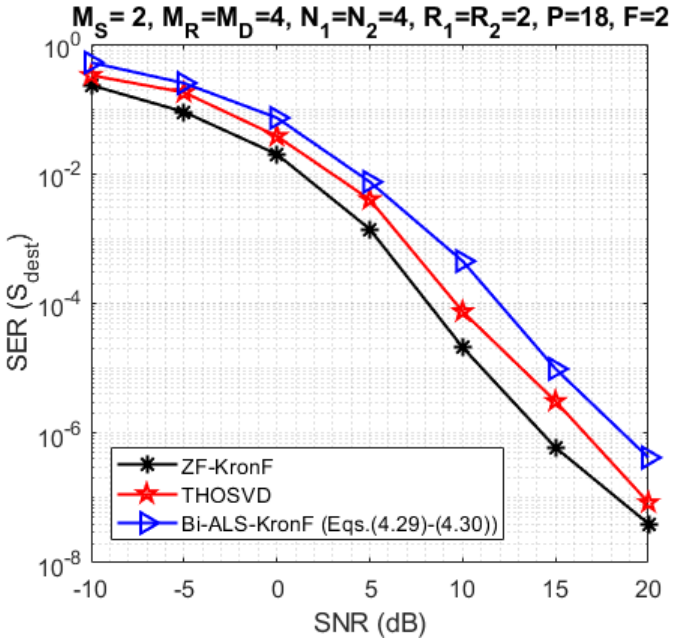


Figure 29 – SER comparison with THOSVD, Bi-ALS-KronF Eqs.(4.29)-(4.30) and ZF receivers at the destination.

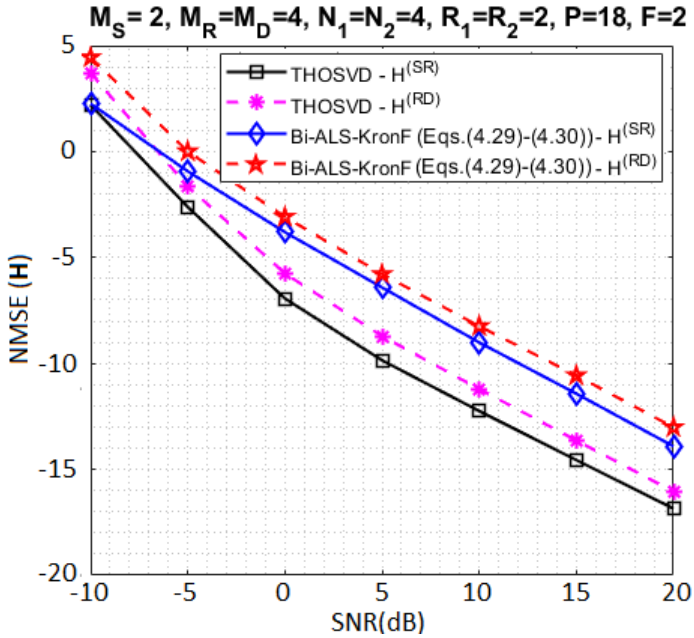


Figure 30 – Channel NMSE comparison with THOSVD and Bi-ALS-KronF Eqs.(4.29)-(4.30) receivers.

is because the THOSVD is a closed-form solution, while the Bi-ALS algorithm is iterative. Moreover, the channel estimation in the first hop is slightly better than the one in the second hop. This is due to error propagation in the retransmission of symbol matrices after decoding at the relay.

In Table 24, a comparison of the complexities of Bi-ALS-KronF receiver, both versions corresponding to Eqs.(4.27)-(4.28) and Eqs.(4.29)-(4.30) and THOSVD is provided. Based on this table we can define the ratios $O_1 = O_{Bi-ALS-KronF(4.27)-(4.28)}/O_{Bi-ALS-KronF(4.29)-(4.30)}$, $O_2 = O_{THOSVD}/O_{Bi-ALS-KronF(4.27)-(4.28)}$ and $O_3 = O_{THOSVD}/O_{Bi-ALS-KronF(4.29)-(4.30)}$, which expresses how many times Bi-ALS-KronF (4.27)-(4.28) is more computational complexity than Bi-ALS-KronF (4.29)-(4.30) and how many times THOSVD is more complexity demanding than Bi-ALS-KronF algorithms. We have

$$O_1 = \frac{i_1\left(F^3M_S^2PN + R^2PFM_R\right) + \left(\sum_{l=1}^{L} N_lR_l\right)\prod_{q=1}^{L} N_qR_q}{i_2\left(M_S^2PR + R^2N + F^3M_R^2M_S\right) + \left(\sum_{l=1}^{L} N_lR_l\right)\prod_{q=1}^{L} N_qR_q} \tag{4.52}$$

$$O_2 = \frac{P^2FM_SR + F^2M_S^2M_R + FM_SM_R(\sum_{l=1}^{L} N_lR_l)\prod_{q=1}^{L} N_qR_q}{i_1\left(F^3M_S^2PN + R^2PFM_R\right) + \left(\sum_{l=1}^{L} N_lR_l\right)\prod_{q=1}^{L} N_qR_q} \tag{4.53}$$

$$O_3 = \frac{P^2FM_SR + F^2M_S^2M_R + FM_SM_R(\sum_{l=1}^{L} N_lR_l)\prod_{q=1}^{L} N_qR_q}{i_2\left(M_S^2PR + R^2N + F^3M_R^2M_S\right) + \left(\sum_{l=1}^{L} N_lR_l\right)\prod_{q=1}^{L} N_qR_q} \tag{4.54}$$

where $i_1$ and $i_2$ are the average numbers of iterations for convergence of the Bi-ALS-KronF (4.27)-(4.28) and Bi-ALS-KronF (4.29)-(4.30) algorithms, respectively. Figure 31 shows the complexity ratios $O_1$, $O_2$ and $O_3$ calculated using average values for $i_1$ and $i_2$ obtained from all

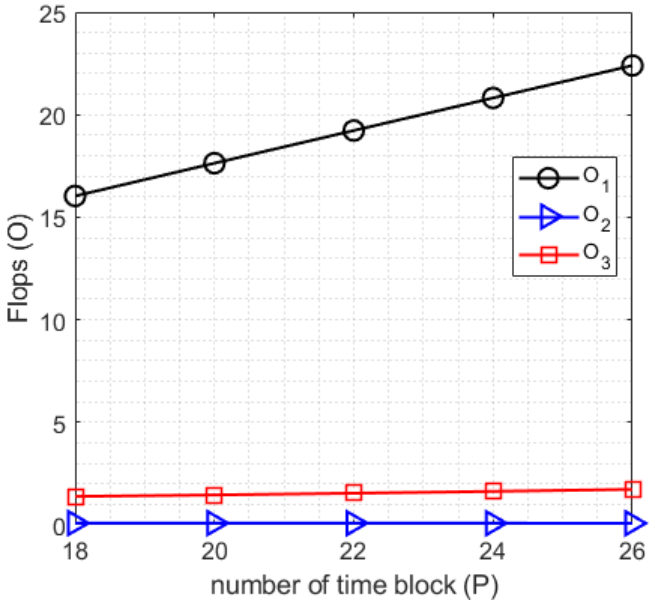


Figure 31 – Complexity ratio of THOSVD, Bi-ALS-KronF Eqs.(4.29)-(4.30) and Bi-ALS-KronF Eqs.(4.27)-(4.30x) receivers.

the Monte Carlo runs and considering the variation of the number of time blocks $P \in \{18, 26\}$. From this figure, we can note that even as the number of time blocks increases, the complexity ratios $O_2$ and $O_3$ for the three receivers are linear, while the complexity ratio $O_1$ for Bi-ALS-KronF Bi-ALS-KronF (4.27)-(4.28) compared to Bi-ALS-KronF (4.29)-(4.30) increases as $P$ increases. The Bi-ALS-KronF (4.29)-(4.30) is much less computationally demanding than Bi-ALS-KronF (4.27)-(4.28) and THOSVD algorithms due the simplification of the pseudo-inverse where this algorithm needs less number of iterations to converge, such that $O_{Bi-ALS-KronF(4.27)-(4.28)} >> O_{THOSVD} >> O_{Bi-ALS-KronF(4.29)-(4.30)}$.

## 4.6 Chapter summary

In this chapter, we have proposed a new coding scheme based on the multiple Kronecker product of symbol matrices, leading to the so-called MSMKron coding. Combining the MSMKron with the TSTF to transmit the symbols we propose the TSTF-MSMKron coding. This new coding makes it possible to improve the gains in diversity and throughput. Based on the proposed TSTF-MSMKron, a new two-hop CDMA-OFDM MIMO system was proposed. We have shown that the tensors of signals received at the relay and destination nodes satisfy two generalized Tucker models whose core tensors are the TSTF coding tensors. The contributions in this chapter extend previous works in different ways, either by using a new coding or extending to a newly received signal tensor model.

By assuming the TSTF coding tensors known, two semi-blind receivers have been derived to jointly estimate the transmitted information symbols and the channels. One

called the Bi-ALS-KronF receiver, is composed of two stages. The first stage is based on the iterative ALS algorithm to estimate the Kronecker product $\mathbf{S}$ and the channels, while the second stage applies the closed-form KronF algorithm to separate the symbol matrices. The other one, called THOSVD receiver, is a closed-form solution that allows simultaneously estimating the channel and the symbol matrices by means of SVD computations as with the KronF method. Necessary conditions for system identifiability have been established for each receiver, showing that the THOSVD receiver is more constraining than the Bi-ALS-KronF one for the choice of the number of time blocks and consequently from the data rate point of view.

Extensive Monte Carlo simulations have allowed us to illustrate the impact of all the design parameters on the SER performance. The performances of the proposed semi-blind receivers have been compared in terms of SER and channel NMSE. As expected, the closed-form THOSVD receiver outperforms the iterative Bi-ALS-KronF receiver. Moreover, a comparison with the standard TSTF coding has corroborated the SER improvement brought by the MSMKron coding which allows to increase the diversity gain. Also, regarding the parameters, it can be noted that the system configuration influences the efficiency of the parameter estimation.

# 5 Conclusions and Perspectives

## 5.1 Conclusions

This thesis has addressed the study of semi-blind receivers applied to point-to-point and two-hop MIMO systems. In particular, a new coding called TSTF-MSMKron and a particular case of the MKRST coding were proposed. By exploiting the proposed codings, new received signal models based on tensor decomposition and new semi-blind receivers were presented that perform the joint estimation of the transmitted symbols and the channels. Performance analysis of each proposed system was provided to illustrate its behavior and effectiveness, evaluating the improvements of the techniques addressed for MIMO systems. In the sequel, we provide a brief conclusion of each chapter that has proposed original contributions.

In **Chapter 3**, we presented a particular case of the MKRST coding where the precoding matrix corresponds to a symbol matrix that is assumed known. It allows us to propose a new point-to-point MIMO system based on tensor decomposition. By exploiting the proposed received signal tensor model, we have derived five semi-blind receivers to jointly estimate the transmitted symbols and channel. Simulation results showed that the MKRST coding increases spatial diversity when the number of symbols per data stream or the number of received antennas increases. Based on the results, also note that the semi-blind receivers are efficient, especially when based on closed-form solutions, to estimate the parameters without channel knowledge, knowing only the pilot symbol matrix.

In **Chapter 4**, we proposed a new coding scheme based on the multiple Kronecker product of symbol matrices, leading to the so-called MSMKron coding. Combining the proposed MSMKron with the TSTF coding to transmit the symbols, we proposed a new coding called TSTF-MSMKron. This new coding makes it possible to improve gains in time, frequency and space diversity and throughput. TSTF-MSMKron coding allows us to propose a new two-hop CDMA-OFDM MIMO. We have shown that the tensors of signals received at the relay and destination nodes satisfy two generalized Tucker models whose core tensors are the TSTF coding tensors. By exploiting the proposed received signal tensor model, we have derived two semi-blind receivers to jointly estimate the transmitted symbols and channels. The first proposed receiver was based on the Bi-ALS and KronF algorithms, where the first was applied to estimate the channel and the Kronecker product, while the second was applied to separate the symbol matrices. The second proposed receiver is based on the closed-form THOSVD algorithm which allows simultaneously estimating the channel and the symbol matrices by means of SVD computations as with the KronF method. Simulation

results allowed us to illustrate the impact of the design parameters on the SER performance. TSTF-MSMKron coding provides an increase in spatial, time and frequency diversities when the number of symbols per data stream or the number of antennas at the relay or destination increases. The semi-blind receivers are efficient, especially when they are based on closed-form solutions, to estimate the parameters without channel knowledge, knowing only one symbol of each symbol matrix. On the other hand, the closed-form THOSVD receiver is more constraining than the iterative Bi-ALS-KronF one in terms of the number of time blocks and consequently from the data rate point of view.

## 5.2 Perspectives and next steps

Given the results presented and the main conclusions highlighted above, in this section, we raise the main perspectives that can be derived from the research carried out in this thesis:

- To extend the two-hop MIMO systems proposed for the multi-hop case using the amplify-and-forward (AF) protocol, and present new receivers to jointly estimate the channels and symbols. In addition, study different settings of the codings applied at the source and at the relay.
- To take into account allocation tensors as in [35] combined with the coding extensions presented and to propose new received signals tensor models and receivers to estimate the symbols and the channels in multi-hop MIMO systems. The allocation tensors allow us to control the sending and receiving of the symbols and can indicate which antenna transmitted or received the information.
- To develop relaying systems with TSTF-MSMKron coding for double directional dual-polarized MIMO systems and IRS-assisted systems.

# References


[1] A. Goldsmith. *Wireless communications*. Cambridge university press, 2005.

[2] A. Mchangama, J. Ayadi, et al. "MmWave massive MIMO small cells for 5G and beyond mobile networks: An overview". In: *2020 12th International Symposium on Communication Systems, Networks and Digital Signal Processing (CSNDSP)*. IEEE. 2020, pp. 1–6.

[3] G.J. Foschini, M.J. Gans, et al. "On limits of wireless communications in a fading environment when using multiple antennas". In: *Wireless personal communications* 6.3 (1998), pp. 311–336.

[4] V. Tarokh, N. Seshadri, and A.R. Calderbank. "Space-time codes for high data rate wireless communication: Performance criterion and code construction". In: *IEEE transactions on information theory* 44.2 (1998), pp. 744–765.

[5] L. Zheng and D.N.C. Tse. "Diversity and multiplexing: A fundamental tradeoff in multiple-antenna channels". In: *IEEE Transactions on information theory* 49.5 (2003), pp. 1073–1096.

[6] A.J. Paulraj, D.A. Gore, et al. "An overview of MIMO communications-a key to gigabit wireless". In: *Proceedings of the IEEE* 92.2 (2004), pp. 198–218.

[7] S. Onoe. "1.3 Evolution of 5G mobile technology toward 1 2020 and beyond". In: *2016 IEEE International Solid-State Circuits Conference (ISSCC)*. IEEE. 2016, pp. 23–28.

[8] R. Chataut and R. Akl. "Massive MIMO systems for 5G and beyond networks—overview, recent trends, challenges, and future research direction". In: *Sensors* 20.10 (2020), p. 2753.

[9] A. Shaikh and M.J. Kaur. "Comprehensive survey of massive MIMO for 5G communications". In: *2019 Advances in Science and Engineering Technology International Conferences (ASET)*. IEEE. 2019, pp. 1–5.

[10] Y. Huo et al. "Technology Trends for Massive MIMO towards 6G". In: *arXiv preprint arXiv:2301.01703* (2023).

[11] P. Yang et al. "6G wireless communications: Vision and potential techniques". In: *IEEE network* 33.4 (2019), pp. 70–75.

[12] A. Sendonaris, E. Erkip, and B. Aazhang. "User cooperation diversity. Part I. System description". In: *IEEE transactions on communications* 51.11 (2003), pp. 1927–1938.

[13] A.L.F. de Almeida, G. Favier, and J.C.M. Mota. "PARAFAC-based unified tensor modeling for wireless communication systems with application to blind multiuser equalization". In: *Signal Processing* 87.2 (2007), pp. 337–351.

[14] M.N. da Costa, G. Favier, and J.M.T. Romano. “Tensor modelling of MIMO communication systems with performance analysis and Kronecker receivers”. In: *Signal Processing* 145 (2018), pp. 304–316.

[15] A. Venugopal and H. Leib. “A tensor based framework for multi-domain communication systems”. In: *IEEE Open Journal of the Communications Society* 1 (2020), pp. 606–633.

[16] A.L.F. de Almeida and G. Favier. “Double Khatri–Rao space-time-frequency coding using semi-blind PARAFAC based receiver”. In: *IEEE Signal Processing Letters* 20.5 (2013), pp. 471–474.

[17] G. Favier, C.A.R. Fernandes, and A.L.F. de Almeida. “Nested Tucker tensor decomposition with application to MIMO relay systems using tensor space–time coding (TSTC)”. In: *Signal Processing* 128 (2016), pp. 318–331.

[18] D.C. Araújo, A.L.F. de Almeida, et al. “Tensor-based channel estimation for massive MIMO-OFDM systems”. In: *IEEE Access* 7 (2019), pp. 42133–42147.

[19] S.V.N. Randriambelonoro, G. Favier, and R. Boyer. “Semi-blind joint symbols and multipath parameters estimation of MIMO systems using KRST/MKRSM coding”. In: *Digital Signal Processing* 109 (2021), p. 102908.

[20] L.R. Ximenes, G. Favier, and A.L.F. de Almeida. “Semi-blind receivers for non-regenerative cooperative MIMO communications based on nested PARAFAC modeling”. In: *IEEE transactions on signal processing* 63.18 (2015), pp. 4985–4998.

[21] L.R. Ximenes, G. Favier, and A.L.F. de Almeida. “Closed-form semi-blind receiver for MIMO relay systems using double Khatri–Rao space-time coding”. In: *IEEE Signal Processing Letters* 23.3 (2016), pp. 316–320.

[22] D.S. Rocha. “Nested tensor decomposition applied to cooperative MIMO communication systems”. PhD thesis. Brazil: University of Ceará, 2019.

[23] D.S. Rocha, G. Favier, and C.A.R. Fernandes. “Closed-form receiver for multi-hop MIMO relay systems with tensor space-time coding”. In: *Journal of Communication and Information Systems* 34.1 (2019), pp. 50–54.

[24] Q. Wang, L. Zhang, et al. “Space-time-frequency coding for MIMO relay system based on tensor decomposition”. In: *Radioelectronics and Communications Systems* 63 (2020), pp. 77–87.

[25] X. Han, J. Ying, et al. “A nested tensor-based receiver employing triple constellation precoding for three-hop cooperative communication systems”. In: *Digital Signal Processing* 133 (2023), p. 103862.

[26] A. Cichocki, D. Mandic, et al. “Tensor decompositions for signal processing applications: From two-way to multiway component analysis”. In: *IEEE signal processing magazine* 32.2 (2015), pp. 145–163.

[27] G. Favier. *From Algebraic Structures to Tensors*. John Wiley & Sons, 2019.

[28] X. Han, A.L.F. de Almeida, and Z. Yang. "Channel estimation for MIMO multi-relay systems using a tensor approach". In: *EURASIP Journal on Advances in Signal Processing* 2014.1 (2014), pp. 1–14.

[29] I.V. Cavalcante, A.L.F. de Almeida, and M. Haardt. "Joint channel estimation for three-hop MIMO relaying systems". In: *IEEE Signal Processing Letters* 22.12 (2015), pp. 2430–2434.

[30] F.H.P. Fitzek and M.D. Katz. *Cooperation in wireless networks: principles and applications*. Springer, 2006.

[31] T. Cover and A.E. Gamal. "Capacity theorems for the relay channel". In: *IEEE Transactions on information theory* 25.5 (1979), pp. 572–584.

[32] Y. Liu, S. Li, et al. "Tensor-based semi-blind channel estimation for three-hop MIMO relay systems". In: *2015 International Conference on Wireless Communications & Signal Processing (WCSP)*. IEEE. 2015, pp. 1–5.

[33] W.C. Freitas Jr, G. Favier, and A.L.F. de Almeida. "Generalized Khatri-Rao and Kronecker space-time coding for MIMO relay systems with closed-form semi-blind receivers". In: *Signal Processing* 151 (2018), pp. 19–31.

[34] P.M.R. de Oliveira, C.A.R. Fernandes, et al. "PARATUCK semi-blind receivers for relaying multi-hop MIMO systems". In: *Digital Signal Processing* 92 (2019), pp. 127–138.

[35] G. Favier and A.L.F. de Almeida. "Tensor space-time-frequency coding with semi-blind receivers for MIMO wireless communication systems". In: *IEEE Transactions on Signal Processing* 62.22 (2014), pp. 5987–6002.

[36] M.R. Zanatta, J.P.C.L. da Costa, et al. "Tensor-based framework with model order selection and high accuracy factor decomposition for time-delay estimation in dynamic multipath scenarios". In: *IEEE access* 8 (2020), pp. 174931–174942.

[37] J.P.A. Maranhão, J.P.C.L. da Costa, et al. "Tensor based framework for Distributed Denial of Service attack detection". In: *Journal of Network and Computer Applications* 174 (2021), p. 102894.

[38] J.M. Junior, J.P.C.L. da Costa, et al. "M-estimator based Chinese remainder theorem with few remainders using a kroenecker product based mapping vector". In: *Digital Signal Processing* 87 (2019), pp. 60–74.

[39] A.L.F. de Almeida. "Tensor modeling and signal processing for wireless communication systems". PhD thesis. France: Université de Nice Sophia Antipolis, 2007.

[40] P.R.B. Gomes, A.L.F. de Almeida, et al. “A nested-PARAFAC based approach for target localization in bistatic MIMO radar systems”. In: *Digital Signal Processing* 89 (2019), pp. 40–48.

[41] J.P.C.L. da Costa, R.K. Miranda, and M.R. Zanatta. “Tensor based blind source separation for current source density analysis of evoked potentials from somatosensory cortex of mice”. In: *2017 8th International IEEE/EMBS Conference on Neural Engineering (NER)*. IEEE. 2017, pp. 664–667.

[42] T.G. Kolda and B.W. Bader. “Tensor decompositions and applications”. In: *SIAM review* 51.3 (2009), pp. 455–500.

[43] P. Comon et al. “Tensor decompostions: state of the art and applications”. In: *INSTITUTE OF MATHEMATICS AND ITS APPLICATIONS CONFERENCE SERIES*. Vol. 71. Oxford; Clarendon; 1999. 2002, pp. 1–24.

[44] F. Roemer. “Advanced algebraic concepts for efficient multi-channel signal processing”. PhD thesis. Germany: Universitätsbibliothek Ilmenau, 2013.

[45] W.C. Freitas Jr, G. Favier, and A.L.F. de Almeida. “Sequential closed-form semiblind receiver for space-time coded multihop relaying systems”. In: *IEEE Signal Processing Letters* 24.12 (2017), pp. 1773–1777.

[46] G. Favier. *Matrix and Tensor Decompositions in Signal Processing, Volume 2*. John Wiley & Sons, 2021.

[47] N. Pitsianis and C.F. Van Loan. *Approximation with Kronecker Products. Linear Algebra for Large Scale and Real Time application*. 1993.

[48] K.K. Wu, Y. Yam, et al. “Kronecker product approximation with multiple factor matrices via the tensor product algorithm”. In: *2016 IEEE International Conference on Systems, Man, and Cybernetics (SMC)*. IEEE. 2016, pp. 004277–004282.

[49] B. Sokal, A.L.F. de Almeida, and M. Haardt. “Semi-blind receivers for MIMO multi-relaying systems via rank-one tensor approximations”. In: *Signal Processing* 166 (2020), p. 107254.

[50] L. De Lathauwer, B. De Moor, and J. Vandewalle. “A multilinear singular value decomposition”. In: *SIAM journal on Matrix Analysis and Applications* 21.4 (2000), pp. 1253–1278.

[51] F. Roemer and M. Haardt. “Tensor-based channel estimation (TENCE) for two-way relaying with multiple antennas and spatial reuse”. In: *2009 IEEE International Conference on Acoustics, Speech and Signal Processing*. IEEE. 2009, pp. 3641–3644.

[52] A.Y. Kibangou and G. Favier. “Non-iterative solution for PARAFAC with a Toeplitz matrix factor”. In: *2009 17th European Signal Processing Conference*. IEEE. 2009, pp. 691–695.

[53] G. Favier and A.L.F. de Almeida. “Overview of constrained PARAFAC models”. In: *EURASIP Journal on Advances in Signal Processing* 2014.1 (2014), pp. 1–25.

[54] A.L.F. de Almeida, G. Favier, and J.C.M. Mota. “A constrained factor decomposition with application to MIMO antenna systems”. In: *IEEE Transactions on Signal Processing* 56.6 (2008), pp. 2429–2442.

[55] G. Favier, M.N. da Costa, et al. “Tensor space–time (TST) coding for MIMO wireless communication systems”. In: *Signal Processing* 92.4 (2012), pp. 1079–1092.

[56] I.V. Oseledets. “Tensor-train decomposition”. In: *SIAM Journal on Scientific Computing* 33.5 (2011), pp. 2295–2317.

[57] L.R. Tucker. “Some mathematical notes on three-mode factor analysis”. In: *Psychometrika* 31.3 (1966), pp. 279–311.

[58] R.A. Harshman et al. “Foundations of the PARAFAC procedure: Models and conditions for an" explanatory" multimodal factor analysis”. In: (1970).

[59] J.B. Kruskal. “Three-way arrays: rank and uniqueness of trilinear decompositions, with application to arithmetic complexity and statistics”. In: *Linear algebra and its applications* 18.2 (1977), pp. 95–138.

[60] J.B. Kruskal. “Rank, decomposition, and uniqueness for 3-way and N-way arrays”. In: *Multiway data analysis* (1989), pp. 7–18.

[61] R.A. Harshman. “Determination and proof of minimum uniqueness conditions for PARAFAC1”. In: *UCLA working papers in phonetics* 22.111-117 (1972), p. 3.

[62] L. De Lathauwer. “A link between the canonical decomposition in multilinear algebra and simultaneous matrix diagonalization”. In: *SIAM journal on Matrix Analysis and Applications* 28.3 (2006), pp. 642–666.

[63] N.D. Sidiropoulos, G.B. Giannakis, and R. Bro. “Blind PARAFAC receivers for DS-CDMA systems”. In: *IEEE Transactions on Signal Processing* 48.3 (2000), pp. 810–823.

[64] N.D. Sidiropoulos and R. Bro. “On the uniqueness of multilinear decomposition of N-way arrays”. In: *Journal of Chemometrics: A Journal of the Chemometrics Society* 14.3 (2000), pp. 229–239.

[65] F. Yates. “The analysis of replicated experiments when the field results are incomplete”. In: *Empire Journal of Experimental Agriculture* 1.2 (1933), pp. 129–142.

[66] B.C. Mitchell and D.S. Burdick. “Slowly converging PARAFAC sequences: swamps and two-factor degeneracies”. In: *Journal of Chemometrics* 8.2 (1994), pp. 155–168.

[67] H.A.L. Kiers. “A three–step algorithm for CANDECOMP/PARAFAC analysis of large data sets with multicollinearity”. In: *Journal of Chemometrics: A Journal of the Chemometrics Society* 12.3 (1998), pp. 155–171.

[68] A.Y. Kibangou and A.L.F. de Almeida. “Consensus-based in-network computation of the PARAFAC decomposition”. In: *arXiv preprint arXiv:1406.1572* (2014).

[69] P. Comon, X. Luciani, and A.L.F. de Almeida. “Tensor decompositions, alternating least squares and other tales”. In: *Journal of Chemometrics: A Journal of the Chemometrics Society* 23.7-8 (2009), pp. 393–405.

[70] G. Tomasi and R. Bro. “A comparison of algorithms for fitting the PARAFAC model”. In: *Computational Statistics & Data Analysis* 50.7 (2006), pp. 1700–1734.

[71] J.G. Andrews et al. “What will 5G be?” In: *IEEE Journal on selected areas in communications* 32.6 (2014), pp. 1065–1082.

[72] A.S. Cacciapuoti et al. “Beyond 5G: THz-based medium access protocol for mobile heterogeneous networks”. In: *IEEE Communications Magazine* 56.6 (2018), pp. 110–115.

[73] E.G. Larsson, O. Edfors, et al. “Massive MIMO for next generation wireless systems”. In: *IEEE communications magazine* 52.2 (2014), pp. 186–195.

[74] R.W. Heath and N. others Gonzalez-Prelcic. “An overview of signal processing techniques for millimeter wave MIMO systems”. In: *IEEE journal of selected topics in signal processing* 10.3 (2016), pp. 436–453.

[75] C. Qian, X. Fu, and N.D. Sidiropoulos. “Algebraic channel estimation algorithms for FDD massive MIMO systems”. In: *IEEE Journal of Selected Topics in Signal Processing* 13.5 (2019), pp. 961–973.

[76] M.N. da Costa. “Tensor space-time coding for MIMO wireless communication systems”. PhD thesis. Université Nice Sophia Antipolis; Universidade estadual de Campinas (Brésil), 2014.

[77] D. Tse and P. Viswanath. *Fundamentals of wireless communication*. Cambridge university press, 2005.

[78] Z. Rong and T.S. Rappaport. *Wireless communications: Principles and practice, solutions manual*. Prentice Hall, 1996.

[79] N.D. Sidiropoulos and R.S. Budampati. “Khatri-Rao space-time codes”. In: *IEEE Transactions on Signal Processing* 50.10 (2002), pp. 2396–2407.

[80] A.L.F. de Almeida and W.C. Freitas Jr. “Blind receiver for multi-layered space-frequency coded MIMO schemes based on temporally extended linear constellation precoding”. In: *2011 IEEE Vehicular Technology Conference (VTC Fall)*. IEEE. 2011, pp. 1–5.

[81] P.H.U. de Pinho, M.F.K.B. Couras, et al. “Semi-supervised receivers for MIMO systems with multiple Khatri-Rao coding”. In: *2019 13th International Conference on Signal Processing and Communication Systems (ICSPCS)*. IEEE. 2019, pp. 1–7.

[82] A.L.F. de Almeida, G. Favier, and J.C.M. Mota. “Space–time spreading–multiplexing for MIMO wireless communication systems using the PARATUCK-2 tensor model”. In: *Signal Processing* 89.11 (2009), pp. 2103–2116.

[83] A.L.F. de Almeida, G. Favier, and L.R. Ximenes. “Space-time-frequency (STF) MIMO communication systems with blind receiver based on a generalized PARATUCK2 model”. In: *IEEE Transactions on Signal Processing* 61.8 (2013), pp. 1895–1909.

[84] A.L.F. de Almeida, G. Favier, and J.C.M. Mota. “Space-time multiplexing codes: A tensor modeling approach”. In: *2006 IEEE 7th Workshop on Signal Processing Advances in Wireless Communications*. IEEE. 2006, pp. 1–5.

[85] E.C. Van Der Meulen. “Three-terminal communication channels”. In: *Advances in applied Probability* 3.1 (1971), pp. 120–154.

[86] J.N. Laneman, D.N.C. Tse, and G.W. Wornell. “Cooperative diversity in wireless networks: Efficient protocols and outage behavior”. In: *IEEE Transactions on Information theory* 50.12 (2004), pp. 3062–3080.

[87] K.R. Liu, A.K. Sadek, et al. *Cooperative communications and networking*. Cambridge university press, 2009.

[88] Z. Zhou et al. “Energy-efficient cooperative communication based on power control and selective single-relay in wireless sensor networks”. In: *IEEE transactions on wireless communications* 7.8 (2008), pp. 3066–3078.

[89] A. Bletsas et al. “A simple cooperative diversity method based on network path selection”. In: *IEEE Journal on selected areas in communications* 24.3 (2006), pp. 659–672.

[90] M. Girnyk. “Cooperative communication for multi-user cognitive radio networks”. PhD thesis. Sweden: KTH Royal Institute of Technology, 2012.

[91] P. H. U. de Pinho et al. “Semi-blind receivers for two-hop MIMO relay systems with a combined TSTF-MSMKron coding”. In: *Sensors* 23.13 (2023), p. 5963.

[92] Z. Wang, Y. Cai, et al. “Mixed-timescale channel estimation for MIMO relay multi-user systems based on the PARAFAC decomposition”. In: *IEEE Communications Letters* 25.4 (2020), pp. 1288–1292.

[93] J. Du, S. Ye, et al. “Tensor-Based Joint Channel Estimation for Multi-Way Massive MIMO Hybrid Relay Systems”. In: *IEEE Transactions on Vehicular Technology* 71.9 (2022), pp. 9571–9585.

[94] L.R. Ximenes, G. Favier, et al. “PARAFAC-PARATUCK semi-blind receivers for two-hop cooperative MIMO relay systems”. In: *IEEE Transactions on Signal Processing* 62.14 (2014), pp. 3604–3615.

[95] D.S Rocha, C.A.R. Fernandes, and G. Favier. “MIMO multi-relay systems with tensor space-time coding based on coupled nested Tucker decomposition”. In: *Digital Signal Processing* 89 (2019), pp. 170–185.

[96] A.L.F. de Almeida, G. Favier, and J.C.M. Mota. “Space–time spreading–multiplexing for MIMO wireless communication systems using the PARATUCK-2 tensor model”. In: *Signal Processing* 89.11 (2009), pp. 2103–2116.

[97] C. Jin et al. “Nonlinear coherent optical systems in the presence of equalization enhanced phase noise”. In: *Journal of Lightwave Technology* 39.14 (2021), pp. 4646–4653.

[98] I. B. Djordjevic. “Spread Spectrum, CDMA, and Ultra-Wideband Communications”. In: *Advanced Optical and Wireless Communications Systems*. Springer, 2022, pp. 647–712.

# Appendix

# APPENDIX A – Resumo Estendido em Língua Portuguesa

**Título**: Receptores semi-cegos para sistema de relé de duplo-salto com codificação baseada em múltiplos produtos de Khatri-Rao e Kronecker
**Autor:** Pablo Henrique Ursulino de Pinho
**Orientador:** Dr.-Ing João Paulo J. da Costa
**Co-orientador:** Dr. Gérard Favier
**Programa de Pós-Graduação em Sistemas Mecatrônicos**
**Brasília, 30 de Abril de 2024**

**Palavras-chave:** Decomposição tensorial. Codificações Khatri-Rao e Kronecker. Receptores semi-cegos. Sistema MIMO.

## Introdução

Os sistemas de comunicação sem fio experimentaram grande crescimento no número de usuários desde o início dos anos 90 [1]. O surgimento de dispositivos conectados e a introdução de novos aplicativos, como veículos autônomos, cidades inteligentes, casas inteligentes, Internet das Coisas (IoT) e realidade virtual, abriram o caminho para a integração de sistemas MIMO sem fio, do inglês *multiple input multiple output* [2]. Os sistemas MIMO foram projetados para suportar a crescente demanda por serviços multimídia de alta qualidade, com as melhores compensações entre o desempenho do erro em termos de SER (do inglês, *symbol error rate*), taxa de transmissão, etc. Esses sistemas usam várias antenas nas extremidades do transmissor e do receptor, o que permite o aumento da diversidade de espaço e leva a sistemas de comunicação com canais MIMO. A implantação de múltiplas antenas em sistemas sem fio permite melhorar a confiabilidade em termos da taxa de erro e da taxa de transmissão em relação aos sistemas de antena de transmissão única, mantendo a mesma largura de banda de energia e transmissão [3,4,5,6].

Nos últimos anos, os sistemas MIMO cooperativos atraíram muita atenção para as redes móveis 5G por aumentar a área de cobertura de transmissão, taxas de dados e desempenho de comunicações sem fio [10]. Os ganhos dos sistemas MIMO cooperativos estão relacionados à diversidade espacial pelo uso de múltiplas antenas para transmitir e receber sinais e multiplexação espacial relacionada ao uso de múltiplas antenas para transmitir fluxos de dados independentes.

Durante as últimas décadas, os modelos tensoriais tem sido amplamente utilizados para projetar sistemas de comunicação sem fio [13, 14, 15, 16, 17]. Veja o seu uso no contexto de sistemas MIMO ponto a ponto [18, 19], e sistemas MIMO cooperativos 20, 21, 22, 23, 24, 25]. Os modelos tensoriais têm a capacidade de capturar a natureza multidimensional do canal sem fio, bem como suas propriedades exclusivas [26, 27]. Essas abordagens também nos permitem desenvolver receptores semi-cegos para estimar em conjunto os canais e as matrizes de símbolos, sob condições mais relaxadas do que os métodos baseados em matriz. No contexto de sistemas cooperativos, alguns resultados foram publicados em receptores baseados em tensores. Alguns trabalhos são dedicados ao uso de sequências de treinamento para estimar os canais de maneira supervisionada, como em [28, 29] onde múltiplos links do relé são explorados para estimar todos os canais parciais envolvidos na comunicação. Esses trabalhos dependem de métodos supervisionados de estimativa de canal, que podem ser consumidos por largura de banda, especialmente para um moderado a grande número de antenas. Isso explica o desenvolvimento de receptores semi-cegos para estimar em conjunto os símbolos de informação transmitidos e os canais, isto é, sem o uso de sequências de treinamento, como no caso dos sistemas introduzidos brevemente.

Para melhorar a estimativa das informações transmitidas, também é necessário explorar as codificações de espaço, tempo e frequência. Vários trabalhos combinam sistemas MIMO cooperativos com codificações de espaço/tempo/frequência para aumentar a diversidade do sistema e obter o melhor desempenho na estimativa dos símbolos e do canal [17, 32, 33, 34]. Dependendo da codificação escolhida para o sistema de relé, diferentes modelos de tensores são obtidos para os sinais recebidos nos nós de relé e destino. A exploração desses modelos permite derivar duas famílias de receptores. A primeira são os receptores supervisionados e a segunda são os receptores semi-cegos.

Nesta tese, abordamos novos receptores semi-cegos para estimar em conjunto as matrizes de canal e dos símbolos nos sistemas de comunicação MIMO ponto a ponto e cooperativos. Em particular, uma das principais contribuições desta tese depende do novo esquema de codificação obtido pela combinação das codificações TSTF e MSMKron nos nós da fonte e retransmissão . Esse novo esquema de codificação, chamado de codificação TSTF-MSMKron pode ser visto como uma generalização das codificações propostas em [33] e [35]. A codificação TSTF-MSMKron é aplicada a um sistema de comunicação OFDM-CDMA de dois saltos. Além disso, apresentamos um caso particular da codificação MKRST, onde uma matriz de símbolos é assumida conhecida, sendo assim considerada como a matriz de pré-codificação. A codificação MKRST é aplicada a um sistema MIMO ponto a ponto. Ao aplicar as codificações propostas, novos modelos de sinais recebidos com base nas decomposições tensoriais são apresentados e, ao explorar esses modelos, receptores semi-cegos são propostos para estimar em conjunto as matrizes de símbolos transmitidos e dos canais em sistemas MIMO de dois saltos e ponto a ponto. São realizadas extensas simulações de Monte Carlo para ilustrar o comportamento e a eficácia dos esquemas propostos.

# Modelo do sistema

Considere um sistema MIMO OFDM-CDMA de dois saltos equipado com $M_S$, $M_R$ e $M_D$ antenas nos nós da fonte, relé e destino, respectivamente. Os canais fonte-relé ($\mathcal{H}^{(SR)} \in \mathbb{C}^{M_R \times M_S \times F}$) e relé-destino ($\mathcal{H}^{(RD)} \in \mathbb{C}^{M_D \times M_R \times F}$) são assumidos como flat Rayleigh fading, representado por tensores de 3-ordem cujo os coeficientes são variáveis aleatórias independente e identicamente distribuídas, constantes durante os últimos $P$ blocos de transmissão.

O protocolo DF é considerado no relé, e a transmissão ocorre em dois saltos. Durante o primeiro salto, os símbolos codificados são transmitidos pela fonte para o relé, através do canal $\mathcal{H}^{(SR)}$, e decodificados no relé. Durante o segundo salto, os símbolos estimados são recodificados e depois re-transmitidos pelo relé para o destino através do canal $\mathcal{H}^{(RD)}$. Cada matriz de símbolos $\mathbf{S}^{(l)} = [s^{(l)}_{n_l,r_l}] \in \mathbb{C}^{N_l \times R_l}$, com $r_l \in \{1, R_l\}$, $n_l \in \{1, N_l\}$, para $l \in \{1, L\}$, é composta de $R_l$ fluxos de dados, cada um contendo $N_l$ símbolos.

O sinal recebido no relé forma um sinal $\mathcal{X}^{(SR)}$ que satisfaz a decomposição Tucker-$(L+1, L+3)$ generalizada dada por:

$$\mathcal{X}^{(SR)} = \mathcal{G}^{(S)} \times_1 \mathcal{H}^{(SR)} \times_2 \mathbf{S}^{(1)} \times_3 \ldots \times_{L+1} \mathbf{S}^{(L)} \times_{L+2} \mathbf{I}_F \times_{L+3} \mathbf{I}_P, \tag{A.1}$$

onde $\mathbf{S}^{(l)}$ são os símbolos decodificados pela codificação TSTF-MSMKron para $l \in \{1, L\}$ e $\mathcal{G}^{(S)}$ é o tensor do núcleo do modelo Tucker. O conhecimento do tensor do núcleo implica a unicidade desse modelo. O sinal recebido no destino é similar ao sinal recebido no relé com as seguintes correspondências:

$$\left(\mathcal{G}^{(S)}, \mathcal{H}^{(SR)}, \mathbf{S}^{(l)}\right) \leftrightarrow \left(\mathcal{G}^{(R)}, \mathcal{H}^{(RD)}, \mathbf{S}^{(l)}_R\right), \tag{A.2}$$

$$(M_R, M_S) \leftrightarrow (M_D, M_R), \tag{A.3}$$

tal que:

$$\mathcal{X}^{(RD)} = \mathcal{G}^{(R)} \times_1 \mathcal{H}^{(RD)} \times_2 \mathbf{S}^{(1)}_R \times_3 \ldots \times_{L+1} \mathbf{S}^{(L)}_R \times_{L+2} \mathbf{I}_F \times_{L+3} \mathbf{I}_P, \tag{A.4}$$

onde $\mathcal{X}^{(RD)} \in \mathbb{C}^{M_D \times N_1 \times \ldots \times N_L \times F \times P}$. O sistema relé OFDM-CDMA proposto é ilustrado na Figura 32.

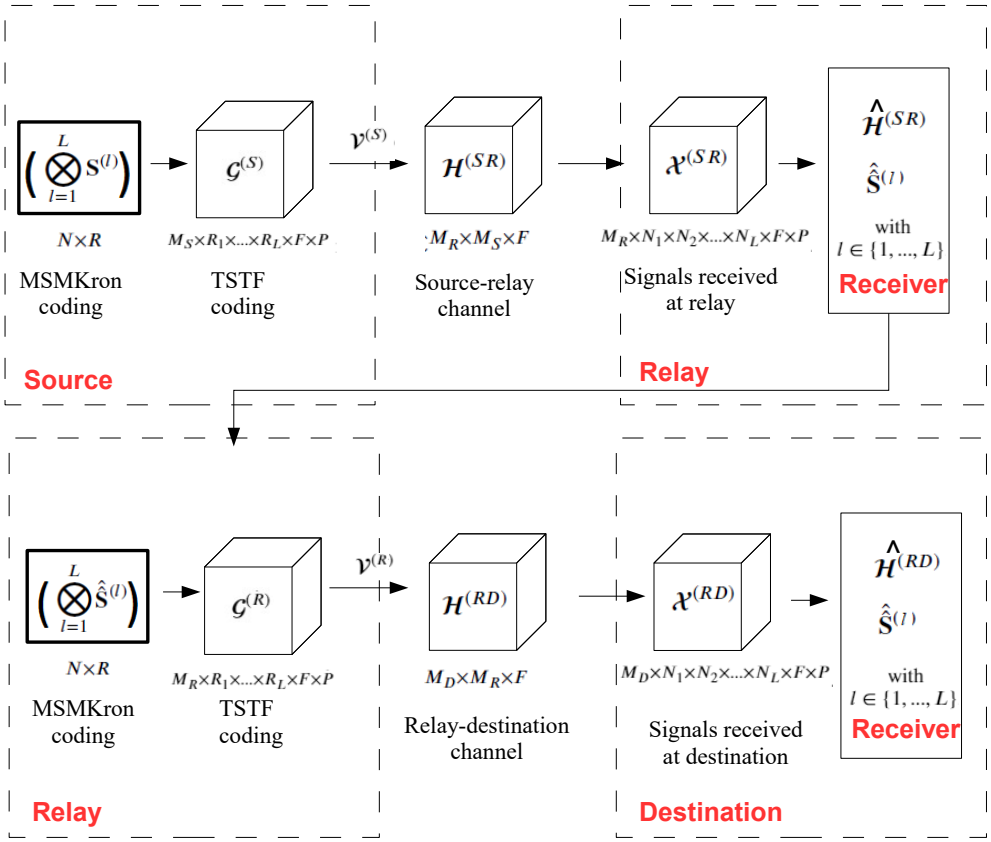


Figure 32 – Diagrama de blocos do sistema de comunicação MIMO OFDM-CDMA proposto.

## Receptores semi-cegos

Dois receptores semi-cegos são apresentados para estimar os tensores do canal e as matrizes de símbolos, nos nós de relé e destino. Assumimos que os tensores de codificação $\mathcal{G}^{(S)}$ e $\mathcal{G}^{(R)}$ são conhecidos. Também assumimos que um símbolo de cada matriz de símbolos é conhecido para eliminar ambiguidades de escala. As matrizes de símbolo $\mathbf{S}^{(l)}$ e o tensor do canal $\mathcal{H}^{(SR)}$ são estimados no relé, enquanto as matrizes de símbolos $\mathbf{S}_R^{(l)}$ e o tensor do canal $\mathcal{H}^{(RD)}$ são estimados no destino. Os receptores propostos são detalhados para o relé. Os mesmos receptores podem ser derivados para o destino, usando as correspondências (A.2) e (A.3). O primeiro receptor é baseado no algoritmo ALS para estimar o canal e o produto Kronecker entre as matrizes de símbolos, seguido pelo método KronF para separar as matrizes de símbolos, enquanto o segundo é uma solução de forma fechada, permitindo que estime em conjunto o canal e as matrizes de símbolos através do algoritmo THOSVD. Os dois receptores são apresentados nas tabelas a seguir.

Table 27 – Receptor Bi-ALS-KronF para estimação dos canais e matrizes de símbolos.

**Receptor Bi-ALS-KronF para estimar $\mathbf{S}^{(l)}$, $\mathcal{H}^{(SR)}$ e $\mathcal{H}^{(RD)}$.**

**Entrada:** tensores $\mathcal{X}^{(SR)}$, $\mathcal{X}^{(RD)}$, $\mathcal{G}^{(S)}$, $\mathcal{G}^{(R)}$

**Saída:** Matrizes de símbolos e canais estimados

**Primeiro salto: fonte - relé**

**- Etapa 1: algoritmo Bi-ALS**

$it = 0$

1) Inicialização de $\mathbf{S}^{(l)}[0]$ com símbolos gerados aleatóriamente apartir do alfabeto e $s_{11}^{(l)} = 1$, para $l \in \{1, L\}$.

2) Atualiza as estimações de $\mathbf{H}^{(SR)}_{FM_S \times M_R}$ e $\mathbf{S}$ usando Eqs.(4.27)-(4.28) ou (4.29)-(4.30).

3) Calcula o erro (4.31) e $|err[i-1] - err[i]|$.

-**se** $|err[i-1] - err[i]| \leq \epsilon$ ou $it =$ número máximo de iterações

- **para**

- **caso contrário** $it \rightarrow i + 1$;

4) Elimina as ambiguidades de escala usando Eq.(4.35).

**- Etapa 2: algoritmo KronF**

5) Constrói o tensor de posto um: $\hat{\hat{\mathcal{S}}} = \text{reshape}\left(\hat{\hat{\mathbf{S}}}, [R_1 N_1, ..., R_L N_L]\right)$.

6) Estima cada vetor $\hat{\mathbf{s}}^{(l)}$ através do algoritmo KronF na Tabela 1, e desvetoriza com a Eq.(4.33).

7) Elimina as ambiguidades de escala usando Eq.(4.37).

8) Projeta os símbolos estimados no alfabeto do símbolo.

**Segundo salto: relé - destino**

**- Etapa 1: algoritmo Bi-ALS**

- Aplica os estágios 1) ao 4) do primeiro salto, usando as correspondências (A.2)-(A.3).

**- Etapa 2: algoritmo KronF**

- Aplica as etapas 5) ao 8) do primeiro salto, usando as correspondências (A.2)-(A.3).

Table 28 – Receptor THOSVD para estimação dos canais e matrizes de símbolos.

**Receptor THOSVD para estimar $\mathbf{S}^{(l)}$, $\mathcal{H}^{(SR)}$ e $\mathcal{H}^{(RD)}$.**

**Entrada:** tensores $\mathcal{X}^{(SR)}$, $\mathcal{X}^{(RD)}$, $\mathcal{G}^{(S)}$, $\mathcal{G}^{(R)}$

**Saída:** Canais e matrizes de símbolos estimados

**Primeiro salto: fonte - relé**

1) Calcula a estimação LS $\mathbf{Z}^{(SR)}$ definida em (4.38).

2) Constrói o tensor de posto um $\mathcal{Z}^{(SR)}$ de tamanho $R_1N_1\times...\times R_LN_L\times FM_SM_R$ a partir de $\mathbf{Z}^{(SR)}$.

3) Calcula a SVD de cada desdobramento de modo-$n$ de $\mathcal{Z}^{(SR)}$, e calcula a estimação $\hat{\mathbf{s}}^{(l)} = \text{vec}\left(\hat{\mathbf{S}}^{(l)}\right)$ e $\hat{\mathbf{h}}^{(SR)} = \text{vec}\left(\hat{\mathbf{H}}^{(SR)}_{M_R\times FM_S}\right)$ como o primeiro vetor singular esquerdo de cada desdobramento de modo-$n$.

4) Desvetoriza $\hat{\mathbf{s}}^{(l)}$ e $\hat{\mathbf{h}}^{(SR)}$ para obter a estimação $\hat{\hat{\mathbf{S}}}^{(l)}$ e $\hat{\hat{\mathbf{H}}}^{(SR)}_{M_R\times FM_S}$.

5) Elimina as ambiguidades de escala.

6) Projeta os símbolos estimados no alfabeto do símbolo.

**Segundo salto: relé - destino**

- Aplica as etapas 1) ao 6) do primeiro salto,usando as correspondências (A.2)-(A.3).

# Resultados

## Impacto dos parâmetros de design

Nesta seção, avaliamos o desempenho da SER do sistema proposto sob o conhecimento perfeito do canal. Nesse caso, usamos o receptor ZF-KronF para estimar as matrizes de símbolo transmitido por meio da Eq. (4.42). Os resultados apresentados nas Figuras 34 a 38 foram obtidos para ambos os saltos, mas aqui são apresentados apenas para o relé.

Figura 33 apresenta o impacto na SER para diferentes números de símbolos por fluxo de dados: $N_1 = N_2 \in \{8, 12, 16\}$, onde $\mathbf{S}_{relay}$ e $\mathbf{S}_{dest}$ denotam a SER no relé e no destino, respectivamente. A partir desses resultados de simulação, pode-se concluir que a SER melhora quando o número de símbolos aumenta, o que implica um aumento da diversidade de codificação, pois $N = N_1N_2$ é uma dimensão da forma contraída $y_c^{(SR)}$ e $y_c^{(RD)}$ nos tensores de dados, o que não é o caso de $R = R_1R_2$. Por outro lado, a taxa de transmissão diminui como mostrado na Tabela 26. Além disso, observe que a SER no relé é melhor que a no destino. Isso acontece porque, com o protocolo DF, os símbolos são estimados e decodificados antes de serem retransmitidos pelo relé para o destino, o que induz um erro de propagação devido à decodificação.

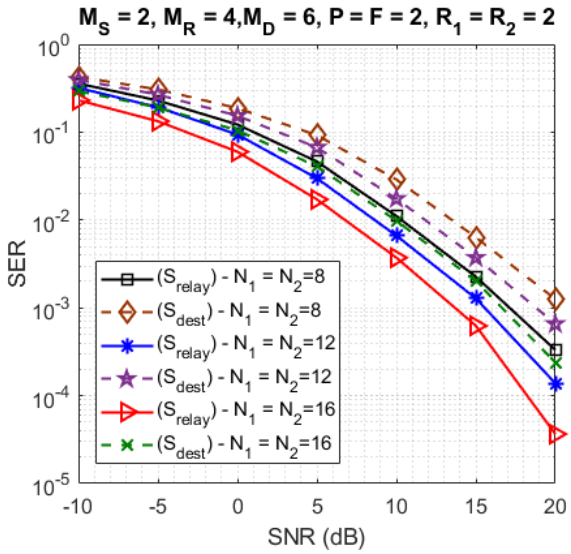


Figure 33 – Impacto do número de símbolos por fluxo de dados.

Figuras 34 a 38 apresentam a SER obtida no relé ($\mathbf{S}_{relay}$). Figura 22 compara a SER para três diferentes números de fluxos de dados: $R_1 = R_2 \in \{4, 6, 8\}$. A partir desta figura, pode-se concluir que o aumento de $R_1$ e $R_2$ implica um aumento do número de símbolos a serem estimados, sem aumentar o número de dados no tensor $\mathcal{Y}^{(SR)}$ para estimar os símbolos, induzindo assim uma degradação da SER, enquanto a taxa de transmissão aumenta (veja Tabela 26).

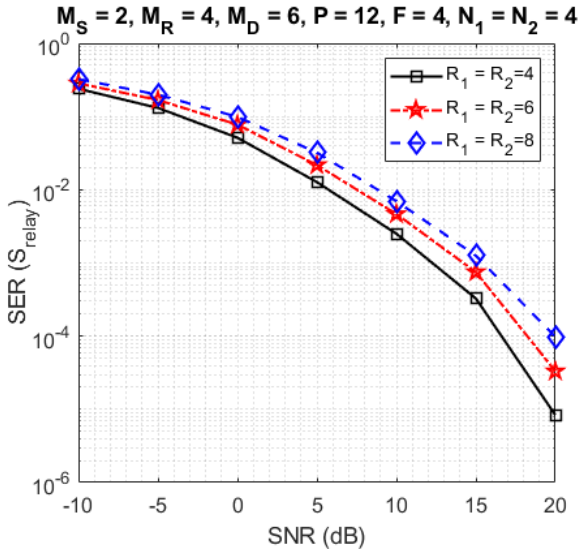


Figure 34 – Impacto do número de fluxos de dados.

Na Figura 35, os resultados das simulações comparam a $\text{SER}_{global}$ com as SERs individuais para $\mathbf{S}^{(1)}$ e $\mathbf{S}^{(2)}$, quando $N_1 = 4$, $N_2 = 12$ e $R_1 = R_2 = 2$. Considerando essa configuração, o produto de Kronecker para $\mathbf{S}^{(1)}$ e $\mathbf{S}^{(2)}$ induz uma alta diversidade para $\mathbf{S}^{(1)}$ que para $\mathbf{S}^{(2)}$, devido ao fato de que cada símbolo de $\mathbf{S}^{(1)}$ é repetido $12R_2$ vezes enquanto cada

símbolo de $\mathbf{S}^{(2)}$ é repetido somente $4R_1$ vezes. O que implica em uma menor SER para $\mathbf{S}^{(1)}$ que para $\mathbf{S}^{(2)}$.

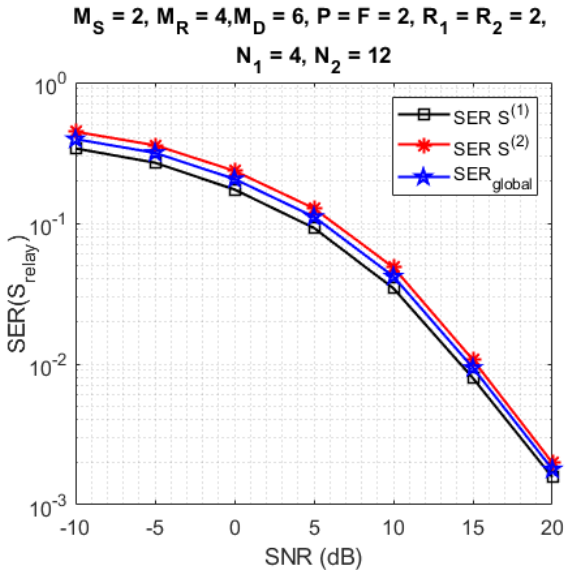


Figure 35 – Impacto na the SER matrizes de símbolos individuais.

Figura 36 apresenta os resultados considerando diferentes configurações para o número de subportadoras ($F$) e blocos de tempo ($P$). Observe que uma melhoria de desempenho é obtida quando $F$ e/ou $P$ são/é aumentado(s), devido a um aumento da diversidade da frequência e/ou de tempo. Por outro lado, a taxa de transmissão diminui. Também podemos observar que, para o mesmo valor do produto $FP = 8$ ou $FP = 16$, o ganho da diversidade é o mesmo, implicando SERs muito próximas, o que ilustra o papel simétrico desempenhado pela diversidade da frequência e do tempo no desempenho da SER.

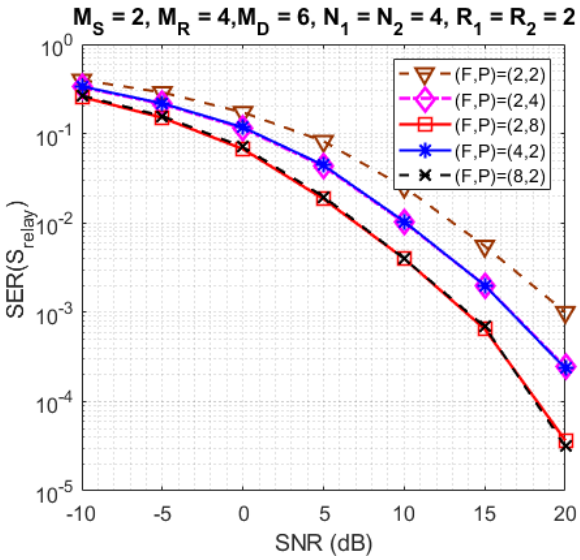


Figure 36 – Impacto das configurações diferentes de ($F$,$P$).

Na Figura 37, a SER é comparada para diferentes números de matrizes de símbolos

($L \in \{2, 3, 5\}$). Os parâmetros de design foram escolhidos para que a taxa de transmissão seja a mesma para os três valores de $L$. A codificação MSMKron com $L = 5$ fornece o melhor desempenho da SER em comparação com $L \in \{2, 3\}$. Esses resultados corroboram o ganho de codificação fornecido pelo produto de Kronecker das matrizes de símbolos.

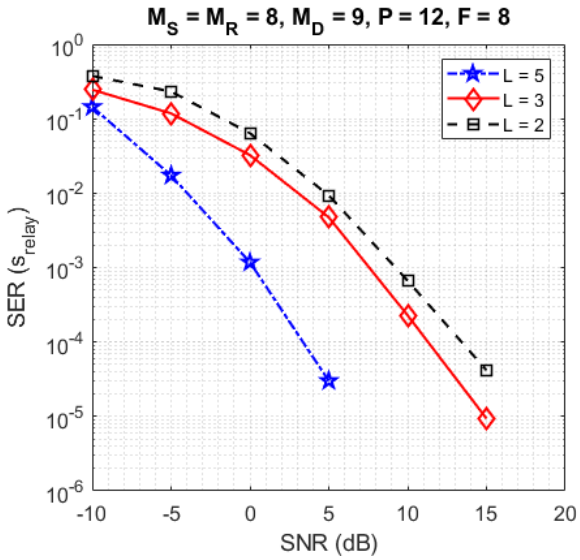


Figure 37 – Impacto de $L$ na SER.

Na Figura 38, a codificação TSTF-MSMKron proposta é comparada com a codificação TSTF, ou seja, usando apenas uma matriz de símbolos $\mathbf{S} \in \mathbb{C}^{N \times R}$ ao invés de um produto de Kronecker de várias matrizes de símbolos. Com a codificação TSTF, a matriz de símbolos é estimada usando a Eq. (4.28). Como esperado, a partir da Figura 38, nós concluímos que a codificação TSTF-MSMKron fornece uma melhor SER do que a codificação TSTF, graças a uma maior diversidade de codificação imposta pelo produto de Kronecker das matrizes de símbolos. Em contrapartida, a taxa de transmissão para a codificação TSTF-MSMKron é menor que a taxa de transmissão com a codificação TSTF. Veja Tabela 26.

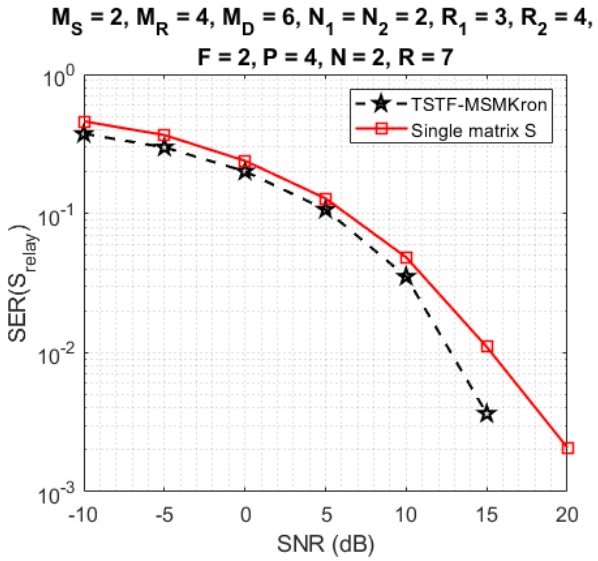


Figure 38 – Comparação das codificações TSTF-MSMKron e TSTF.

## Comparação dos receptores THOSVD e Bi-ALS-KronF

A partir das Figuras 39 e 40, podemos concluir que o receptor THOSVD fornece uma melhor performance na SER comparado ao receptor Bi-ALS-KronF. Isso se deve à forma fechada do receptor THOSVD, permitindo estimar conjuntamente as matrizes do canal e dos símbolos, enquanto o receptor Bi-ALS-KronF é composto por duas etapas, uma iterativa e uma de forma fechada. Por outro lado, o receptor THOSVD é mais restritivo em termos de condições de identificabilidade ($M_S R \leq P$) do que o receptor Bi-ALS-KronF, induzindo uma redução da taxa de transmissão, como pode ser visto na Tabela 26. Também pode-se notar que a SER no relé é melhor que a SER no destino devido à propagação de erro causada pela decodificação no relé. Como esperado, o receptor ZF-KronF fornece a melhor SER devido ao conhecimento a priori dos canais.

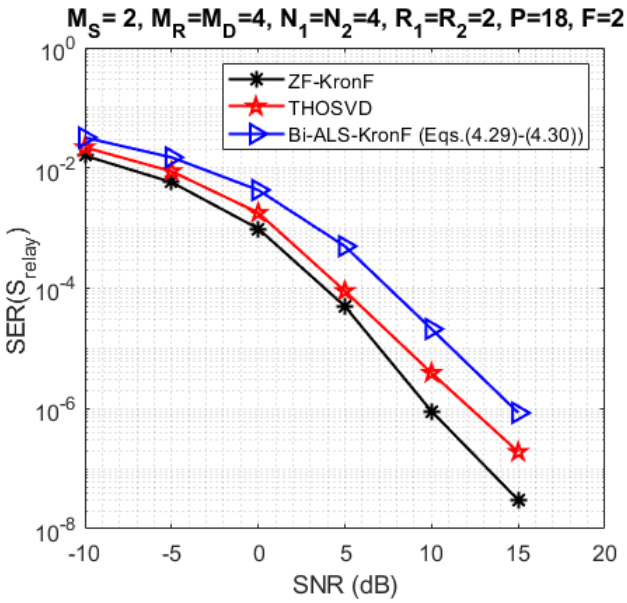


Figure 39 – Comparação da SER com os receptores THOSVD, Bi-ALS-KronF Eqs.(4.29)-(4.30) e ZF no relé.

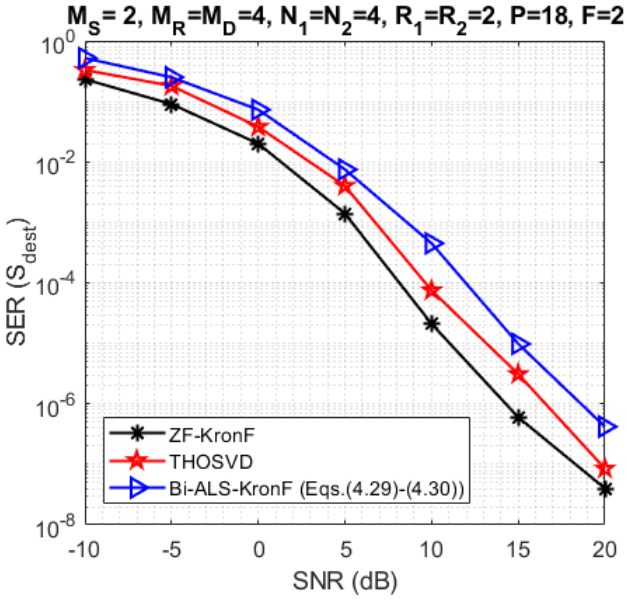


Figure 40 – Comparação da SER com os receptores THOSVD, Bi-ALS-KronF Eqs.(4.29)-(4.30) e ZF no destino.

Na Figura 41, os resultados obtidos para a NMSE do canal em cada salto são apresentadas. Observe que o receptor THOSVD fornece melhores resultados do que os receptores Bi-ALS-KronF. Como para a SER, isso ocorre porque o THOSVD é uma solução de forma fechada, enquanto o algoritmo Bi-ALS é iterativo. Além disso, a estimativa do canal no primeiro salto é um pouco melhor que a do segundo salto. Isso se deve à propagação de erros na retransmissão das matrizes de símbolos após a decodificação no relé.

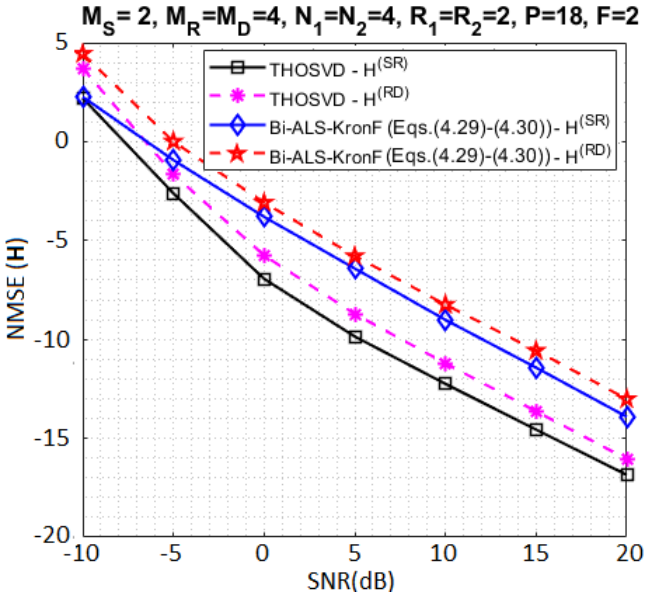


Figure 41 – Comparação da NMSE para a estimação do canal com os receptores THOSVD e Bi-ALS-KronF Eqs.(4.29)-(4.30).

# Conclusão

Ao explorar o modelo do sinal recebido, derivamos dois receptores semi-cegos para estimar em conjunto os símbolos transmitidos e os canais. O primeiro receptor proposto foi baseado nos algoritmos Bi-ALS e KronF, onde o primeiro foi aplicado para estimar o canal e o produto Kronecker, enquanto o segundo foi aplicado para separar as matrizes de símbolos. O segundo receptor proposto é baseado no algoritmo THOSVD de forma fechada, que permite estimar simultaneamente o canal e as matrizes de símbolo por meio do cálculo de SVDs, como no método KronF. Os resultados da simulação nos permitiram ilustrar o impacto dos parâmetros de design no desempenho da SER. A codificação TSTF-MSMKron fornece um aumento nas diversidades espaciais, de tempo e frequência quando o número de fluxos de dados ou o número de antenas na fonte ou relé aumenta. Os receptores semi-cegos são eficientes, especialmente quando são baseados em soluções de forma fechada, para estimar os parâmetros sem o conhecimento do canal, conhecendo apenas um símbolo de cada matriz de símbolos. Por outro lado, o receptor THOSVD de forma fechada é mais restritivo do que o Bi-ALS-KronF iterativo implicando em uma baixa taxa de transmissão.